INSTITUT FÜR HYDROLOGIE
ALBERT-LUDWIGS-UNIVERSITÄT FREIBURG I.BR.

Laurin Wissmeier

Implementation of distributed solute transport into the catchment model TAC^{d} and event based simulations using oxygen-18

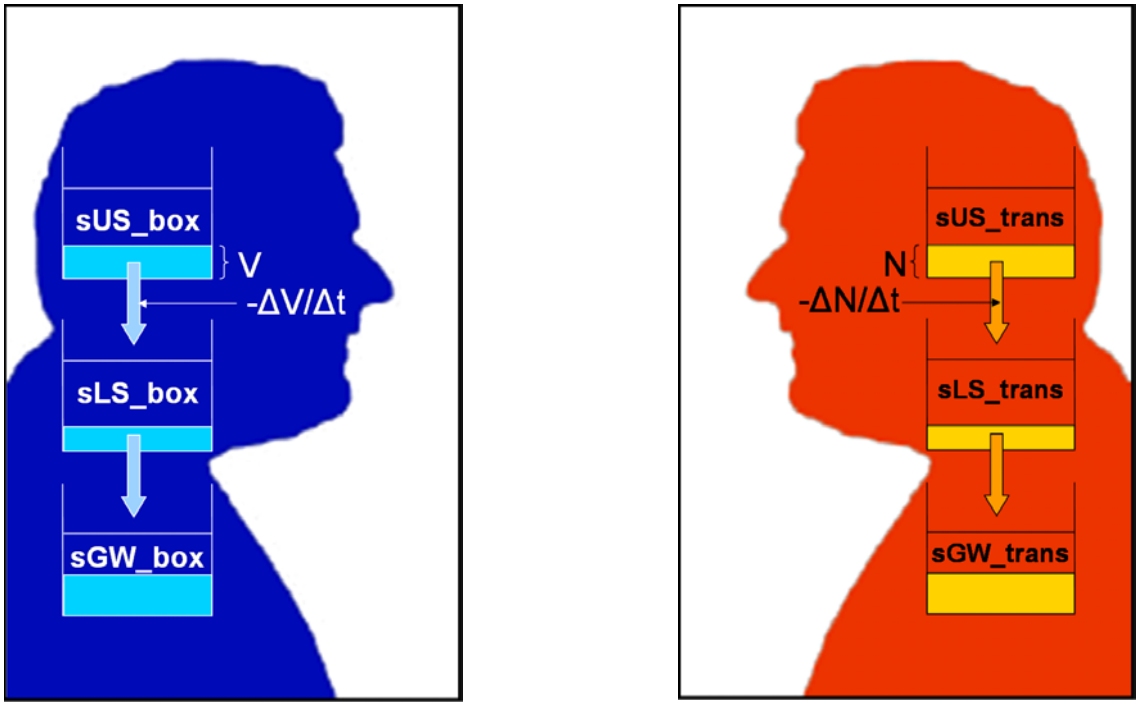

Diplomarbeit unter Leitung von PD Dr. S. Uhlenbrook
Freiburg i. Br., Januar 2005

INSTITUT FÜR HYDROLOGIE
ALBERT-LUDWIGS-UNIVERSITÄT FREIBURG I.BR.

Laurin Wissmeier

Implementation of distributed solute transport into the catchment model TAC^{d} and event based simulations using oxygen-18

Referent: PD Dr. Stefan Uhlenbrook
Koreferent: Dr. Jens Lange

Diplomarbeit unter Leitung von PD Dr. S. Uhlenbrook
Freiburg i. Br., Januar 2005

Contents

List of figures

List of tables

Notations

a	wind correction parameter	[-]
A	wet cross section	[m²]
a.s.l.	above sea level	[m]
accufractionstate	PCRaster function	
ADE	advection-dispersion equation	
AvVol	average volume in channel segment of kinematic function	[m³]
b	wind correction parameter	[-]
bStream	stream cell	
c	constant parameter for vertical flux	[mm/time step]
C	solute concentration	[quantity/m³]
C*	Courant number	[-]
catchmenttotal	PCRaster function	
cExf	exfiltration from groundwater into stream	[mm/time step]
ckg_trans	unit conversion for solute (kg/h => kg/s)	[-]
cMmToCubM	unit conversion for water (mm/h => m³/s)	[m²]
c_p	specific heat capacity of dry air at constant pressure	[kJ/(kg*K)]
cSlopeFactor	slope factor	[-]
DFG	Deutsche Forschungsgemeinschaft; German Research Society	
d_i	distance from location to gauging station i	[m]
dt	time derivative	
dx	space derivative	
e	actual vapor pressure	[hPa]
EML	environmental modeling langusge	
e_s	saturated vapor pressure	[hPa]
ETP	potential evapotranspiration	[mm/h]
$f(x_i)$	elevation correction factor of cell x_i	[-]
G	soil heat flux	[Wh/m²]
HoriAng	horizon angel in direction of sun	[°]
k	number of grid cells	
k*	storage coefficient	[1/time step]
kinematic	kinematic wave routing; PCRaster function	
LDD	local drainage direction	
MTD	micro-topographic depression storage	
n	Manning roughness coefficient	[s/m$^{1/3}$]
N	amount of solute within the solute storage	[quantity]

$N(x_i)$	mean annual precipitation of cell x_i, calculated via altitude regression	[mm]
N_A	Avogadro's number	[-]
N_i	^{18}O concentration in number of molecules/ m^3	[$10^{25}/m^3$]
nRGTypes	runoff generation type	
p	wetted perimeter	[m]
P	gauged precipitation	[mm]
P_{corr}	corrected precipitation	[mm]
POTRAD 5	POtential RADiation equator model	
Q	discharge	[m^3/s]
Q*	water flux	[mm/time step]
Q_{eff}	model efficiency	[-]
$Q_{i, obs}$	observed runoff at time step i	[mm/time step]
$Q_{i, sim}$	simulated runoff at time step i	[mm/time step]
$Q_{log\ eff}$	logarithmic model efficiency	[-]
$Q_{x, t+1}$	new discharge at "upstream end" of grid cell	[m^3/s]
$Q_{x+1, t}$	present discharge in grid cell	[m^3/s]
$Q_{x+1, t+1}$	new discharge at next time step	[m^3/s]
R	^{18}O /^{16}O ratio in sample	[-]
r	weighting coefficient of inverse distance regionalization	[-]
R^2	coefficient of determination	[-]
r_a	bulk aerodynamic resistivity	[s/m]
repeat...until...	PCRaster iterative section	
R_N	net radiation	[Wh/m^2]
r_s	bulk surface resistivity	[s/m]
R_{St}	^{18}O /^{16}O ratio in standard VSMOW	[-]
S	sine of slope gradient	[-]
sActET	actual evapotranspiration from the storages	[mm/time step]
sActET_SOF	evapotranspiration from the MTD-storage	[mm/time step]
sAlpha	parameter of the kinematic function	[-]
sBalance	sum of balance errors, water	[mm]
sBalance_trans	sum of balance errors, solute	[quantity]
sBalanceRouting	sum of balance errors, water in routing routine	[m^3/s]
sCoverage	fraction of vegetation coverage according to landuse	[-]
sDirectIntoStream	stream input from open water ares	[mm/time step]
sEfficiency	model efficiency	[-]
sGW_box	groundwater storage	[mm]
SHADE	function in POTRAD 5	

sInSoil	output from precipitation regionalization, in- and output from interception and snow module input in urban runoff routine and soil routine; (depending on context)	[mm/time step]
sInterceptionET	evaporation from interception storage	[mm/time step]
sIntoStream	stream input of water	[mm/time step]
sIntoStream_trans	stream input of solute	[quantity/time step]
sIntPrec	intercepted precipitation	[mm]
sIntPrec_trans	intercepted solute	[quantity]
sIntPrecNew	input into interception storage	[mm/time step]
sLeafarea	leaf area index	[m²/m²]
slogEfficiency	logarithmic model efficiency	[-]
sLS_box	lower storage	[mm]
sMeltWater	amount of melted snow	[mm/time step
sMTD_box	storage of micro-topographic depressions	[mm]
soiloutput	PCRaster function of soil routine	
soilwater	PCRaster function of soil routine	
SolAlt	angle from sun to theoretical horizon	[°]
sPotET	potential evapotranspiration	[mm/time step]
sPrec	precipitation input	[mm]
sPrec_trans	solute input	[quantity]
sQ_	lateral fluxes	[mm/time step]
sQ_exf	exfiltration from groundwater into stream	[mm/time step]
sQ_GW	lateral groundwater flow	[mm/time step]
sQ_inf;	infiltration from stream into groundwater	[mm/time step]
sQ_LS	lateral outflow from lower storage	[mm/time step]
sQ_LSfull	overflow from full lower storage	[mm/time step]
sQ_SOF	lateral outflow from MTD-storage	[mm/time step]
sQ_step	output of kinematic function	[m³/s]
sQ_US	lateral outflow from upper storage	[mm/time step]
sRefreeze	amount of refreezing water per time step	[mm/time step]
sSlope	slope of cell	[-]
sSlopePerRGT	mean slope of all cells with the same nRGtype	[-]
sSnowET	snow evaporation	[mm/time step]
sSnowPack	snow pack, snow cover	[mm water equivalent]
sSoilMoisture	soil moisture storage	[mm]
sSSD_night	mean daily sunshine duration	[h]
sStorageLeak	vertical outflow from upper storage	[mm/time step]
sStorageMax	maximum storage capacity of interception storage	[mm]
sStreamWidth	stream width	[m]

sTemp	air temperature	[°C]
sToGroundwater	percolation from lower or upper storage	[mm/time step]
Storages $_{1,j}$	sum of storage levels of water of all storages at first time step of simulation period	[mm]
Storages $_{i,j}$	sum of storage levels of water of all storages at actual time step	[mm]
Storages_trans $_{1,j}$	sum of storage levels of solute of all storages at first time step of simulation period	[quantity]
Storages_trans $_{i,j}$	sum of storage levels of solute of all storages at actual time step	[quantity]
sToRunoffGeneration	output from soil routine, vertical percolation into underlying storages	[mm/time step]
sUrbanFlux	fraction of input that is directed to the next stream channel as urban runoff	[mm/time step]
sUrbanIntoStream	stream input from urban areas	[mm/time step]
sUrbanSplit	fraction of sealed area within a urban cell	[-]
sUrbanState	input into the soil routine in urban areas	[mm/time step]
sUS_box	water level in the upper storage	[mm]
sVolumeError	difference between gauged and simulated runoff	[mm]
sWaterContent	water content of snow cover	[mm]
sWaterContent_trans	mobile solute content in snow layer	[quantity]
sWaterDepth	water depth	[m]
t	beginning of time step	
t+1	end of time step	
t_i	number of seconds within a time step	
u_{fluid}	fluid velocity	[m/s]
u_w	wind speed	[m/s]
V	volume of water within the water storage	[mm]
v	flow velocity vector	[m/s]
V(t)	storage level at time t	[mm]
V_o	storage level at time t=0	[mm]
VE	volume error	[mm]
WSB FLAB	knowledge based system for declaration of runoff generation types	
w	diffusion coefficient	[1/time step]
x	"upstream side" of grid cell	
x+1	"downstream side" of grid cell	
z(x)	interpolated value at location x	
$z(x_i)$	measured value at gauging station i	
β	parameter of the kinematic function	
γ	psychrometric constant	[hPa/K]
$\delta^{18}O$	delta ^{18}O notation	[‰]
λ	latent heat of evaporation	[kJ/kg]
ρ	air density	[kg/m³]

ρ^*	density of water at 10°C (0.997 kg/l)	[kg/m³]
$\bar{q}$	average lateral input over the length of the grid cell	[m³/m/s]
$\bar{\bar{D}}$	hydrodynamic dispersion tensor	[m²/s]
^{18}O	oxygen-18	
^{16}O	oxygen-16	
$\overline{Q_{obs}}$	mean observed runoff for whole observation period	[m³/s]
$\overline{Q_{sim}}$	mean simulated runoff for whole observation period	[m³/s]
$\bar{Q}$	"diagonal" average in space-time diagram	[m³/s]
$-\Delta N/\Delta t$	solute flux	[quantity/time step]
Δt	time step discretization	[time]
Δx_{cell}	space discretization	[length]
$\Delta\zeta$	gradient of saturated vapor pressure curve	[hPa/K]
$\bar{N}$	mean annual catchment precipitation	[mm/a]
0.3	maximum thickness of water film on surface in interception routine	[mm]
18.016	average molecular mass of $H_2{}^{16}O$	[g/mol]
20.016	average molecular mass of $H_2{}^{18}O$	[g/mol]

PCRaster parameters and can be found in the parameter table in Appendix A

Summary

The objective of this thesis was the development of a solute transport model based on the existing catchment model *TAC*^{d} (Tracer Aided Catchment model, distributed). As *TAC*^{d} seeks to reproduce water fluxes in a process-orientated way, solute transport can be tied in with the description of water fluxes.

The dynamic GIS *PCRaster* was used for the construction of the solute transport model. A high linkage of dynamic, space related operations and the database signifies *PCRaster*'s excellence for distributed hydrological modeling.

A coupled solute transport model fully relies on the correct representation of water fluxes. Due to mixing of water, it is also dependent on the correct representation of water volumes within the storages of the catchment. Since the incorrect water balance in previous model versions has indicated faults in the *TAC*^{d} model script, a complete review of the *TAC*^{d} source code was necessary. While intensively checking the code for mistakes in its formulation, numerous bugs could be detected and rectified. As a result, the water balance and the solute balance work out even in the present model version.

Continuous simulations of solute distributions within mountainous, snow influenced, meso-scale catchments can be performed by the presented model of solute transport. Based on the revised water model, the solute model is represented by another system of solute storages and fluxes, which are built in full analogy to the water model. In other words, the solute model is a mirror image of the water model, in a way that each water storage and flux is represented by one solute storage and flux. Thus, the solute is routed through all sections of the land phase water cycle. The connection between the water model and the solute model is given by the following equation:

$$\frac{\Delta N}{N \cdot \Delta t} = \frac{\Delta V}{V \cdot \Delta t} \qquad \textit{Eq. 5.3}$$

V:	volume of water within the water storage
$-\Delta V/\Delta t$:	water flux
N:	amount of solute within the solute storage
$-\Delta N/\Delta t$:	solute flux

Without including further solute reactions the model can be used for transport simulation of any conservative, non-reactive substance such as ^{18}O or deuterium. The flexibility of the model structure allows area wide solute input as well as input from point sources. Both, instantaneous and continuous input can be simulated. Subsurface mineralization of water

can also be captured if mineralization rates are available. In addition, the solute can be introduced via precipitation or directly into each section of the land phase hydrological water cycle (e.g. dry deposition into interception storages). Solute concentrations can be reported in stream discharges at the catchment outlet as well as in the different storages at arbitrary locations within the catchment.

In order to verify the produced model code, several tests with synthetic input data were carried out. Here the model's behavior under straightforward and well-defined conditions could be examined. After tests with synthetic data sets were successfully completed, the model was applied to the Dreisam catchment under natural conditions with 'real-life 'data sets. The environmental isotope oxygen-18 was used for simulations of event-based concentration distributions within the catchment area and in stream discharges. No further calibration is necessary for solute transport, because the dynamics of processes within the solute model are fully dependent on the parameterization of the water model. Thus, solute simulations can help to detect inadequate conceptionalization of water fluxes, when data uncertainties are sufficiently small.

From model applications of ^{18}O simulations the following conclusions can be drawn:

- If data requirements for the solute model are satisfied, simulation accuracy is within the analytical error of laboratory measurements of ^{18}O. This claim has already been achieved by the presented applications within the Brugga subcatchment.
- The water model seems to overestimate the contribution of urban runoff to total stream input in catchments with a high degree of urbanization.
- Other fast runoff components such as shallow translatory flow and saturated overland flow are only important when the cells under consideration are directly connected to the river network. Otherwise, their influence is swept off by dilution with pre-event water.
- The incorporation of processes such as Piston Flow, retardation in an immobile subsurface phase and dispersion/ diffusion within the channel system would lead to better results of ^{18}O simulations, because of their damping effect on $\delta^{18}O$ concentrations at the catchment outlet.
- In order to capture the time lag between stream input and discharge at the catchment outlet, the module for solute translation within the channel system has to be revised.

The presented model applications have shown that the model for solute transport can be used as a diagnostic tool for the adequate conceptualization of water fluxes. Preparations for the advancement of the model extension in respect to realistic simulations of reactive, non-conservative solutes have been made. In general, the solute model is seen as a framework for further development of solute transport modeling with TAC^d.

Zusammenfassung

Ziel dieser Diplomarbeit war die Entwicklung eines Stofftransportmodells auf Basis des distribuierten Einzugsgebietsmodells *TAC*^{d} (Tracer Aided Catchment model, distributed). Aufgrund der prozessorientierten Simulation der Wasserflüsse und -Volumina in *TAC*^{d}, können die Stoffflüsse direkt mit dem Wassertransport verknüpft werden.

Für die programmtechnische Umsetzung des Stofftransportmodells wurde, genauso wie für *TAC*^{d}, die Programmierungsumgebung *PCRaster* verwendet. Die enge Verknüpfung von GIS-Operationen und -Datenbank, zeichnet *PCRaster* als dynamisches GIS für die Programmierung distribuierter hydrologischer Modelle aus.

Weil ein wassergekoppeltes Stofftransportmodell in besonderem Masse von der naturgetreuen Simulation der Wasserflüsse abhängt und da die modellinterne Wasserbilanz der Vorläuferversionen auf eine fehlerhafte Programmierung hin deutete, wurde erheblicher zeitlicher Aufwand in die eingehende Überprüfung des bestehenden *TAC*^{d} Programmcodes investiert. Daraufhin konnte eine Vielzahl von Logikfehlern in nahezu allen Modulen erkannt und behoben werden, so dass in der aktuellen Programmversion weder die Wasserbilanz noch die hinzugefügte Stoffbilanz eine Verletzung des Massenerhaltungsgesetzes anzeigen.

Mit Hilfe des erarbeiteten Modells für den advektiven Stofftransport können kontinuierliche Simulationen von Konzentrationsverteilungen in einem schneebeeinflussten, mesoskaligen Einzugsgebiet durchgeführt werden. Basierend auf dem überarbeiteten Wasserflussmodell *TAC*^{d}, wird das Stofftransportmodell von einem System von gekoppelten Stoffspeichern und Stoffflüssen gebildet. Dieses System ist in völliger Analogie zum Wassermodell aufgebaut, sodass jeder Wasserspeicher und –Fluss von einem gleichartigen Stoffspeicher und –Fluss repräsentiert wird. Das bedeutet, dass der gelöste Stoff genauso wie das Wasser durch alle Stationen des festländischen Wasserkreislaufs transportiert wird. Die Verbindung von Wassermodell und Stoffmodell wird durch die folgende Gleichung hergestellt:

$$\frac{\Delta N}{N \cdot \Delta t} = \frac{\Delta V}{V \cdot \Delta t} \qquad \textit{Eq. 5.3}$$

V:	Wasservolumen im Wasserspeicher
-ΔV/Δt:	Wasserfluss
N:	Stoffmenge (Fracht) im Stoffspeicher
-ΔN/Δt:	Stoffffluss

Ohne dass weitere Stoffreaktionen berücksichtigt werden, kann das Modell den Transport von konservativen Stoffen wie z.B. Sauerstoff-18 und Deuterium simulieren. Die Flexibilität der Modellstruktur ermöglicht die Simulation von punktuellem, konzentriertem als auch flächenhaften, diffusem Stoffeintrag. Zudem kann der Stoff als Konzentration im Niederschlag oder als Fracht per Trockendeposition direkt in den Interzeptionsspeicher oder jeden anderen Speichertyp eingetragen werden. Auch Mineralisierung im Untergrund kann berücksichtigt werden, wenn Mineralisierungsraten bekannt sind. Die resultierenden Konzentrationen können im Abfluss am Einzugsgebietsauslass oder in jedem beliebigen Speicher des Einzugsgebiets ausgelesen werden.

Um den Programmcode des Stofftransportmodells zu verifizieren, wurden mehrere Tests mit synthetischen Datensätzen durchgeführt. Dabei konnte das Modell unter definierten Abflussbedingungen und gezieltem Stoffeintrag auf mögliche Fehler in der Formulierung des Codes hin untersucht werden. In einem weiteren Schritt wurde das Modell unter natürlichen Bedingungen mit realen Daten getestet. Das Umweltisotop Sauerstoff-18 wurde zur ereignisbasierten Simulation von Konzentrationsverteilungen im Einzugsgebiet und im Gerinneabfluss verwendet. Da die Dynamik des Stoffmodels völlig von der Parametrisierung des Wassermodells abhängt, ist für die Verwendung des Stofftransportmodells keine weitere Kalibrierung notwendig. Das Stofftransportmodell kann daher helfen Modellunsicherheiten aufzudecken, vorausgesetzt die Datenunsicherheit ist ausreichend klein ist.

Die Modellanwendung auf ereignisbasierte Simulationen von Sauerstoff-18 erlaubt folgende Schlüsse:

- Wenn die Datenanforderung des Stofftransportmodells hinreichend erfüllt ist, können Simulationsergebnisse im Bereich der analytischen Genauigkeit der Laboranalysen von ^{18}O erreicht werden.
- Der Anteil des Siedlungsflächenabflusses im Verhältnis zum gesamten Gerinneeintrag wird im Wassermodell in Gebieten mit einem hohen Versiegelungsgrad überschätzt.
- Andere schnelle Abflusskomponenten, wie hangparalleler Interflow und Sättigungsflächenabfluss, sind nur dann für den Stofftransport relevant, wenn die betreffende Zelle direkt ans Gerinne angeschlossen ist. Andernfalls wird ihr Einfluss durch Verdünnung mit Vorereigniswasser zunichte gemacht.
- Die Berücksichtigung von Prozessen wie Piston Flow, Retardierung (Adsorpton/Desorption) in eine immobile Phase und Dispersion im Gerinne würden zu verbesserten Ergebnissen bei der Simulation von ^{18}O führen.
- Um die Abflussdynamik des Stoffes im Gerinne besser nachbilden zu können bedarf es einer verbesserten Routine für den Gerinnetransport von Stoffen. Dieser Schwachpunkt ist offensichtlich in Einzugsgebieten mit längeren Fliesszeiten im Gerinne von größerer Bedeutung.

Die Modellanwendungen haben gezeigt, dass das Stofftransportmodell im Sinne einer „multi response calibration/validation“ als diagnostisches Werkzeug zur Überprüfung der naturgetreuen Abbildung der Wasserflüsse verwendet werden kann. Darüber hinaus wurden in der vorliegenden Arbeit Vorbereitungen zur Simulation von reaktiven nicht-konservativen Stoffen getroffen. Generell sollte das hier erarbeitete Modell als Grundbaustein für die weitere Entwicklung der Stofftransportmodellierung mit *TAC*^{d} betrachtet werden.

Keywords: distributed, process-orientated, conservative, solute transport, ^{18}O-simulation, Dreisam catchment

1 Introduction

The rapid development of hydrological models within the last decade results in an almost unmanageable number of modeling approaches for nearly all hydrological problems. The internet search engine 'Google' (*GOOGLE 2004*) yields about 6050 entries for the search key "hydrology, 'distributed model'". However, the potential of solute transport models that operate on the catchment scale is yet far from exhausted. Many of the water related issues of the 21st century can only be handled by distributed, process-orientated solute transport models. One typical domain is water quality modeling e.g. the assessment of vulnerability in respect of agricultural, industrial or urban pollution or predictions of contaminants in stream discharges. Other aspects are predictions of the effects of alterations in climatic input (global warming) or landuse (urbanization), evaluation of process understanding in a river basin modeling systems and a gain of information about the origin of waters and their residence times. In order to cope with these crucial issues, solute transport models can only yield realistic simulations when the underlying water models reflect natural flow processes in an appropriate process-orientated way.

Even though computer models are of great value for hydrological sciences, their limitations have to be respected. Also the best process-orientated, physically based models only reflect the knowledge and expertise of the modeler. However, models can be used to evaluate, whether the implemented knowledge adequately represents natural processes, or not. Due to the fast progress in experimental hydrology, a close cooperation of model developers and experimentalists is essential to keep process knowledge within a model up to date.

This thesis is based on results from the project "runoff generation and catchment modeling", which was funded by the German Research Society (*DFG, 2000-2004*).

1.1 Objective

The objective of this thesis was the development of a solute transport model based on the existing catchment model *TAC*^{d} (Tracer Aided Catchment model, distributed). As *TAC*^{d} seeks to reproduce water fluxes in a process-orientated way, solute transport can be tied in with the description of water fluxes. For the development of the solute model, it could be reverted to numerous previous studies (*UHLENBROOK 1999, ROSER 2001, OTT 2002, SIEBER 2003, TILCH ET AL. 2003, JOHST 2003, AUS DER BEEK 2004, DIDSZUN 2004*).

As a second objective, the developed solute transport model had to be tested and evaluated. For this purpose, several tests with synthetic input data were carried out, such that the model's behavior could be examined under straightforward and well-defined conditions. After tests with synthetic data sets were successfully completed, the model was applied to the Dreisam catchment (southern Black Forest) under natural conditions with

'real-life 'data sets. The environmental isotope oxygen-18 (^{18}O) was used for simulations of concentration distributions within the catchment and in stream discharges. Data for ^{18}O concentrations in precipitation and climatic input for selected events was available from *DIDSZUN* (*2004*).

Furthermore, preparations for the advancement of the model extension in respect to realistic simulations of reactive, non-conservative solutes have been made. Thereby, also suggestions for further development of the water model were compiled.

1.2 State of the art

"The state of the art is not necessarily close to the state of nature" (*PILKEY 1997, P. 265*). Nevertheless, this chapter wants to give a brief overview of recent approaches for distributed solute transport modeling. For coupled water and solute transport models, the underlying water model usually determines the type of the solute transport, even though in some models simplifications are applied for solute transport. Therefore, the categorization of solute transport models follows the classification of the underlying water models.

Many physically based solute transport models where developed for applications in porous groundwater aquifers. Except for those restricted cases, where analytical functions can be derived (*MALOSZEWSKI & ZUBER 1992, MALOSZEWSKI & ZUBER 1993*), the models use spatial and temporal numerical discretization methods for calculations of water flow as for solute transport. Usually, groundwater-solute transport models apply different solving schemes for the differential form of the transport equation:

$$-\nabla \cdot (\vec{v}C - \overline{\overline{D}} \cdot \nabla C) = \frac{\partial C}{\partial t} \qquad \textit{Eq. 1.1}$$

(from *BECKIE 2001*)

v: flow velocity vector
$\overline{\overline{D}}$: hydrodynamic dispersion tensor
C: solute concentration

Those solute transport models are incorporated in groundwater flow models like *MODFLOW* (*MODFLOW 2004*) or *FEFLOW* (*FEFLOW 2004*). Sophisticated solutions account for transient, multi-phase flow in anisotropic aquifers including 3-dimensional dispersion and the effects of numerous solute reactions like diffusion and retardation. For these physically based simulations of water and solute fluxes, the physical properties, the boundary and the initial conditions in the simulated area have to be well known.

These prerequisites are much harder to fulfill when simulations are transferred from porous groundwater aquifers to entire meso-scale river basins (in the order of 100 km²).

Nevertheless, it has been tried to simulate water and corresponding solute fluxes on the catchment scale by applying physical equations of flow also to the unsaturated zone. Vertical flow in the unsaturated zone is usually calculated by solving the Richards equation. Despite the physical basis of the equations, conceptualization is inherent also in those models. Due to the assumed homogeneity within a discretization unit, non-plausible values for physical properties may have to be calibrated in order to yield acceptable simulation results (*BEVEN 1996*). Examples for this category of models are *MIKE SHE* (*MIKE SHE 2004*) and *SHETRAN* (*SHETRAN 2004*), which shall be briefly discussed in the following.

MIKE SHE:

MIKE SHE is a commercial hydrological model integrating physically based modules for unsaturated (Richards equation), saturated (advection-dispersion equation, ADE) and overland flow (kinematic wave routing). *MIKE SHE* is based on the *SHE* (Système Hydrologique Européen) model, which was developed by *ABBOTT ET AL.* (*1986A, B*). *MIKE SHE* features a close coupling of surface water and subsurface flow like infiltration of stream water or exfiltration from the groundwater. The solute module incorporated in *MIKE SHE* can handle basic advective/dispersive solute transport, equilibrium and non-equilibrium adsorption as well as first order decay. In addition, modules for advanced biological degradation and macro pore flow (dual porosity) are available. (*MIKE SHE 2004*)

SHETRAN:

The SHETRAN model and its later version SHESED, which contains a sediment component (*WICKS & BATHURST, 1996*), were also inherited from the Système Hydrologique Européen (*SHE*) model (*ABBOTT ET AL., 1986A, B*). Thus, the general model approach is very similar to *MIKE SHE*. *SHETRAN* was developed by the WRSRL (Water Resource Systems Research Laboratory). According to *EWEN ET AL.* (*2000*), *"SHETRAN is a 3D, coupled surface/subsurface, physically based, spatially distributed, finite difference model for coupled water flow, multi-fraction sediment transport and multiple, reactive solute transport in river basins."* (from *EWEN ET AL. 2000, P. 250*)

An independent grid oriented Phosphorus component (GOPC) (*NASR ET AL., 2003*) has been developed for modeling phosphorus for a catchment where SHETRAN has been applied for water flow and sediment. A module for Nitrate transport is under testing. A river network component based on the solution of the full Saint-Venant equation as well as a regional groundwater component below the variably saturated subsurface model and a capability for preferential flow in the subsurface is under development. (*SHETRAN 2004*)

The treatment of water fluxes and solute transport with physical equations fails in areas where detailed knowledge of physical properties is restricted by large heterogeneities. This is usually the case in fractured aquifers, where the detailed geometry of fractures is

unknown. Especially in mountainous areas, runoff generation processes are mostly determined by subsurface layers with a high fraction of boulders and blocks or fractured base rock aquifers. Thus, a certain degree of conceptualization is inevitable in those catchments. Starting from more physical based catchment models, a wide spectrum of conceptual models with large differences in their level of agreement exists (*REFSGAARD 1996*). Two representative models for this type are *WaSiM ETH* (*SCHULLA & JASPER 2000*) and *HBV-96* (*HBV 2004, LINDSTRÖM ET.AL. 1997*), which are partly very similar to *TAC*^{d}.

WASIM ETH:

The *WaSiM ETH* (Water balance Simulation Model) is a girded, process-oriented water balance model. It was developed and maintained by *SCHULLA* (*1997, SCHULLA & JASPER 2000*) at the ETH Zürich. The model includes different schemes to calculate potential evapotranspiration (Penman-Monteith 1975, Wendling 1975, Hamon 1983) and two different soil routines (Version 1: TOPMODEL-approach (*BEVEN 1997*); Version 2: Richards-equation-approach with multi layer soil). By numerically solving the universal Richards-equation for unsaturated flow and the Laplacian advection-dispersion-equation (ADE) for saturated flow in porous aquifers, the *WaSiM ETH* is put on a physical basis. Nevertheless, the runoff generation routine still comprises conceptualizations for fractured aquifers. Thus, the complex soil routine and the close coupling to a groundwater model are the most evident differences between *WaSiM ETH* and *TAC*^{d}. The interception routine, methods for precipitation regionalization and the evapotranspiration model (Penman-Monteith) are the same in both models. In Version 2 of the *WaSiM ETH* a solute transport routine is included, which is very similar to the one presented in this thesis. It also couples solute fluxes to water fluxes. Thus, it can be used for advective transportation of conservative tracers with or without evapotranspiration influence and additional radioactive decay. (*SCHULLA & JASPER 2000*)

HBV-96

The *HBV-96* is the distributed and revised successor of the conceptual *HBV* model (*LINDSTRÖM ET AL 1997*). The original *HBV* model was developed by *BERGSTRÖM* (*1976*). The snow routine and the soil routine of the *TAC*^{d} were adopted from the *HBV*. A short description of this model can be found at *HBV-96* (*2004*). The two main features for transformation of precipitation into runoff are the soil routine and the runoff generation routine.

"Water not retained in the soil is routed through two stores, an upper one interpreted conceptually as saturated soil and a lower one representing groundwater. Water can percolate from the upper to the lower store, which has a slow linear outflow. In HBV-96, the upper store is nonlinear. In previous versions, the store is linear until a second and faster outlet comes into operation above a specified level.(...) Each variant of the model gives a nonlinear response to water input, with a dependence also on recent history through the initial level of soil moisture. Fast pathways operate only when the basin is already very wet, or

becomes wet through a large input of rain or snowmelt. The number of adjustable parameters allows the model to be fitted to a wide range of basin conditions. The HBV-96 version has one parameter less and is easier to calibrate." (from *HBV-96 2004*)
The HBV-96 model, usually working on a daily basis, does not yet contain a routing scheme for stream runoff.

The *HBV-N* model is a model for nitrogen simulations, which can be coupled to the HBV-96 (*ARHEIMER & BRANDT 1998*).
"The HBV-N model is a process-based, semi-distributed conceptual model, which has recently been used by national authorities in large-scale estimates of Swedish nitrogen (N) load, retention and source apportionment for the Baltic Sea. (...) In the N routine, leakage concentrations are assigned to the water percolating from the unsaturated zone of the soil to the response reservoir of the hydrological HBV model. Different concentrations are applied to water originating from the land use categories forest, urban, arable and other land. The arable land may be further divided into a variety of crops and management practices, for which the N leaching is achieved by using the field-scale model SOIL-N. In addition to the diffuse soil leaching, N is also added from point sources, such as rural households, industries, and wastewater treatment plants. Atmospheric deposition is added to lake surfaces, while deposition on land is implicitly included in the soil-leaching. The model simulates residence, transformation and transport of N in groundwater, rivers and lakes. The equations used to account for the N turnover processes are based on empirical relations between physical parameters and concentration dynamics. Inorganic N and organic N are treated separately in the simulations and the calculations are made with a daily time-step." (from *ARHEIMER 2004*)
In the latest developments, simulation of phosphorus was included in the *HBV-N* model resulting in the *HBV-NP*.
"HBV-NP is a dynamic mass-balance model, which is run at a daily time-step, including all sources in the catchment coupled to the water balance." (from *HBV-NP 2004*)
In contrary to the solute transport in TAC^d, *HBV_NP* is semi-distributed working with different subcatchments for regionalizing solute reactions. Further information is given at *HBV-NP* (*2004*) and *ARHEIMER & BRANDT 1998*.

Because of the vast number of existing modeling approaches, only the most similar to TAC^d could be selected for a closer description. Due to the rapid progress of model development in hydrological sciences, review books like *COMPUTER MODELS OF WATERSHED HYDROLOGY* (*SINGH P. 1995*) are out-dated within few years.

1.3 Procedure

The model version of *TAC*^{d}, which was extended and applied by *OTT* (*2002*), was used as a starting point for the development of a solute transport model. Originally, it was intended to calculate nitrogen transport in the Dreisam catchment on a daily basis with a less detailed, lumped method similar to the one used by *EISELE* (*2003*), however it became apparent that a universal and powerful method for solute transport could be developed by coupling solute fluxes cell by cell to distributed water fluxes. With this approach, an expendable framework for process-orientated and distributed simulations of conservative solute transport was created.

Since a coupled solute transport model fully relies on the correct representation of water fluxes, much time and effort was put in a complete review of the *TAC*^{d} source code. As the incorrect water balance of prior model versions has indicated faults in the *TAC*^{d} model script, the code was intensively checked for mistakes in its formulation. That way, numerous bugs could be detected and rectified (see chapter 4).

For the actual development of the solute transport, a virtual test site of 10 by 10 cells was installed in order to achieve a higher degree of transparency in flow processes. Within this test site, the solute model was gradually extended to the different modules. Problems during the formulation of the code did not arise from the theoretical principles, but from the complexity of the model structure namely the number of interconnections between storages and modules. Each water flux had to be coupled to a corresponding solute flux (see chapter 5).

After the code development was completed, the model was tested with synthetic input data under several different conditions (see chapter 5.8) including two substantial tests for code verification. Firstly, the solute balance was checked for violations of mass conservation. Secondly, in the case of precipitation input with constant solute concentrations, the concentrations have to remain constant within all storages of the catchment even under transient flow conditions. Consequently, the discharge at the outlet has to reflect the original input concentration in precipitation. In addition, tests for point source and area-wide input of solute were conducted with synthetic input data.

In the following, the model was applied to event-based simulations of ^{18}O in stream discharges. For this purpose, some modifications of the solute model had to be carried out. $\delta^{18}O$-values had to be converted into units of concentration, namely number of ^{18}O molecules per cubic meter of water. In the case of ^{18}O, also loads within the solute model are subject to evapotranspiration. Thus, evapotranspiration had to be integrated into the solute model, even though fractionation could be neglected for event-based simulations. The model was applied to three different events, of which two were simulated in the Dreisam river basin and all its subcatchments and one only in the Brugga river basin.

Literature from other models was of limited help, because the objective was to use *TAC*^{d} for solute simulations, in which case the coupling of solute transport had to be tailored individually to the representation of water fluxes.

2 *PCRaster* – a dynamic GIS

PCRaster is used as a programming environment for *TAC*^{d} and its connected solute transport model.

2.1 Concepts of *PCRaster*

PCRaster provides a development environment for hydrological and geoscientific simulations including a modern environmental modeling language (EML). *PCRaster* is under intensive development and constant advancement. Within the last 9 months, several bug fixes and updates for all its components were released, including a user shell (*NutShell 1.89*) and an iterative section (*repeat…until…*).

The *PCRaster* environmental modeling language is specially designed for the tasks of hydrological modeling. Similar to programming languages *like GRASS* (*GRASS 2004*) and *Simile* (*SIMILE 2004*), *PCRaster* combines the advantages of common technical database languages like MATLAB (*MATLAB 2004*) and GIS systems (e.g. ESRI; *ESRI 2004*).

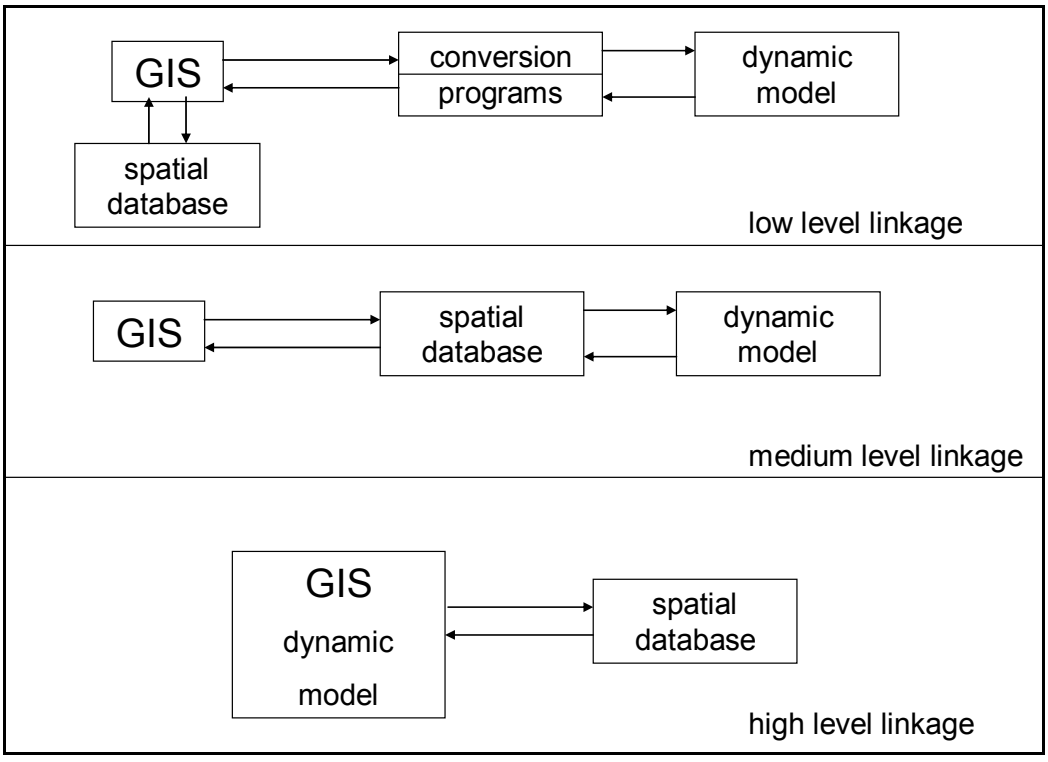

Figure 2.1: Level of linkage in dynamic GIS modeling languages (from van Deursen 1995)

Figure 2.1 illustrates the level of linkage between the GIS and the dynamic section within a modeling system. In order to gain the spatio-temporal flexibility, which is necessary for the simulation of hydrological processes, a high-level linkage between the database and GIS-system is of great advantage. This high-level linkage is realized in *PCRaster*.

Therefore, the use of an external data conversion program can be avoided. Hence, *PCRaster* is called a dynamic GIS (*VAN DEURSEN 1995*).

WESSELING ET AL. (*1996A,B*) and define the objectives of the development of *PCRaster* as follows:

"1. provide a set of operators operating on spatio-temporal data in which widely accepted generic hydrological processes have been coded using accepted, clearly understood algorithms.
2. provide these operators in a suitable way that they can be glued together in a model by a hydrologist using his or her hydrological understanding, rather than computer expertise.
3. embed this set of tools for model construction in a GIS-like software environment providing database management and generic visualization routines for the spatio-temporal data read and written by the model.
4. provide standard interfaces to other programming languages so that new or alternative operators can be added by the user in ways that are fully compatible with the EML." (from *WESSELING ET AL. 1996B, P. 41*)

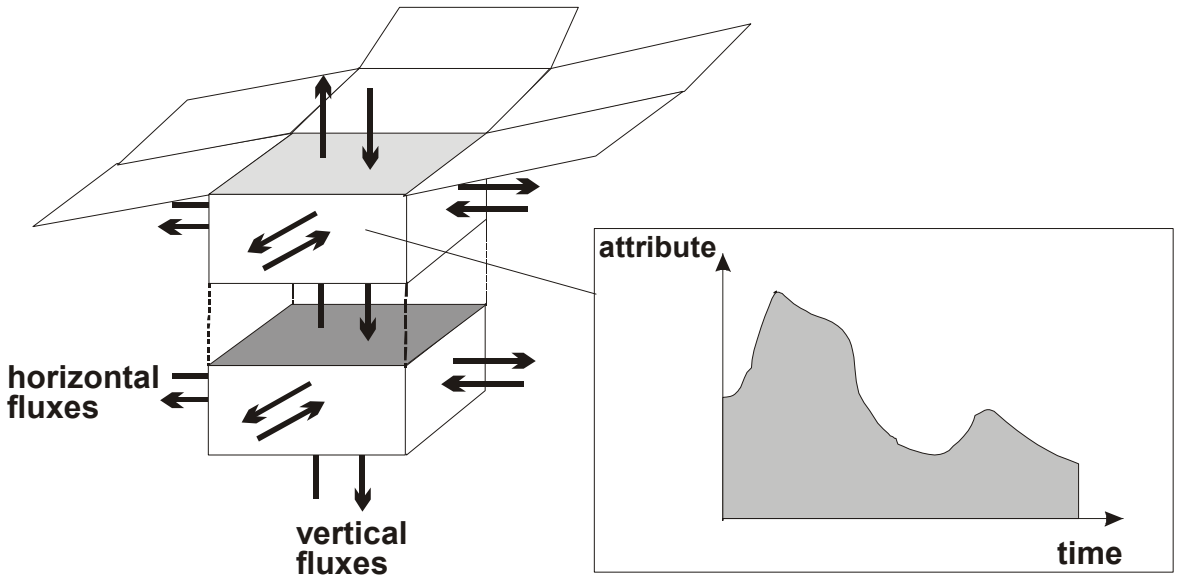

Figure 2.2: Spatial fluxes and time-variable cell attributes (from Roser 2001, after van Deursen 1995)

Figure 2.2 shows the spatio-temporal conceptionalization of *PCRaster*. The natural system is horizontally discretized in rectangular raster cells. These cells contain numerous attributes (e.g. temperature, storage levels, runoff generation type). Time dependent attributes are also called variables. In the presented example, a variable is assigned to each of the vertically arranged storages, which represent the vertical discretization. An arbitrary number of variables can be layered on top of each other. Thus, the vertical resolution can be chosen according to the needs of the problem set. This structure, where 3 dimensional

processes can be simulated via 2 dimensional mapstacks is referred to as 2.5 dimensional (*PCRASTER 2004A, ROSER 2001*).

A *PCRaster* model script is divided into five major sections. Each of those sections is responsible for a different task in data management:

- *BINDING:*
  Definition of variables and assignment of containing data type (Boolean, scalar, nominal, directional, LDD);
- *AREAMAP:*
  Assignment of the spatial base map (clone) and the spatial discretization;
- *TIMER:*
  Definition of the time step discretization and number of time steps in the model run;
- *INITIAL:*
  Assignment and calculation of constants and assignment of initial values for variables
- DYNAMIC:
  Sequential definition of model operations (core of the model)

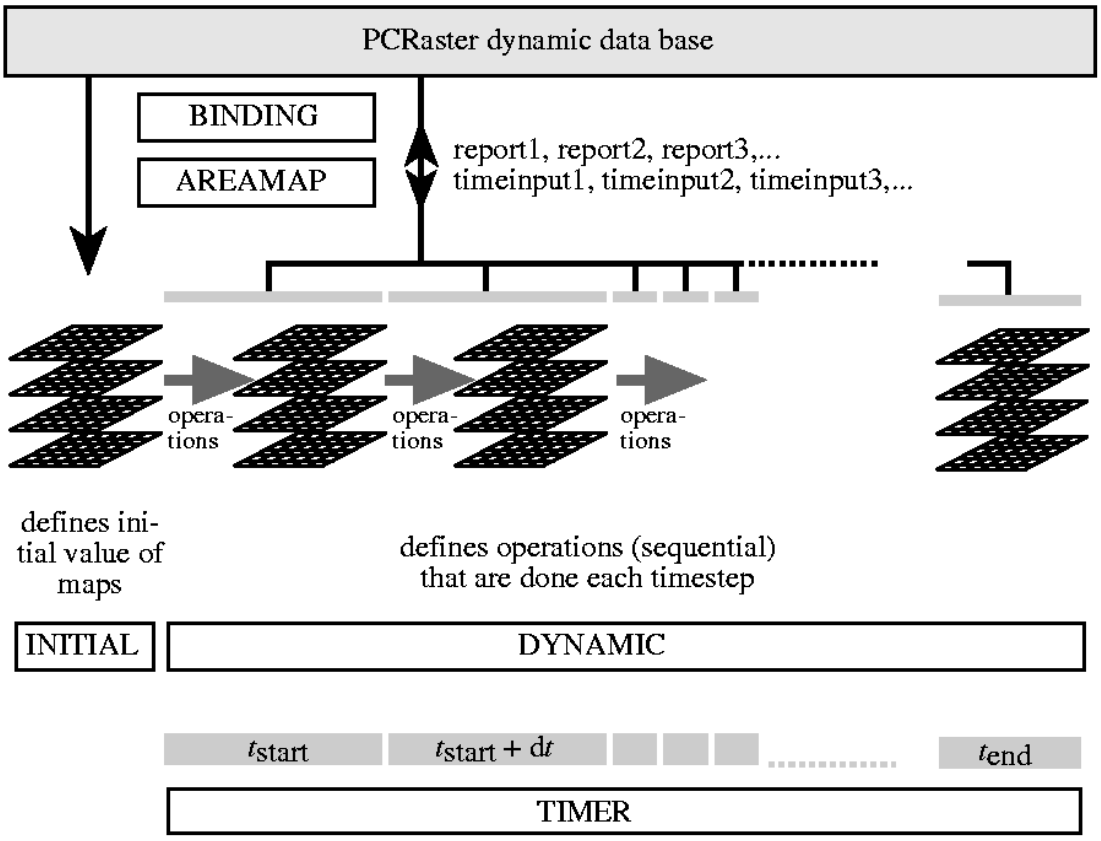

Figure 2.3: Script structure in PCRaster (from PCRaster 2004a)

The interconnections between those sections are illustrated in Figure 2.3. Via the command *timeinput*, data can be imported into the *DYNAMIC* section. The *report* function

exports data from model runs into the database. Afterwards, this data can be processed with additional visualization tools like *timeplot, display* or *aguila*. An *INITIAL* section always precedes the *DYNAMIC* section in order to calculate constants and starting values.

The dynamic modeling language of PCRaster provides a set of more than 120 spatial and temporal operators that can be used for building (static) cartographic models and dynamic models. These include:

POINT OPERATORS:
analytical and arithmetic functions, Boolean operators, conditional statements, operators for relations, comparison, rounding, (random) field generation

WINDOW OPERATORS:
for calculations in moving windows of variable size (high pass filtering, edge filtering, moving averages, etc.)

AREA OPERATORS:
for calculations in specified areas or classes

SPREAD OPERATORS:
for calculation of distances or cost paths over a map

GEOMORPHOLOGIC OPERATORS:
functions for hillslope and catchment analysis, definition of hydrological topology

HYDROLOGICAL OPERATORS:
for modeling transport (drainage) of material over a local drain direction map with routing functions

TIME OPERATORS:
for retrieving and storing temporal data in iterative Dynamic Models
(from *PCRASTER 2004A*)

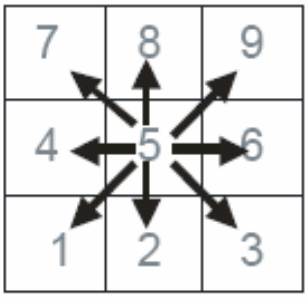

Furthermore, it is possible to develop additional functionality in *Delphi* or *C++* and include it in the form of dynamic linked libraries (.dll).

A special functionality for the designation of flow directions is implemented in *PCRaster*. Flow directions are assigned to cells either according to the steepest gradient of the digital elevation model or manually. Their definition follows the D8-method:

Figure 2.4: D8-method of flow direction

In Figure 2.4 the D8-method is illustrated. According to the elevation gradients, each cell receives a nominal value from one to nine, which determines the direction of drainage into the next downstream cell. The value is saved in a special map called *LDD* (*local drainage direction*). Whether a neighboring cell is located downstream or upstream is in fact defined by the *LDD*. The *LDD* value 5 is assigned to cells, which have no further outflow, for example dead end lakes in arid zones (Aral Lake) or Ponors in Karst systems. In addition,

those cells, where water leaves the catchment at the outlet are indicated by the *LDD* value 5.

PCRaster distinguishes between spatial and non-spatial data. The localization of spatial data within the areamap (clone) is saved in addition to the actual piece of information. Non-spatial data has no localization within the catchment or in other words, its value is the same in all cells of the areamap.

PCRaster provides a modeling environment for hydrologists and geoscientists, which are usually no experts in informatics. Thus, the language is easy to learn and includes the most commonly used hydrological features in predefined functions. Nevertheless, a fundamental knowledge of numerical methods is essential for a critical assessment of modeling results. It has to be respected that numerical models are approximations of natural processes and their accuracy largely depends on the applied time and space discretization.

2.2 Conclusion of the development environment

The dynamic GIS *PCRaster* is a modern environmental modeling language specially designed for the needs of hydrologists. A high linkage of dynamic, space related operations and the database signifies its excellence for distributed modeling. In addition, it provides special functionality for the most common hydrological tasks. It is easy to learn and thus, no specialist knowledge in computer sciences is necessary.

3 The catchment model *TAC*^{d}

The semi-distributed catchment model TAC was developed by *UHLENBROOK* in 1999 (*UHLENBROOK 1999*), as a forerunner version of the fully distributed *TAC*^{d} (tracer aided-catchment model, distributed). *TAC*^{d} was written in the *PCRaster* programming environment by *ROSER* in 2001 (*ROSER 2001*). It belongs to the group of conceptual or grey box models, with a storage analogy for the transformation of surface and underground water fluxes. It consists of several sequentially linked routines, also referred to as modules, which are mostly adopted from other conceptual models (*WaSiM ETH*, *SCHULLA 1997, SCHULLA & JASPER 2000; HBV, BERGSTRÖM 1976, 1992*). In the modules all stations of the land phase hydrological cycle are represented. The addition "distributed" indicates the spatially variable and disintegrated treatment of water fluxes within *TAC*^{d}. The runoff generation routine, as the principal item of the model, is the result of intensive investigations of runoff generation processes in the semi-alpine Black Forest. Besides others, many tracer experiments were accomplished in order to gain detailed knowledge of runoff generation processes (*FRITZ 2001, UHLENBROOK ET AL. 1998, UHLENBROOK 1999, UHLENBROOK & LEIBUNDGUT 2002*). This knowledge was implemented in the conceptualization of runoff generation. *TAC*^{d} was successfully applied to the Dreisam catchment and its subcatchments by *OTT* (*2002*), to the alpine Löhnersbach catchment in Austria by *JOHST* (*2003*), to the H.J. Andrews catchment in Oregon, USA by *AUS DER BEEK* (*2004*) and several other sites throughout Germany.

After some comments on the model structure and discretization, the different modules are discussed in the following chapters. From input regionalization (chapter 3.4) to the routing routine (chapter 0), these chapters are arranged according to the sequential order of the modules in *TAC*^{d} script.

3.1 Model structure

In order to treat a real life catchment with numerical methods, it has to be discretized and therefore generalized. Within *TAC*^{d}, a catchment is reflected by cells of equal size with defined attributes. For most applications, a cell size of 200*200 m² is appropriate, as it could be shown by *OTT* (*2002*). Vertically, the cells are divided into different layers, where each layer reflects a single storage. In fact, storages are nothing more than variables that contain scalar numbers. These scalar numbers can be interpreted as storage levels. The storages are interconnected via vertical or lateral fluxes. Lateral fluxes connect storages in neighboring cells, whereas vertical fluxes connect different storage types in the same cell. Each of those storages in a cell has one or more input and output fluxes and can be assigned to one of the operating model routines. The arrangement of storages in a cell and their specific storage parameters are defined by the runoff generation type (see chapter 3.10). For calculation of storage levels and fluxes it is useful to use units, where cell size does not have to be taken into account. Thus, aside from the wave routing routine, storage

levels are calculated in units of millimeters and water fluxes in units of millimeters per time step.

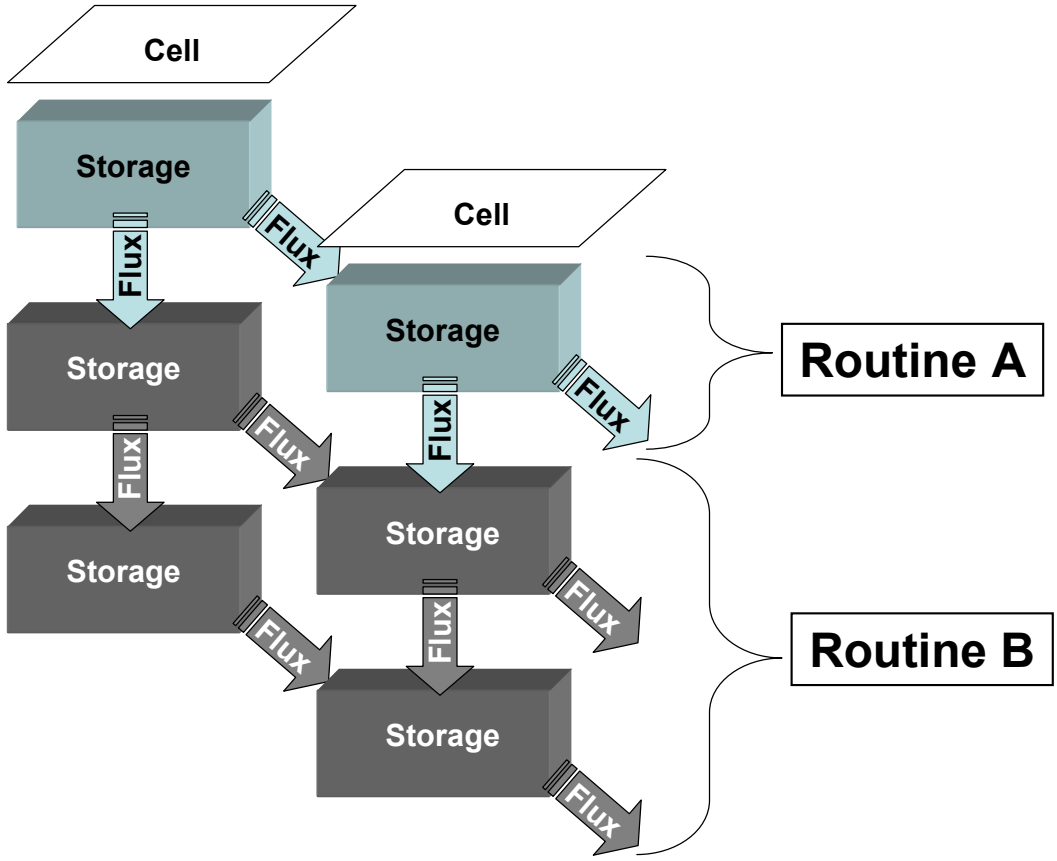

Figure 3.1: Storages, fluxes and routines

As Figure 2.1 shows, a routine can be seen as a system of storages and fluxes that form a logical unit. In addition, this figure shows the vertical arrangement of storages within a cell.

The governing equation for lateral fluxes is the simple differential equation of a linear storage unit.

$$-\frac{dV}{dt} = k^* \cdot V = Q^* \qquad \textit{Eq. 3.1}$$

Q^*: flux [mm/time step]
V: storage level [mm]
k^*: storage coefficient [1/time step]

The integrated solution for an instantaneous input impulse at time t=0 would be an exponential function.

$$V(t) = V_0 \cdot e^{-k^* t} \qquad \textit{Eq. 3.2}$$

V(t): storage level at time t [mm]
V_0: storage level at time t=0 [mm]

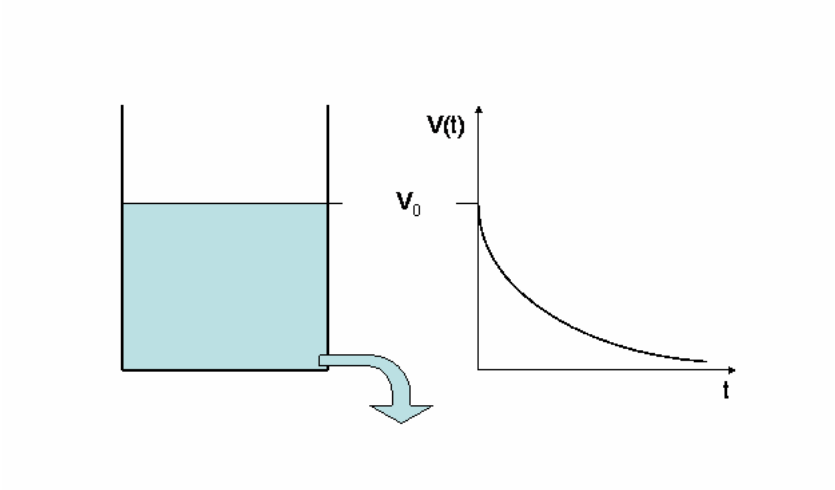

Figure 3.2: Linear storage unit

Figure 3.2 shows a linear storage unit (left) and its response function due to an instantaneous input of water.

Vertical fluxes are represented by constant amounts of percolating water. Thus, they are independent from storage levels until the storages run empty. Obviously, no further percolation occurs in this case.

$$-\frac{dV}{dt} = c \qquad \textit{Eq. 3.3}$$

c: constant parameter for vertical flux [mm/time step]

Figure 3.3 gives an overview of the sequential order of routines within *TAC*^{d} and its connected models.

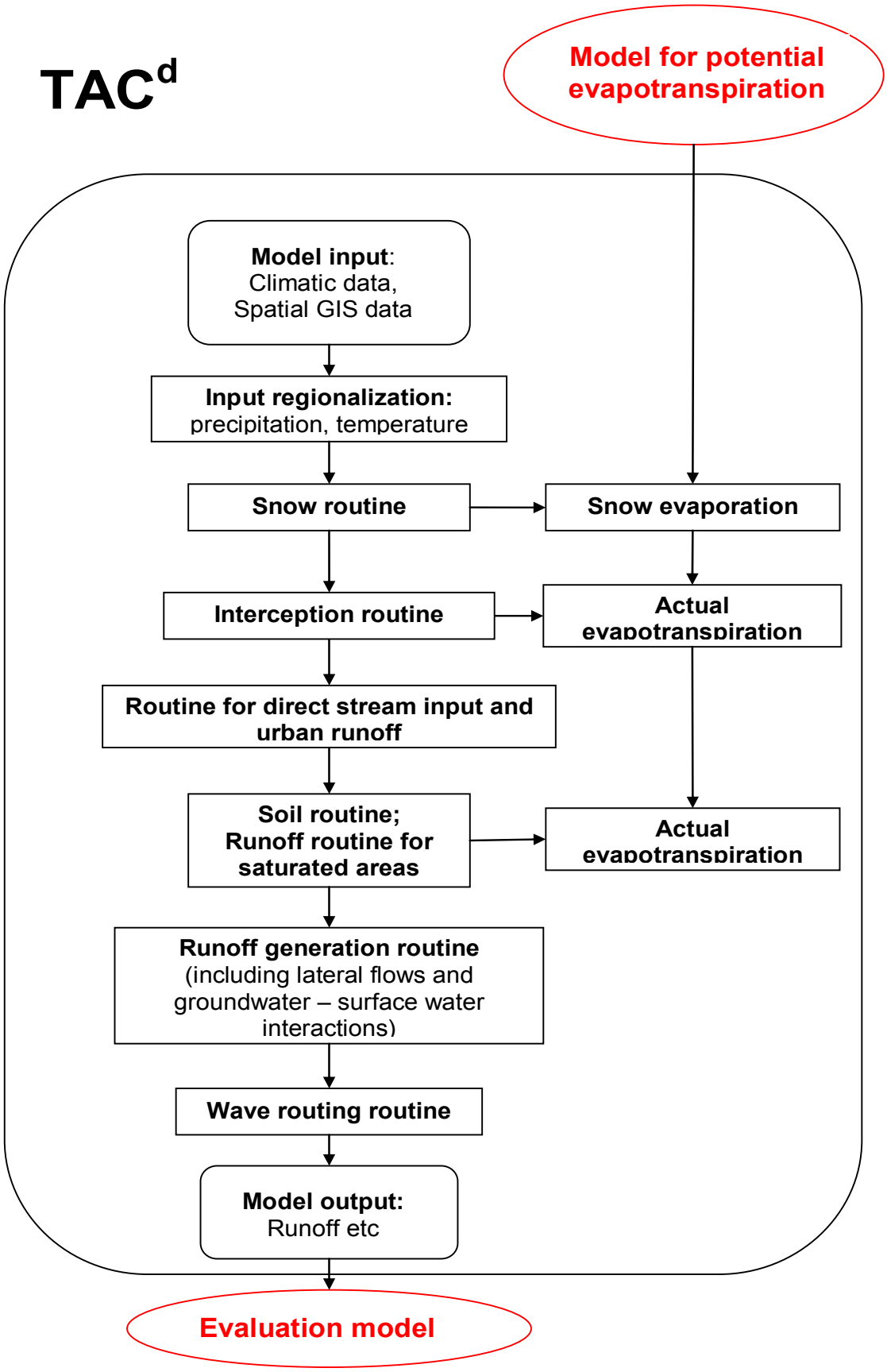

Figure 3.3: Modular structure (external models highlighted in red)

The models of potential evapotranspiration and evaluation (highlighted in red) are not directly included into the actual *TAC^d* script, but can be combined automatically by the batch file.

3.2 Time step discretization in *TAC^d*: from hourly to daily time steps

The choice of time step intervals in rainfall-runoff modeling is mainly restricted by the lack of input data with high resolution. In order to gain maximum information on short-term fluctuations of catchment reactions, an hourly time step is appropriate. When computation time has to be minimized or when data with hourly resolution is not available the modeling time step of *TAC^d* can be changed to daily. In that case, the subsequent procedure has to be followed:

- Maps of potential evapotranspiration have to be provided as 24-hour totals. If hourly input data for the evapotranspiration model is available, those maps can be produced by the present model via selective reports (see *PCRASTER 2004B*). This procedure reads out one map every 24 hours. The concerning map has to reflect the cumulative potential evapotranspiration of the 24 previous time steps. To the produced map files, the file extension of creation time is assigned. Because of restrictions within *PCRaster*, only map files with the file extension of the corresponding modeling time step can be produced by one model and imported as a map stack into another model. Thus, the file extensions of evapotranspiration maps have to be changed form .024, .048, .072 ...to .001, .002, .003.... This can be done by pasting a text file with the renaming commands into a DOS-shell.
  If hourly input data for the evapotranspiration model is not available, a different formula for calculation of potential evapotranspiration has to be used.
- In case hourly temperature data is available, temperature correction due to the cell aspect and solar geometry within the evapotranspiration model can be applied (see chapter 3.3). In this case, regionalized maps of mean daily temperature must be produced and imported into *TAC^d*. File extensions have to be changed in the same way as described for maps of potential evapotranspiration. Then, the temperature correction within *TAC^d* has to be deleted.
  If hourly temperature data is not available, temperature correction due to the cell aspect and solar geometry has to be skipped or calculated with a different approach.
- The calculation of Julian date within *TAC^d* has to be corrected.
- The constants for unit conversions (*cMmToCubM, ckg_trans*) have to be adapted.
- The number of loops (*cNrSteps*) for the wave routing routine and the time step within the loops in seconds (*cTime step*) has to be changed.

It has to be said that the creation and import of map files in *PCRaster* models is a CPU-time consuming procedure.

3.3 Model for potential evapotranspiration

Table 3.1: Data requirements and parameters of the evapotranspiration model

INPUT DATA	PARAMETERS
Sunshine duration, wind speed, relative humidity, temperature gradients	Latitude [°], albedo [-], landuse, effective crop height [m], leaf area index [m²/m²], minimal surface resistivity [s/m]

The model of evapotranspiration was adopted from the *WaSiM ETH* water balance model (*SCHULLA & JASPER 2000* p. 14) and translated into the *PCRaster* code by *OTT* (*2002*). It is based on the *MORECS*-scheme (Meteorological Office Rainfall and Evapotranspiration Calculation System) (*THOMPSON ET AL. 1981*), which was developed and applied in Great Britain for real time assessment of evapotranspiration and soil moisture.
The core of the model is represented by the Penman-Monteith equation (*MONTEITH 1975*) that combines a thermodynamic approach with a resistivity analogy (*DVWK 1996*):

$$ET_P = \frac{1}{\lambda} \frac{3.6 \cdot \frac{\Delta\zeta}{\gamma} \cdot (R_N - G) + \frac{\rho \cdot c_p}{\gamma \cdot r_a}(e_S - e) \cdot t_i}{\frac{\Delta}{\gamma} + 1 + \frac{r_s}{r_a}} \qquad \textit{Eq. 3.4}$$

ET_P: potential evapotranspiration [mm/h]
λ: latent heat of evaporation [kJ/kg]
$\Delta\zeta$: gradient of saturated vapor pressure curve [hPa/K]
γ: psychrometric constant [hPa/K]
R_N: net radiation; conversion from Wh/m² to kJ/m² by a factor 3.6 [Wh/m²]
G: soil heat flux [Wh/m²]
ρ: air density [kg/m³]
c_p: specific heat capacity of dry air at constant pressure [kJ/(kg*K)]
e_s: saturated vapor pressure [hPa]
e: actual vapor pressure [hPa]
r_a: bulk aerodynamic resistivity [s/m]
r_s: bulk surface resistivity [s/m]
t_i: number of seconds within a time step

Due to the strong dependency of evapotranspiration on solar radiation, a module for solar geometry (*POTRAD 5*, *VAN DAM, O., 2004, 2000*) was included. Besides for the calculation of solar radiation, *POTRAD 5* is also used for temperature correction due to the aspect of cells and sun position.
As mentioned before, potential evapotranspiration is imported into *TAC*^{d} via formatted map files. Since the model is not calibrated, it was not directly included in the *TAC*^{d} script. Once the maps are produced, they can be reused for each *TAC*^{d} calibration run. Although

the import and export of maps into or from a *PCRaster* model is time consuming, this method still seems to be more efficient than including the evapotranspiration routine into *TAC*^{d}. Another aspect is the higher flexibility of modeling approaches for evapotranspiration and temperature regionalization, as methods can be changed without modification of the actual *TAC*^{d} code. Detailed descriptions of the evaporation model can be found in OTT (2002) and AUS DER BEEK (2004).

3.4 Input regionalization

For transformation of point measurements into spatial data, different regionalization procedures are used for temperature, precipitation, sunshine duration and relative atmospheric humidity. Their general applicability depends on the number and spatial distribution of point measurements. Also morphological and climate heterogeneities have to be taken into account. Thus, gauging stations have to be more numerous in mountainous areas as in plains.

3.4.1 Temperature

Temperature values have to be provided as linear equations with a base and slope. The regionalization is based on a linear regression relation between temperature values and elevation of the gauging locations. The usually good negative correlation between altitude and temperature fails during inversion weather situations. In this case, temperature stations are split by a certain elevation into different groups and a regression relation is calculated for each group individually. In addition, air temperature at a certain spot strongly depends on the location's exposure to direct sunlight. The shading effects of mountains and buildings considerably reduce its potential reception of short wave radiation. The incoming short wave radiation is transformed via surface absorption and heat conduction into an increase of near surface air temperature. Whether a cell potentially receives direct sunlight, is calculated by *POTRAD 5* (*Potential Radiation Equator Model;* VAN DAM, O. 2004). *POTRAD 5* considers sun position, the aspect of a cell and obstacles in the direction of the sun. Potential sunshine has to be corrected by a measure of cloudiness, the sunshine duration. It is represented by a scalar factor from 0 (no direct sunshine) to 1 (sunshine throughout the whole measurement interval), which determines the duration of direct sunshine within a measurement interval.

3.4.2 Precipitation

Before regionalization of precipitation data, measured values are corrected in order to account for systematic measurement errors due to wind drift. This is done by the following equation:

$$P_{corr} = P \cdot (a + b \cdot u_w) \qquad \textit{Eq. 3.5}$$

P: gauged precipitation [mm]
P_{corr}: corrected precipitation [mm]
u_w: wind speed [m/s]
a,b: wind correction parameters [-]

Afterwards, precipitation is regionalized by a combination of an inverse distance weighting method and altitude regression. The inverse distance weighting method (IDW) weights the influence of a gauging station on local precipitation in respect to its distance:

$$z(x) = \frac{\sum z(x_i) \cdot d_i^{-r}}{\sum d_i^{-r}} \qquad \textit{Eq. 3.6}$$

z(x): interpolated value at location x
$z(x_i)$: measured value at gauging station i
d_i: distance from location to gauging station i [m]
r: weighting coefficient of reciprocal distance, in $TAC^d = 2$

Only a certain percentage of precipitation is additionally weighted by an altitude regression. This was done, because the influence of elevation is unimportant during single events due to the spottiness of rainfall. However, it is evident in mean annual precipitation values. An elevation correction factor was found by using the following equation:

$$f(x_i) = 1 + \frac{N(x_i) - \overline{N}}{\overline{N}} \qquad \textit{Eq. 3.7}$$

$f(x_i)$: elevation correction factor of cell x_i [-]
$N(x_i)$: mean annual precipitation of cell x_i [mm], calculated via altitude regression
$\overline{N}$: mean annual catchment precipitation

3.5 Snow routine

Table 3.2: Variables and parameter of the snow routine

STORAGES	INPUT FLUXES	OUTPUT FLUXES	PARAMETERS
sSnowPack	sPrec, sRefreeze	sMeltWater, sSnowET	sSFCF, sSnowET, cCFMAX
sWaterContent	sPrec, sMeltWater	sInSoil, sRefreeze	cCWH, cCFMAX, cCFR
STORAGES			
sSnowPack: Storage for frozen immobile water			
sWaterContent: Storage of fluid mobile water within the snow layer			
FLUXES			
sPrec: Input of precipitation into either storage, depending on temperature			
sRefreeze: Freezing of fluid water from water content, transfer into sSnowPack			
sMeltWater: Melting of frozen water from sSnowPack, transfer into sWaterContent			
sInSoil: Final output of snow routine consisting of melt water in, case of snow and precipitation			
sSnowET: Snow evaporation from the solid phase (sSnowPack)			
PARAMETERS			
sSFCF: Snowfall correction factor; due to biased measurement errors			
sSnowET: Snow evaporation			
cCWH: Water-holding capacity; connects limit of sWaterContent to sSnowPack			
cCFMAX: Time step-degree factor; determines amount of melted snow per time step and degree Celsius above threshold			
cCFR: Refreezing parameter; modifies time step degree-factor for refreezing			

The snow module was adopted from the *HBV* catchment model, which was developed by *BERSTRÖM* (*1976, 1992*) for snowmelt runoff in Scandinavian countries. Based on a time-degree factor, the module has also proven to be applicable in semi-alpine and alpine areas.

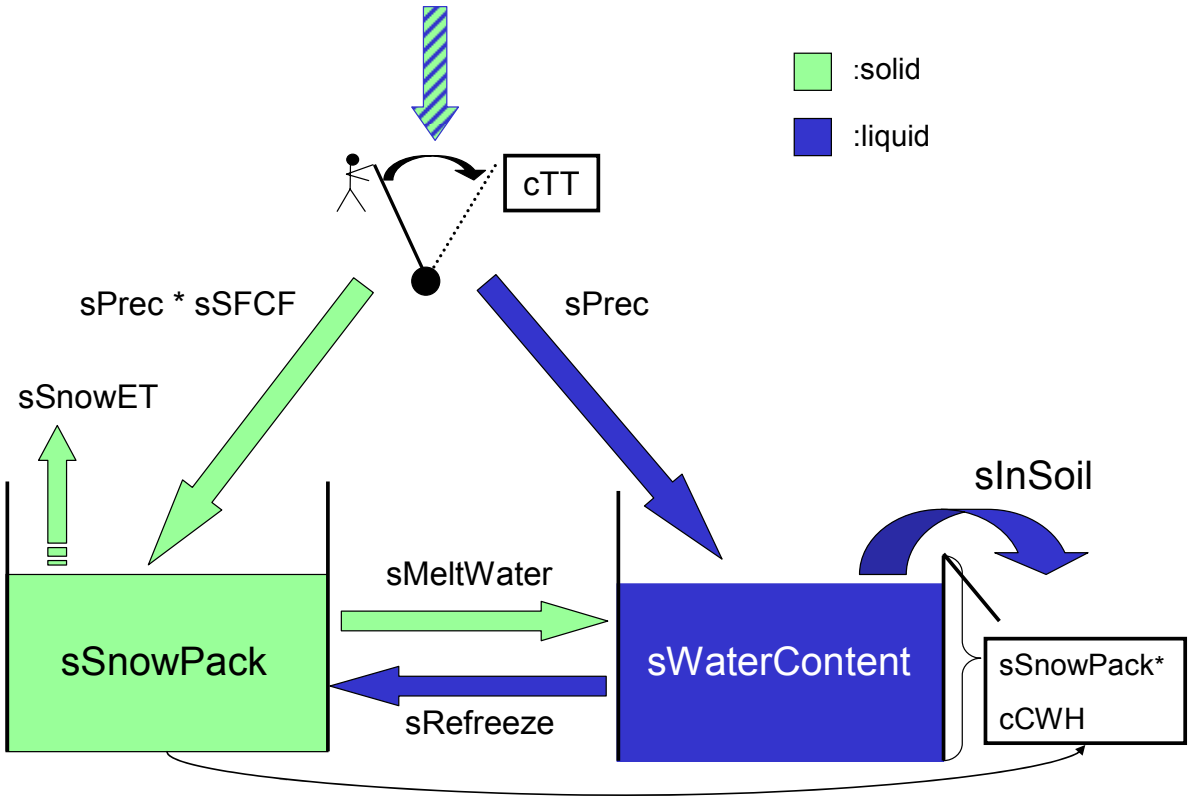

Figure 3.4: Conceptualization of the snow routine

Figure 3.4 illustrates the conceptualization of the snow routine. It uses two different but connected storages (*sSnowPack, sWaterContent*). The first one (*sSnowPack*) reflects the amount of frozen snow in the units of millimeter water equivalent, whereas the second storage (*sWaterContent*) represents the amount of fluid water, stored within the snow-pack. Similar to soil, the snow pack is seen as a porous media that can store a certain amount of water before it drains. The limit of water content is defined by the parameter of water-holding capacity and the actual amount of snow (*cCWH * sSnowPack*). If air temperature drops below the parameterized threshold temperature (*cTT*), precipitation (*sPrec*) multiplied by the snowfall correction factor (*cSFCF*) is added to the snow pack storage. Then the snow evaporation (*sSnowET*) is subtracted. It is notable that, in contrast to the complex model of potential evapotranspiration, snow evaporation is a simple, temperature independent parameter. If air-temperature exceeds the threshold temperature and a snow cover exists, precipitation is added to the water content until the water-holding capacity is reached. Beyond water-holding capacity, precipitation bypasses the snow routine and directly enters the following modules. The storages are linked by the fluxes of refreezing (*sRefreeze*) and melting water (*sMeltWater*) which are again controlled by the exceedance or shortfall of the threshold temperature. As mentioned above melt water is calculated by the time-degree method, shown here in the original *PCRaster* code. The syntax for If-statements in *PCRaster* is *...if(condition,then,else);*.

$$sMeltWater = if\ (sSnowPack > 0\ and\ sTemp > cTT\_melt, cCFMAX * (sTemp - cTT\_melt), 0);$$ **Eq. 3.8**

sMeltWater: amount of melted snow per time step [mm/time step]
sSnowPack: snow cover [mm water equivalent]
sTemp: air temperature [°C]
cTT_melt: threshold temperature [°C]
cCFMAX: time-degree factor [mm/(°C Δt)]

For calculation of refreezing water, the same approach is used:

$$sRefreeze = max\ (cCFR * cCFMAX * (cTT - sTemp), 0);$$ **Eq. 3.9**

sRefreeze: amount of refreezing water per time step [mm/time step]
cCFR: refreezing coefficient [-]

After melt water is subtracted from the snow and added to the water content, the water content is limited again to the water-holding capacity of the corresponding snow pack. The surplus is treated as the output of the snow routine (*sInSoil*). Since snow evaporation is not controlled by air temperature, the amount of snow is also reduced during temperatures below zero. This means that snow pack and therefore water-holding capacity is reduced. Consequently, a formerly full storage of water content would exceed the water-holding capacity and drain. Thus, under certain conditions the snow routine produces an outflow (*sInSoil*), even though air-temperatures are below threshold temperature (see chapter 4.4).

3.6 Interception routine

Table 3.3: Variables and parameters of the interception routine

STORAGE	INPUT FLUXES	OUTPUT FLUXES	PARAMETER
sIntPrec (=> sIntPrecOld)	sIntPrecNew	sInterceptionET, [max (sIntPrecNew + sIntPrecOld – sStoreageMax, 0)]	sStoreageMax, sLeafarea, sCoverage
STORAGES:			
sIntPrec: Interception storage; after sInterceptionET is subtracted named sIntPrecOld			
FLUXES:			
sIntPrecNew: Fraction of precipitation input that is intercepted by vegetation			
sInterceptionET: Loss of evaporating water			
[max (sIntPrecNew + sIntPrecOld – sStoreageMax, 0)]: Overflow of interception storage;			
PARAMETER:			
sStorageMax: Maximum storage capacity of interception storage, dependent on sCoverage and sLeafarea			
sCoverage: Factor of vegetation coverage according to landuse			
sLeafarea: Leafarea index			

The interception routine calculates the storage and loss of water due to wetting of surfaces and evaporation. Its emplacement after the snow routine accounts for the interception of fluid precipitation and melt water, not for snow. Type and habit of vegetation plays a key role in interception processes, because of its dominant influence on surface area. The calculation of interception within *TAC*^{d} follows the scheme presented by *VAN DAM J.* (*2000*) in combination with elements from the *WaSiM ETH* (*SCHULLA 1997, SCHULLA & JASPER 2000*). The governing equations are based on experimental investigations accomplished by *HOYNINGEN-HUENE* (*1983*) and *BRADEN* (*1985*).

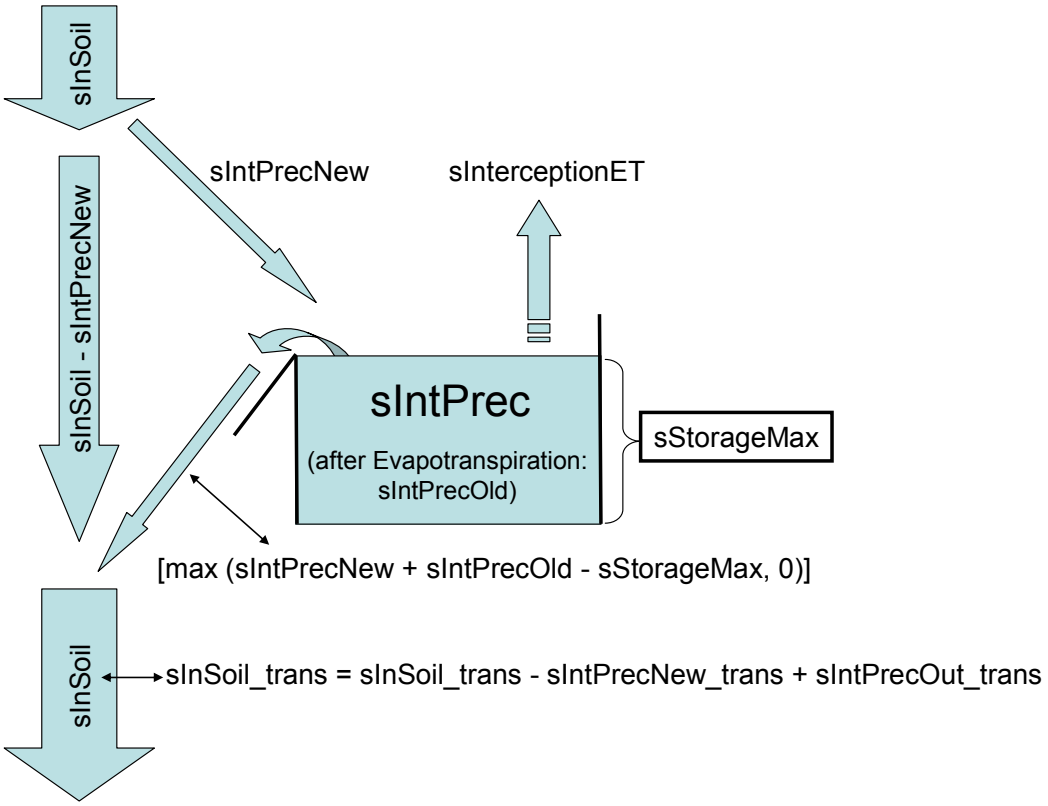

Figure 3.5: Conceptualization of interception

Figure 3.5 illustrates the conceptualization of the interception routine. It is represented by a single storage (*sIntPrec*), which is supplied by the input flux *sIntPrecNew*. The input is only a certain fraction of the output from the snow routine or precipitation regionalization (*sInSoil*). This fraction again is determined by maximum storage capacity (*sStorageMax*) and vegetation coverage (*sCoverage*), as show by the following equation:

$$sInt\,Pr\,ecNew = sStorageMax \cdot \left(1 - \frac{1}{1 + \frac{sCoverage \cdot sInSoil}{sStorageMax}} \right) \qquad \textit{Eq. 3.10}$$

sInSoil:	output from precipitation regionalization or snow module [mm/time step]
sIntPrecNew:	input into interception storage [mm/time step]
sStorageMax:	maximum storage capacity [mm]
sCoverage:	fraction of vegetation coverage [-]

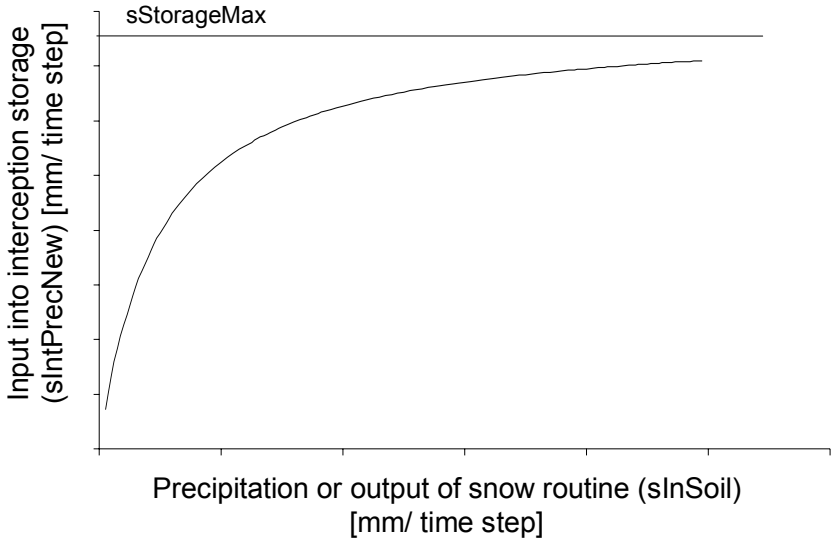

Figure 3.6: Dependency of interception input on water supply (from Johst 2003)

As can be seen in Figure 3.6, the maximum input into the interception routine is limited to maximum storage capacity. This means, that events with large amounts of precipitation input lead to a similar increase of the interception storage level as medium or small events. Therefore, the fraction of water that bypasses the interception storage ranges from zero for very small events to nearly one for big storm events. The storage capacity itself is determined by the following *PCRaster* equation:

*sStorageMax = sCoverage * sLeafarea * 0.3 + (1 - sCoverage) * 0.3;* ***Eq. 3.11***

(from *SCHULLA 1997*)

sStorageMax:	maximum storage capacity [mm]
sCoverage:	fraction of vegetation coverage [-]
sLeafarea:	leaf area index [m²/m²]
0.3:	maximum thickness of water film on surface [mm]

Whenever the storage capacity is exceeded by adding new input to the old storage level, an overflow is activated. Besides evaporation this is the only output flux from the interception storage. If water levels stay below maximum storage capacity, no outflow is subtracted. In this case, the water is trapped and storage levels are only reduced by evaporation.

3.7 Routine for direct stream input and urban runoff

The amount of precipitation that falls directly onto the stream surfaces (*sDirectIntoStream*) is calculated proportionally from the area that is covered by stream and the total cell area:

$$sDirectIntoStream = (MeanStreamLenght * StreamWidth / Cellarea) * sInSoil; \quad \textit{Eq. 3.12}$$

sDirectIntoStream: Direct input into stream flow [mm/time step]
sInSoil: Output of interception routine [mm/time step]

The emplacement of the calculation of direct stream input after the interception routine can be justified in two ways:

- Smaller streams in the mountainous Black Forest are mostly completely roofed by tree canopies.
- Interception can be seen as a compensation for the unaccounted evaporation out of larger open water areas.

The water of direct stream input is subtracted from the following input into the soil routine and then added to stream input (*sIntoStream*).

Table 3.4: Variables and parameter of the urban runoff routine

FLUXES	**PARAMETERS**
sInSoil, sUrbanFlux, sUrbanState, sUrbanIntoStream	cUrbanSplit
FLUXES:	
sInSoil: Output from interception routine and input into soil routine	
sUrbanFlux: Fraction of input that is directed to the next stream channel as urban runoff	
sUrbanState: Remaining input into the soil routine in urban areas	
sUrbanIntoStream: Accumulated urban runoff within stream cells	
PARAMETERS:	
cUrbanSplit: Parameter that determines fractions of urban runoff and soil input	

Urban runoff is calculated for cells with a high proportion of sealed surfaces, such as densely populated areas, roads or rocky outcrops. As also those areas are not completely impermeable (green spaces, backyards etc.), the input precipitation is divided by a parameter (*sUrbanSplit*). One part still enters the soil- and runoff generation routine (*sInSoil*), whereas the other one is directed superficially into the next river channel (*sUrbanFlux*). Due to high flow velocities, this component is expected to reach the next stream cell within the modeling time step. In order to comply with this condition, modeling time steps have to be large compared to the spatial extent of urban or sealed

areas and their distance from downstream river channels. If translation times have to be considered, a different approach, such as the kinematic wave solution (*VAN DER PERK* & Slávik *2003, PCRASTER 2004B*) has to be used. Urban runoff is directed via the map of local drainage direction (*LDD*) into the next downstream river cell. Whenever it enters a stream cell, urban runoff is transformed into stream runoff (*sIntoStream*). In the present version of *TAC*^{d,} this is performed by the function *catchmenttotal*, which sums up all cell values of an upstream-defined area.

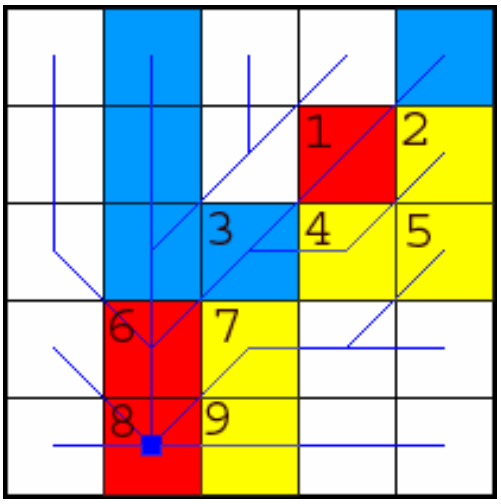

Figure 3.7: Urban runoff routine (urban cells: yellow, stream cells: blue, urban + stream cells: red)

An example for the actual urban runoff routine is given in Figure 3.7. Cell 1 and 6 only receive the urban runoff created within the cell itself, whereas cell 3 receives the urban runoff from cells 2 and 4. Cell 8 only receives the urban runoff from cells 5, 7 and 9 and not from the whole catchment area

3.8 Runoff generation in zones of saturated overland flow

Table 3.5: Variable and parameters of the saturated overland flow routine

STORAGE	INPUT FLUXES	OUTPUT FLUXES	PARAMETERS
sMTD_box	sInSoil	sQ_SOF, sActET_SOF	cMTD_K, cMTD
STORAGE:			
sMTD_box: storage of micro-topographic depressions (MTD)			
FLUXES:			
sInSoil: Input from interception or urban runoff routine			
sQ_SOF: Lateral outflow from the storage			
sActET_SOF: Evapotranspiration from the storage			
PARAMETERS:			
cMTD: Maximum storage capacity of the MTD storage			
cMTD_K: Storage coefficient of the MTD storage			

Since runoff generation in zones of saturated overland flow is considerably different from other runoff generation types, it is outsourced from the runoff generation module. Areas with saturated overland flow as predominant runoff generation process are represented by the two storages of ground water and micro-topographic depression (sMTD). The latter has a low maximum storage capacity (~ 30 mm). This means that only little water can be stored before the overflow is activated. Consequently, those cells have a negligible effect on retention. The MTD-storage has no connection to the underlying groundwater storage, which is therefore only supplied by lateral inflow. Cells of saturated overland flow are excluded from the soil routine. The runoff generation type 7 is assigned to cells with saturated overland flow as predominant runoff generating process (see chapter 3.10).

3.9 Soil routine

Table 3.6: Variables and parameters of the soil routine

STORAGE	INPUT FLUXES	OUTPUT FLUXES	PARAMETERS
sSoilMoisture	sInSoil	sToRunoffGeneration, sActET	cFieldCapacity, cBETA, cLP
STORAGE:			
sSoilMoisture: Soil moisture storage			
FLUXES:			
sInSoil: Input from interception or urban runoff routine			
sToRunoffGeneration: Vertical percolation into underlying storages			
sActET: Evapotranspiration from the storage			
PARAMETERS:			
cFC: Maximum storage capacity of the soil moisture storage, field capacity			
cBETA: Empirical soil parameter			
cLP: Evaporation reduction parameter			

The soil routine, which was adopted from the *HBV*-model (*BERGSTRÖM 1976, 1992*), describes infiltration and percolation through the soil layer with an empirical exponential equation:

$$sToRunoffGeneration/sInSoil = (sSoilMoisture/cFC)^{cBETA}; \qquad \textbf{Eq. 3.13}$$

sToRunoffGeneration:	output from soil routine [mm/time step]
sInSoil:	input from interception or urban runoff routine [mm/time step]
sSoilMoisture:	soil moisture [mm]
cFC:	field capacity [mm]
cBETA:	empirical soil parameter [-]

The calculations are performed by the two external functions *soilwater* and *soiloutput*, which are written in *Delphi*. After converting them into dynamic linked libraries, the functions can be accessed by *PCRaster* commands.

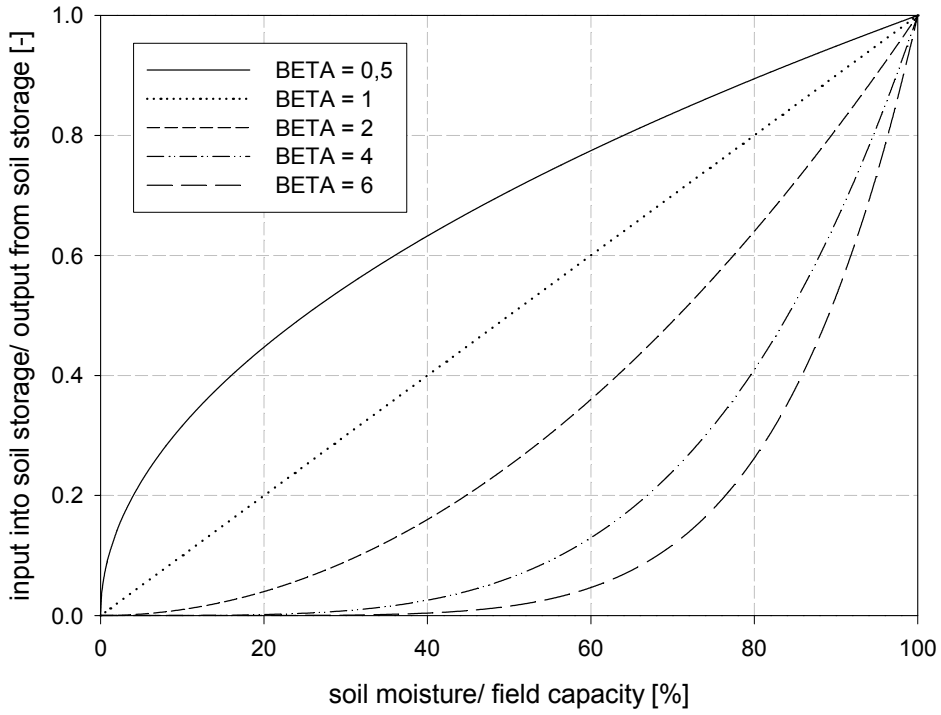

Figure 3.8: Relation of input/ output in dependency of soil moisture/ field capacity for different BETA-coefficients (after Bergström 1992)

Figure 3.8 shows the response of the soil routine with different values for the empirical cBETA - coefficient. When the cBETA - coefficient is small, the fraction of water that enters the runoff generation routine is large, even when soil moisture is low compared to field capacity. This would be the case in areas where macro pore flow and preferential pathways play an important role. Because of the spatially variable representation of cBETA- coefficients and filed capacity, reactions of different soil types can be captured.
Furthermore, the soil routine calculates evapotranspiration using the empirical parameter *cLP*. Before actual evapotranspiration can be computed the potential evapotranspiration, which has not yet been dissipated by actual evapotranspiration from the snow or interception routine, has to be calculated:

sPotET = sPotET - sSnowET - sInterceptionET; ***Eq. 3.14***

sPotET:	potential Evapotranspiration [mm/time step]
sSnowET:	snow evaporation [mm/time step]
sInterceptionET:	evaporation from interception storage [mm/time step]

Since small soil moisture contents result in high suction tensions within the pore space, an increasing resistivity towards evaporation can be observed under drier conditions. The

evaporation model accounts for this fact by linearly reducing actual evapotranspiration, when soil moisture content drops below a certain value. This threshold value is determined by the parameters *cLP* and *cFC*.

$$sActET = sPotET \quad \text{if } sSoilMoisture = cLP * cFC$$
$$sActET = sPotET * (sSoilMoisture / (cLP * cFC)) \quad \text{if } sSoilMoisture < cLP * cFC$$

Eq. 3.15

sActET:	actual evapotranspiration [mm/time step]
sPotET:	potential evapotranspiration [mm/time step]
sSoilMoisture:	soil moisture [mm]
cLP:	parameter of reduction [-]
cFC:	field capacity [mm]

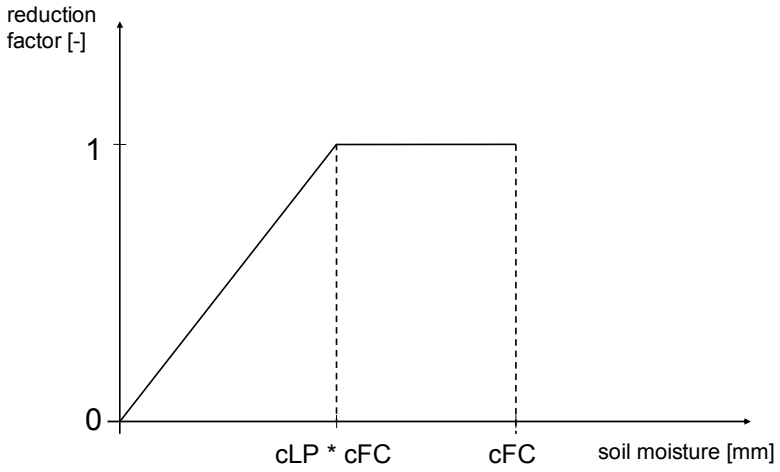

Figure 3.9: Reduction of potential evapotranspiration (from Johst 2003)

The resulting reduction factor is shown in Figure 3.9.

3.10 Runoff generation routine

Table 3.7: Variables and parameters of the runoff generation routine

STORAGES	INPUT FLUXES	OUTPUT FLUXES	PARAMETERS
sUS_box	sToRunoffGeneration, sQ_US, sQ_LSfull	sQ_US, sStorageLeak	cUS_K
sLS_box	sStorageLeak, sQ_LS	sQ_LS, sToGroundwater	cLS_K, cLS_H
sGW_box	sToGroundwater, sQ_GW	sQ_GW,	cGW_K, cGW_H
STORAGES:			
sUS_box: Upper storage			
sLS_box: Lower storage			
sGW_box: Groundwater storage			
FLUXES:			
sToRunoffGeneration: Input from soil routine			
sQ_US: Lateral outflow of upper storage			
sQ_LSfull: Inflow from full lower storage			
sStorageLeak: Vertical outflow from upper storage			
sQ_LS: Lateral outflow from lower storage			
sToGroundwater: Vertical outflow from lower storage; if lower storage does not exist: vertical outflow of upper storage			
sQ_GW: Lateral outflow of groundwater storage			
PARAMETERS:			
cUS_K: Storage coefficient of upper storage			
cLS_K: Storage coefficient of lower storage			
cLS_H: Maximum storage capacity of lower storage			
cGW_K: Storage coefficient of groundwater storage			
cGW_H: Maximum storage capacity of groundwater storage			

The runoff generation routine is the core piece of the *TAC*^{d} model. It was developed for mountainous areas, where direction of flow is predominantly determined by the inclination of hill slopes. Among the many runoff generation processes that could be observed in tracer experiments and other field investigations, the dominating processes are integrated in seven different runoff generation classes. The declaration of runoff generation types in the catchment cells was accomplished by the computer aided WSB-FLAB system (wissensbasiertes System zur Ausweisung von Flächen gleicher Abflussbildung, *PESCHKE ET AL. 1999*). Each cell in the catchment area belongs to one of those runoff generation types (*nRGTypes*). The *nRGType* defines the conceptual composition of the storages within a cell as well as their specific parameters. Those parameters are storage coefficients, maximum storage levels and values for vertical fluxes. Storage coefficients determine the dynamics of lateral fluxes, whereas vertical fluxes are constant values but may only occur under specific conditions (storage levels etc.). Their values are listed in the parameter table (see Appendix A).

Figure 3.10, Figure 3.11 and Figure 3.12 illustrate three systems of cells with different runoff generation types and their connection via lateral fluxes.

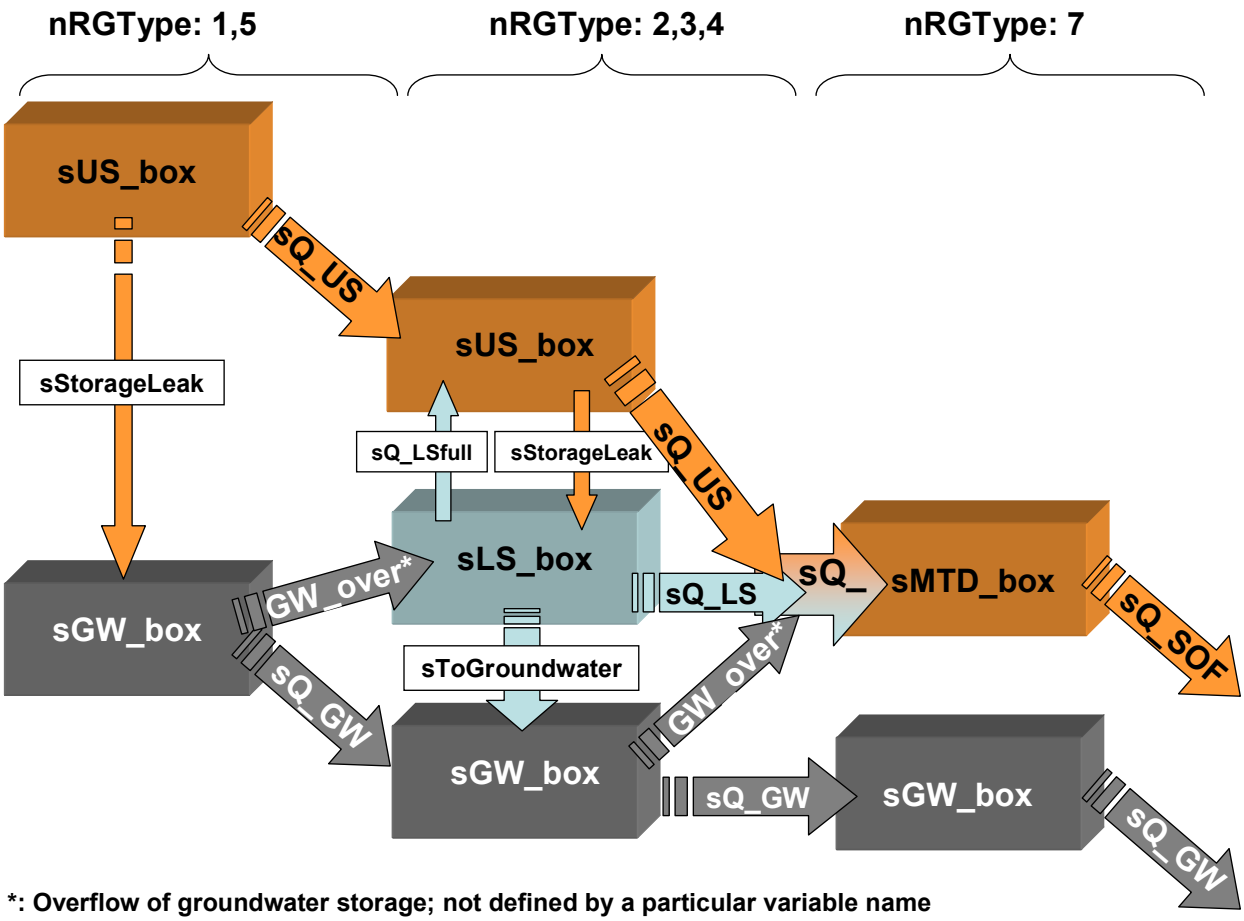

Figure 3.10: System of runoff generation types I

nRGTypes 2, 3 and *4* have the same structure but different parameters, and therefore different flow dynamics. They consist of three storages, the upper storage (*sUS_box*), the lower storage (*sLS_box*), and the groundwater storage (*sGW_box*). Consistently, the lateral outflows are named *sQ_US* for the upper storage, *sQ_LS* for the lower storage and *sQ_GW* for the groundwater storage. If the downstream cell belongs to the same *nRGType* the outflow from the upper storage (*sQ_US*) is directed into the upper storage (*sUS_box*) again, otherwise into the lower storage (*sLS_box*).

nRGTypes 1 and *5* only consist of the two storages *sUS_box* and *sGW_box*. As described in chapter 3.8 also *nRGType 7* consists of the two storages *sMTD_box* and *sGW_box*, but in contrast to the *nRGTypes 1* and *5* they are not connected via a vertical flux (sStorageLeak).

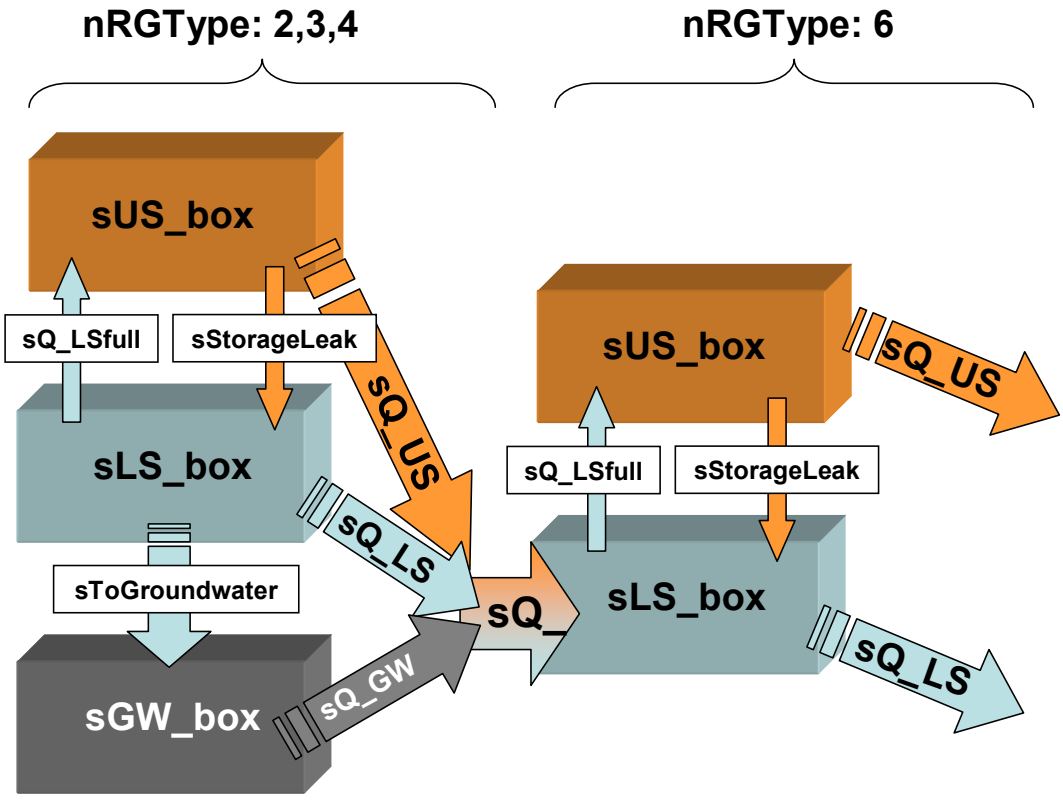

Figure 3.11: System of runoff generation types II

The *nRGType 6* was incorporated for the conceptualization of underground fluxes in alluvial valley fills and porous aquifers, where flow paths are not defined by surface topography. Therefore, the direction of underground flow is altered manually. It is not consistent with surface flow. A different LDD was created, which defines directions of subsurface flow. Only limited linkage between channel runoff and underground flow is allowed (see chapter 3.10.2). Unfortunately, the direction of flow within this runoff generation type is not dependent on storage levels, which results in unrealistic high levels and fluxes caused by lateral inflows at the boundaries to surrounding fracture aquifers (see chapter 7.7).

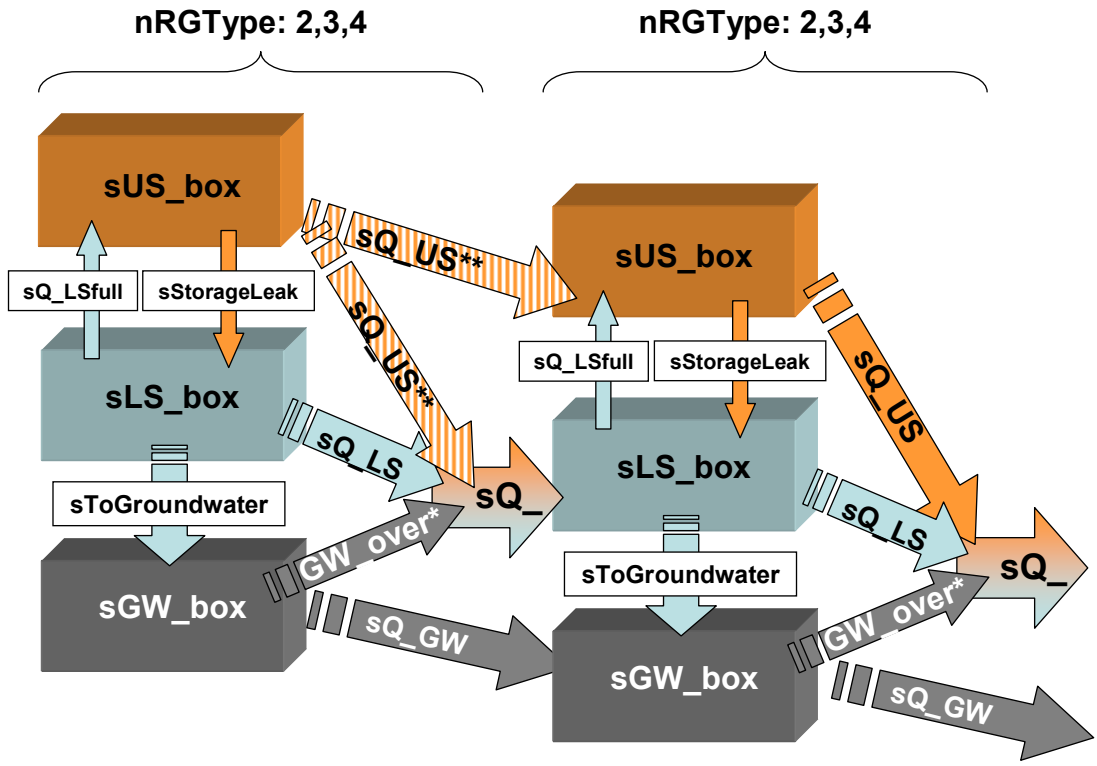

*: Overflow of groundwater storage; not defined by a particular variable name

**:if both nRGTypes are same type, then sQ_US in sUS_box, otherwise into sQ_

Figure 3.12: System of runoff generation types III

3.10.1 Lateral flows

Lateral flows are calculated using the following *PCRaster* equation (here exemplary for the upper storage):

$$sQ\_US = min((sUS\_box * cUS\_K) * cSlopeFactor, sUS\_box); \qquad \textit{Eq. 3.16}$$

sQ_US:	lateral flow [mm/time step]
sUS_box:	storage level of upper storage [mm]
cUS_K:	storage coefficient [1/time step]
cSlopeFactor:	slope factor [-]

As the equation shows, storage coefficients are modified by a dimensionless slope factor that accounts for elevation gradients as the driving force of water fluxes. It is the ratio of the slope of the cell under consideration and the mean slope of all cells of the same runoff generation type:

$$cSlopeFactor = sSlope / sSlopePerRGT; \quad \textit{Eq. 3.17}$$

sSlope: slope of cell [-]
sSlopePerRGT: mean slope of all cells with the same nRGtype [-]

The minimum value of this factor is limited to 0.3 for low angled terrain. Of course, the outflow has to be limited to the actual water content in the storage, even though storage coefficient multiplied by slope factor may be greater than 1 (see chapter 4.3). As it is shown in Figure 3.10 to Figure 3.12, lateral fluxes are bundled in another variable named *sQ_*. Also groundwater overflow is added to this variable. Afterwards, fluxes are redistributed into the following storages, depending on runoff generation type of the downstream cell.

3.10.2 Groundwater – surface water interaction

The interaction between stream flow and groundwater only takes place in those cells, which are defined as *nRGType 6* (valley bottom) and stream cells (*bStream*) at the same time. It is represented by the two parameterized constant fluxes of infiltration (*sQ_inf;* from stream water to groundwater) and exfiltration (*sQ_exf;* from groundwater to stream water). The controlling factor for the direction of flow is the water level in the upper storage of the runoff generation routine. If a certain threshold (*cThres*) is exceeded, exfiltraton (*sQ_exf*) is subtracted from the upper storage (*sUS_box*) of the concerning stream cell and added to the stream flow (*sIntoStream*). Infiltration takes place, when the storage level in the upper storage is lower than the threshold. Obviously, infiltration must not exceed the amount of water, stored in the stream channel and therefore has to be limited.

3.11 Wave routing routine

The wave routing routine was integrated in order to account for translational displacement of water in channels segments. It calculates travel times (translation) of flood waves and their deformation due to lateral inflow by using the kinematic wave approach presented in *CHOW ET AL.* (*1988*). It is based on a classic combination of momentum and mass conservation laws. The following equations are taken from *LISEM* (2004):

$$\frac{dQ}{dx} + \frac{dA}{dt} = \bar{q} \qquad \textit{Eq. 3.18}$$

Q: discharge [m³/s]
A: wet cross section [m²]
$\bar{q}$: lateral input [m³/m/s]
dx, dt: space and time derivative

The relation between A and Q is given by:

$$A = \alpha \cdot Q^{\beta} \qquad \textit{Eq. 3.19}$$

$$\alpha = \left[\frac{n}{\sqrt{S}} p^{2/3} \right]^{\beta} \qquad \textit{Eq. 3.20}$$

β: 0.6
p: wetted perimeter [m]
n: Manning roughness coefficient [-]
S: sine of slope gradient [-]

Differentiating and combining leads to:

$$\frac{dQ}{dx} + \alpha \cdot \beta \cdot Q^{\beta-1} \frac{dQ}{dt} = q \qquad \textit{Eq. 3.21}$$

The finite difference form of this equation is:

$$\frac{Q_{x+1}^{t+1} - Q_x^{t+1}}{\Delta x} + \alpha \cdot \beta \cdot \overline{Q}^{\beta-1} \frac{Q_{x+1}^{t+1} - Q_{x+1}^{t}}{\Delta x} = \overline{q} \qquad \textit{Eq. 3.22}$$

t: beginning of time step
t+1: end of time step
x: "upstream side" of grid cell
x+1: "downstream side" of grid cell
Q_{x+1}^{t+1}: new discharge
Q_x^{t+1}: new discharge at "upstream end" of grid cell (sum of all incoming water generated by the kinematic wave)
Q_{x+1}^{t}: present discharge in grid cell
$\overline{Q} = \frac{\left(Q_x^{t+1} + Q_{x+1}^{t}\right)}{2}$: "diagonal" average in space-time diagram
$\overline{q}$: average lateral input over the length of the grid cell

The wave routing within *TAC*^{d} uses the predefined *PCRaster* function *kinematic*, where equation above is solved by a non-linear implicit scheme using a Newton-Raphson iteration (*WESSELING 2004*).

Unlike explicit schemes, the implicit scheme is unconditionally stable. This means, it can be used also with Courant numbers greater than 1, but major numerical inaccuracies may be the result (*BECKIE 2001*).

$$C^* = \frac{\Delta t}{\Delta x_{cell} / u_{fluid}} \qquad \textit{Eq. 3.23}$$

C^*: Courant number [-]
Δt: time step discretization
Δx_{cell}: space discretization
u_{fluid}: fluid velocity

The Courant number gives a relation between the spatial and temporal discretization steps in a model and relates them to the dynamics of modeled processes (e.g. flow) (*BECKIE 2001*).

Dispersion, as an effect of channel storage, is not implemented explicitly. Nevertheless, deformation of propagating water waves can be observed due to numerical dispersion caused by the iteration scheme. As a rule of thumb, a Courant number of lower than 0.9 is

worthwhile. In order to obtain a smaller Courant number, modeling time steps for the *kinematic* function are reduced by an internal loop construction.

The lateral input into the *kinematic* function has to be provided in the dimensions of cubic meters per meters of cell size per second. The output is given in cubic meters per second. In addition, detailed channel geometry has to be provided. Water depths can be calculated using the following equation:

$$sWaterDepth = sAlpha * (sQ\_step * * cBeta) / sStreamWidth; \qquad \textit{Eq. 3.24}$$

sWaterDepth:	water depth [m]
sStreamWidth:	stream width [m]
sQ_step:	output of *kinematic* function [m³/s]
sAlpha, cBeta:	parameters of the *kinematic* function [-]

By dividing the output flux (*sQ_step*) by the cross section (*A = sWaterDepth * sStreamWidth*) actual flow velocities can be obtained. For stored volumes, water depths have to be multiplied by stream width and cell length.

3.12 Evaluation model

An independent evaluation model was developed within the scope of this thesis. Four different measures of goodness were included. Those are the model efficiency (*sEfficiency*) and logarithmic model efficiency (*slogEfficiency*) according to *NASH AND SUTCLIFF* (*1970*), the coefficient of determination (R^2) and the volume error (*sVolumeError*). Their purpose is to compare measured and simulated hydrographs in order to assess the quality of model simulations. The units in the following equations depend on the observed values (for water fluxes: mm/time step). All measures of goodness, except volume error, are dimensionless.

Model efficiency:

$$Q_{eff} = 1 - \frac{\sum_{i=1}^{n} \left(Q_{i,obs} - Q_{i,sim}\right)^2}{\sum_{i=1}^{n} \left(Q_{i,obs} - \overline{Q_{obs}}\right)^2} \qquad \textit{Eq. 3.25}$$

Q_{eff}: model efficiency [-]
$Q_{i,\,obs}$: observed runoff at time step I [mm/time step]
$Q_{i,\,sim}$: simulated runoff at time step I [mm/time step]
$\overline{Q_{obs}}$: mean observed runoff for whole observation period [mm/time step]

Logarithmic model efficiency:

$$Q_{log\,eff} = 1 - \frac{\sum_{i=1}^{n}\left(log\left(Q_{i,obs}\right) - log\left(Q_{i,sim}\right)\right)^2}{\sum_{i=1}^{n}\left(log\left(Q_{i,obs}\right) - \overline{log\left(Q_{obs}\right)}\right)^2} \qquad \textit{Eq. 3.26}$$

$Q_{log\,eff}$: logarithmic model efficiency [-]

Instead of the logarithm, also the square-root function can be used. Both functions pronounce the weighting of low discharges (*AIMWATER 1999*).

For the coefficient of determination mean simulated runoff values for the whole simulation period are needed. Thus, this measure can only be calculated after the simulation has terminated.

Coefficient of determination:

$$R^2 = \frac{\left(\sum_{i=1}^{n}\left(Q_{i,obs} - \overline{Q_{obs}}\right)\left(Q_{i,sim} - \overline{Q_{sim}}\right)\right)^2}{\sum_{i=1}^{n}\left(Q_{i,sim} - \overline{Q_{sim}}\right)^2 \cdot \sum_{i=1}^{n}\left(Q_{i,obs} - \overline{Q_{obs}}\right)^2} \qquad \textit{Eq. 3.27}$$

R^2: coefficient of determination [-]

$\overline{Q_{sim}}$: mean simulated runoff for whole observation period [mm/time step]

Volume error:

$$VE = \frac{\sum_{i=1}^{n}\left(Q_{i,obs} - Q_{i,sim}\right)}{n} \qquad \textit{Eq. 3.28}$$

VE: volume error [mm/time step]

The Volume error is normalized by the duration of the simulation period. Thus, it represents the average volume error per time step.

The evaluation model works without any data conversions to an external spreadsheet program, if values of mean simulated runoff and mean observed runoff are provided. In a batch file, it can be combined with a *TAC*^{d} simulation run for automatic evaluation.

3.13 Initialization

In order to start the calibration period with realistic values of storage levels, those values have to be determined by an initialization run. Tests have shown that simulations with *TAC*^{d} are extremely sensitive to their initial conditions. For *TAC*^{d} with hourly resolution a data set of at least one year prior to calibration is recommended for initialization. In order to achieve a faster stabilization of storage levels, initialization can be started with best estimations for storage levels. Then the initialization procedure can be repeated several times with the same data set, always using storage levels at the end of one period as initial values for the next run. When calibrating *TAC*^{d}, the effect of a changed parameter set on initial conditions has to be considered. Therefore, initialization has to be repeated for each calibration run (see chapter 4.10).

In the present model version, the following storages can be initialized:

- *sSoilMoisture*
- *sMTD_box*
- *sUS_box*
- *sLS_box*
- *sGW_box*
- *sIntPrecOld*

The storage of river channels (*sQ_step, sWaterDepth*) is initialized by a constant parameter (*sQIni*), which only leads to minor inaccuracies. Even though extensive tests were carried out, a complete initialization of the model could not be accomplished. Consequently, it is suggested that the first 100 to 200 time steps of calibration runs are not included in the model evaluation.

3.14 Conclusion of model conceptualization

The complex, distributed catchment model *TAC*^{d} is designed for process-orientated simulation of runoff generation, concentration and wave routing. Based on the storage analogy, the catchment is discretized in cells with up to three vertically arranged linear storages. Their combination due to lateral flow results in the formation of storage cascades. Areas with similar dominant runoff generation processes are gouped in seven different categories of runoff generation (*nRGType*) and then parameterized by same parameter sets.

Due to its modular structure and the user-friendly modeling language, *TAC*^{d} can be easily adapted to regional catchment characteristics and objectives. However, the complexity of *TAC*^{d}, especially the interaction of different runoff generation types, impedes a controlling overview of all runoff processes within a meso-scale catchment. Thus, the reliable declaration of runoff generation types via topographical, geological and pedological maps, aerial photography, remote sensing and personal user knowledge is essential. Insensitive parameters should be taken from literature as far as possible. During model calibration, the plausibility of parameters in respect to their influence on hydrological processes has to be regarded.

4 Recent modifications of *TAC*^{d}

Since a significant error in water balance indicated mistakes in the formulation of the program code, a profound review of the script was necessary. All model modifications within the modules of water fluxes were carried out in order to eliminate those errors. The conceptual ideas remained untouched as far as possible. As a result, computation times were reduced considerably in comparison to previous versions, although about twice as many calculations have to be performed for the additional model of solute transport. For a general description of the modules, see previous chapters. Because a detailed description of model modifications is mostly relevant for users of *TAC*^{d}, it is written as a technical report using the original *PCRaster* variables.

4.1 Methodology of error analysis

4.1.1 The internal water balance

The main criterion for the correctness and soundness of a catchment model is the internal water balance (*sBalance*). It is the crucial diagnostic tool to test the model for violations of mass conservation. The water balance calculates actual water levels of all storages and the sum of all input- and output-flows for each time step.

$$sBalance = \sum_{i=1}^{n}\left(\sum_{j=1}^{k} Input_{i,j} - \sum_{j=1}^{k} Output_{i,j} + \sum_{j=1}^{k} Storages_{1,j} - \sum_{j=1}^{k} Storages_{i,j}\right) \qquad \textit{Eq. 4.1}$$

sBalance:	sum of balance errors for evaluation period
Input:	input of precipitation
Output:	output of water fluxes
Storages $_{1,j}$:	sum of storage levels of all storages at first time step of simulation period
Storages $_{i,j}$:	sum of storage levels of all storages at actual time step
n:	number of time steps
k:	number of grid cells

Output fluxes are calculated for the water that is entering a stream channel (*sIntoStream*) before the wave routing routine directs the runoff through the river network. Thus, the channel routing routine is included in an extra balancing calculation. Losses due to evapotranspiration have to be included as output fluxes. The input and output fluxes are calculated at each time step and then cumulated over the simulation period. Therefore, balance checks calculate integrative values for the amount of water that was created or eliminated by the model during the simulation period. Consequently, a fundamental error

in the model script results in a continuously rising or dropping water balance. A positive internal water balance means that water disappears within the model, whereas a negative water balance indicates the creation of water. As the water-balance-check can be seen as a simple calculation of mass conservation, it is the fundament of each rainfall-runoff model.

Having said that, it has to be kept in mind that numerical models always suffer from inaccuracies due to time and space discretization (truncation) as well as rounding. This fact results in minimal fluctuations of the water balance also in a fully debugged model. The water balance of *TAC*^{d} is considered sufficiently accurate, when its value stays within millionth of the input amount, and no systematic increase or decline is evident.

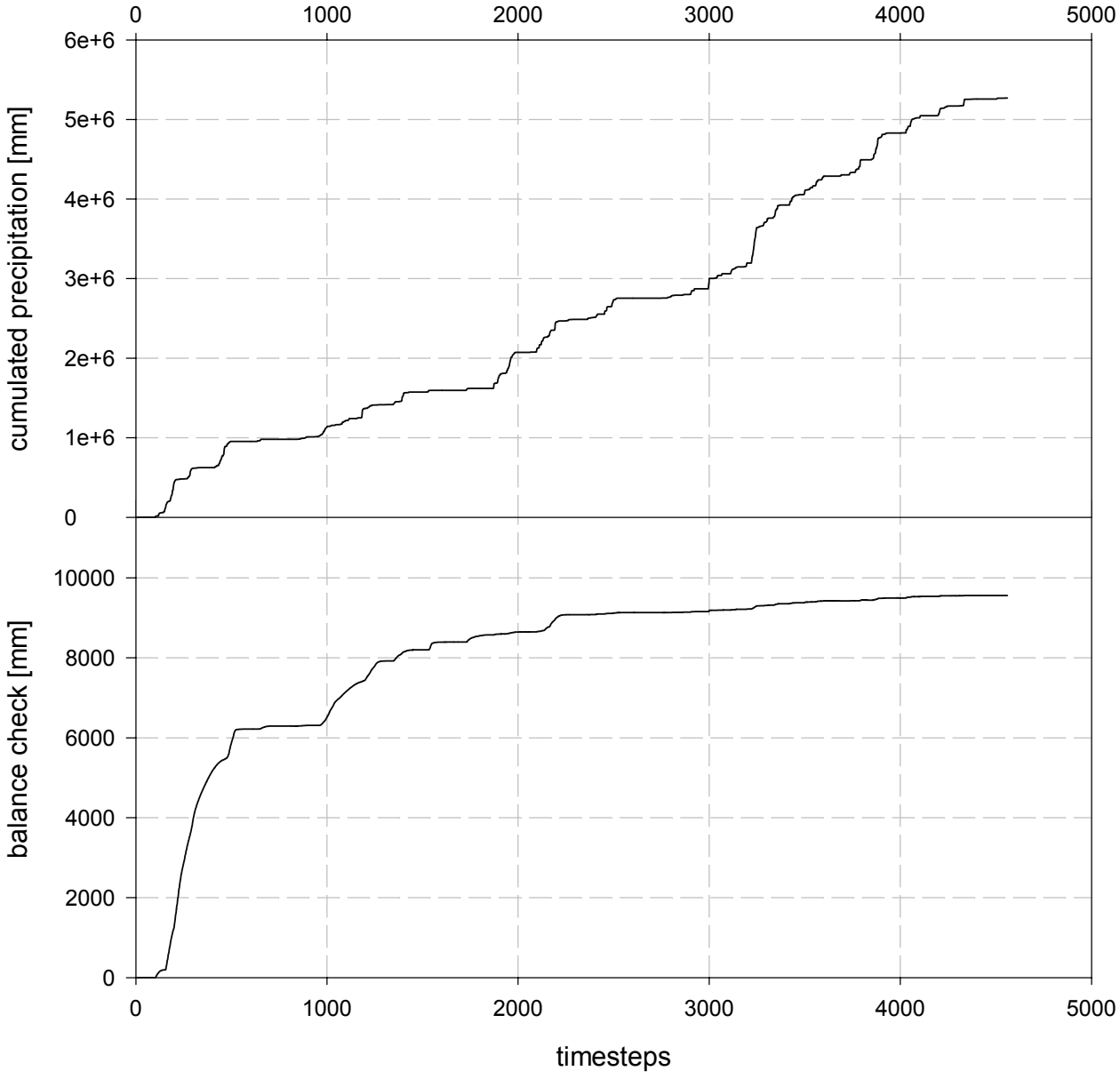

Figure 4.1: Water balance and cumulated precipitation input for 4800 time steps (prior version)

Figure 4.1 shows the water balance of the precursory *TAC*^{d} version for the entire Dreisam catchment and a simulation period of about 4800 hourly time steps. In the upper part of

the graph, cumulated precipitation input is displayed, which adds up to nearly 5.5 million millimeters. The lower part of Figure 4.1 shows the water balance. During the simulation period, the continuously rising water balance, calculated according to equation 4.1 clearly indicates an internal loss of water. Computation errors sum up to a value of nearly 10000 millimeters. Considering the cell-size of 40000 m² this equals a total volume of 400000 m³.

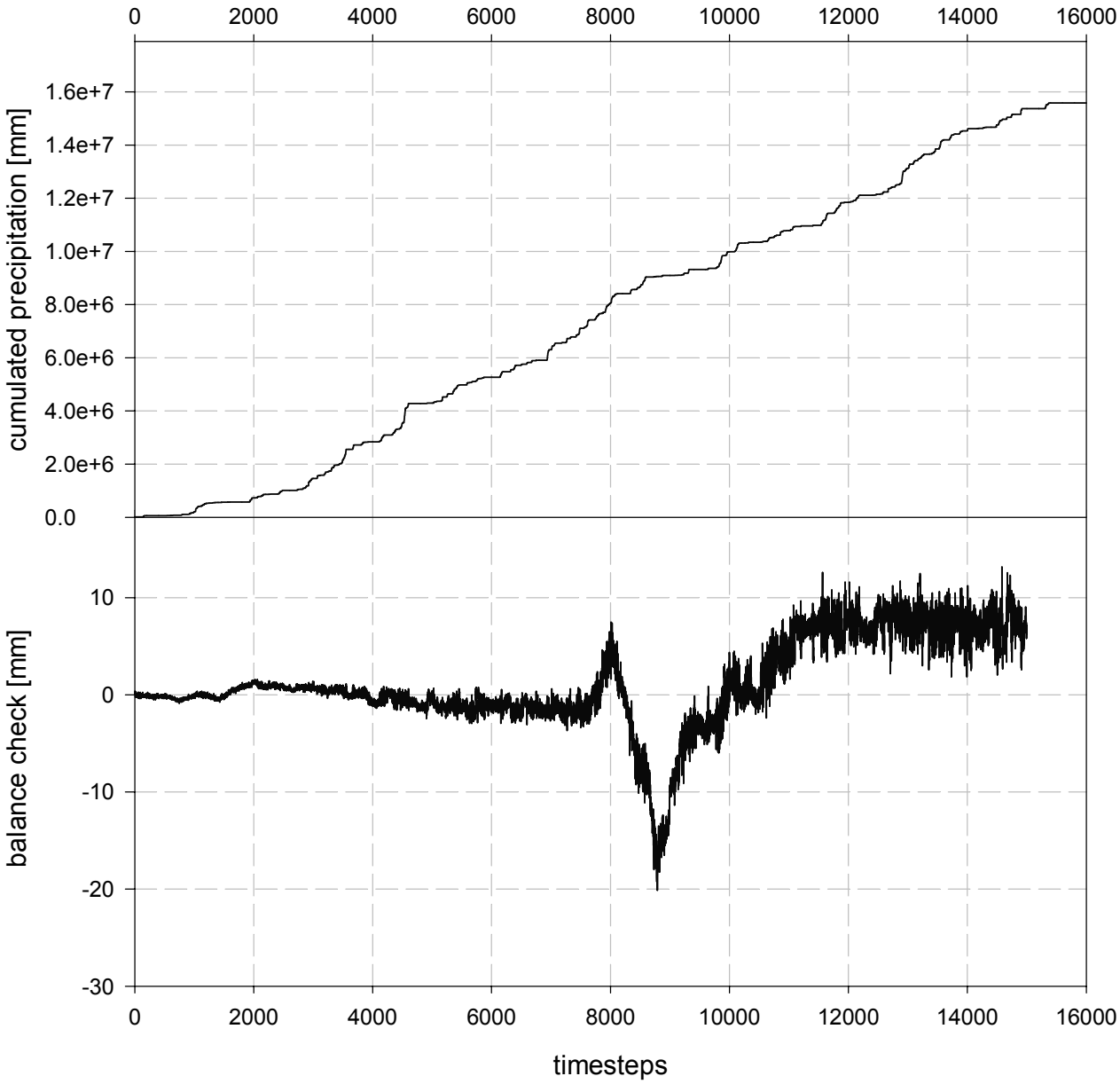

Figure 4.2: Water balance and cumulated precipitation input for 15000 time steps (revised version)

Figure 4.2 shows the water balance of the revised TAC^d for the Dreisam catchment and 15000 hourly time steps. Again, cumulated precipitation input is shown in the upper part of the graph. It adds up to nearly 16 million millimeters. The lower part of Figure 4.2 shows the corresponding water balance. Its maximum amplitudes range from +15 mm to -20mm. Therefore, model inaccuracies stay within millionths of the amount of input. The abrupt drop of the water balance near time step 8000 could not be explained, but it is still

irrelevant for computation accuracy. In addition, the random noise caused by rounding and truncation errors can be observed in this graph. Note that the error of the water balance in the old version results from a simulation period of only 4800 time steps, whereas the balance of the revised version stays stable for 15000 time steps.

For the wave routing routine a separate balancing module (*sBalanceRouting*) is included. It accounts for inputs (*sIntoStream*) into and output (sQ_mm) from the channel system as well as the Volume of water stored within the channel (*AvVol*).

4.1.2 The virtual test site

A virtual test site was installed for testing the model for errors and developing a new solute transport module. The complex structure of TAC^d impedes an overview of all flow processes in a natural catchment. Thus, the virtual test site provides facility to simplify the unmanageable number of interconnected effects in order to observe specific catchment reactions.

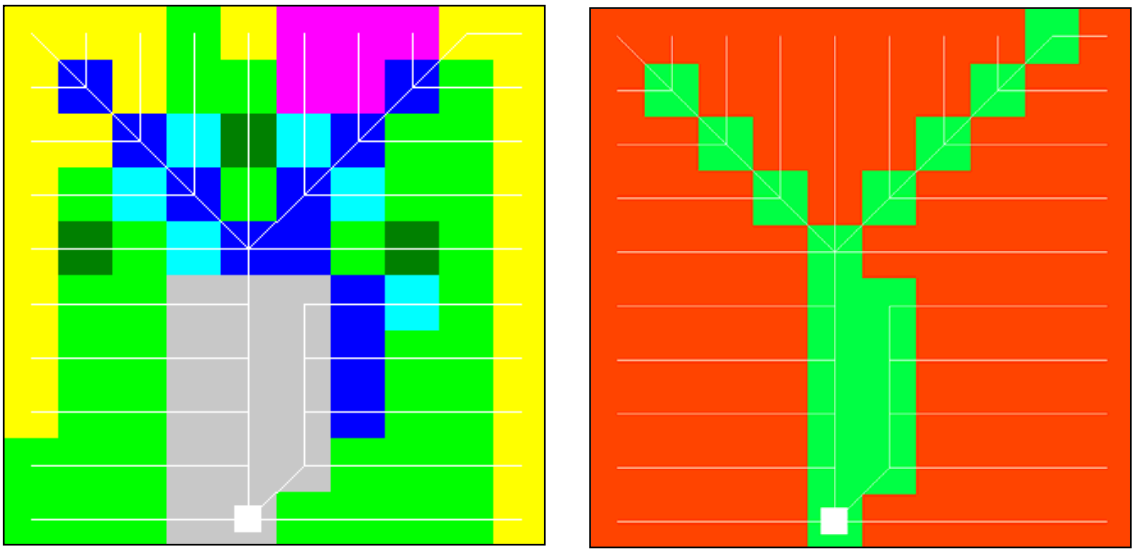

runoff generation type and local drainage direction

stream channel and local drainage direction

Figure 4.3: Virtual test site

Figure 4.3 shows the virtual test site of 10*10 grid cells with its different runoff generation types and the local drainage direction. The advantages of a virtual test site are:

- short computation times
- good overview of processes
- simple changes in catchment characteristics and climatic input
- clearly interpretable effects of parameter tuning

4.2 Modification of potential evapotranspiration

A fundamental error was detected within *POTRAD 5*, which is used for the calculation of potential radiation and temperature correction. Together with the digital elevation model, *POTRAD´s SHADE*-function calculates at each time step whether a cell receives direct sunlight, cloudless sky provided, or is shaded by obstacles. In a first step, the angle between the theoretical horizon at zero degrees and the actual horizon caused by obstacles in the direction of the sun is calculated (*HoriAng*). In a second step, this value is compared to the angle between the sun and the theoretical horizon, called solar altitude (*SolAlt*). If solar altitude exceeds the angle between obstacles and the horizon, a cell can receive direct sunlight. The domain for values of the directional type in *PCRaster* generally covers values from 0 to 360 degrees. This means for the solar altitude that the domain is from 0 to 90 degrees during daytime, where at 90 degrees the sun is located directly in the zenith. During nighttime, the domain covers values from 270 to 360, because negative angles are not defined in *PCRaster*.
In prior model versions, the comparison of those two angles (*HoriAng, SolAlt*) resulted in sunlight throughout the whole catchment during nighttime.

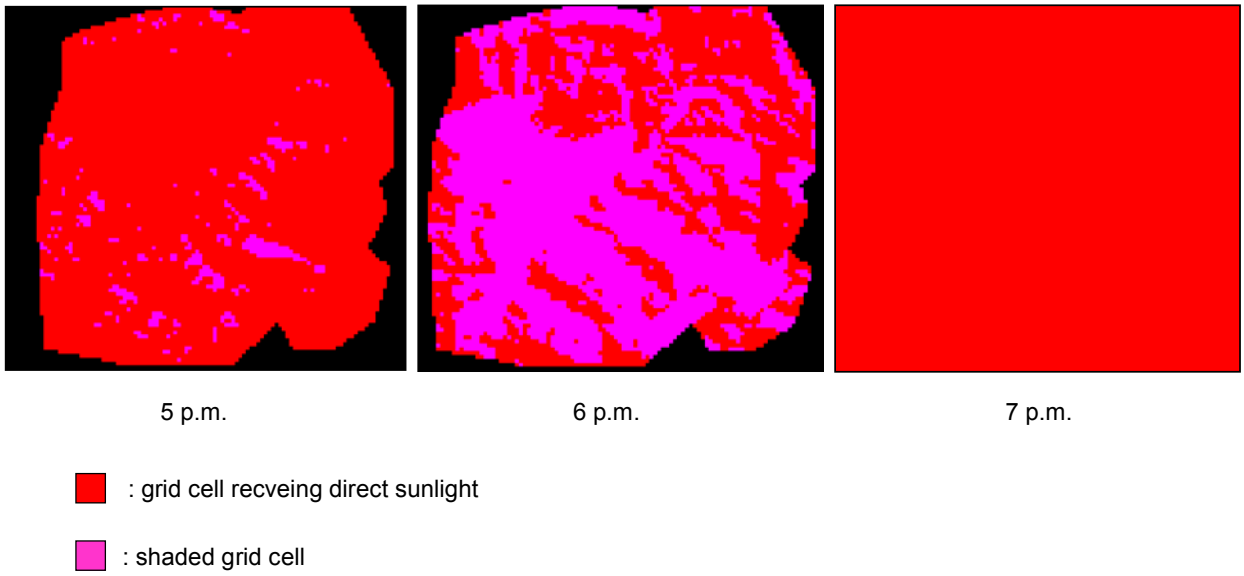

Figure 4.4: Results of the* SHADE*-function on a winter's day at different times

Figure 4.4 shows the results of the former *SHADE*-function in the Dreisam catchment during sunset on a winter's day at 5 p.m., 6 p.m. and 7 p.m. The first two pictures show the increase of shaded cells (purple), as the sun advances towards the theoretical horizon at zero degrees. When the sun drops below the theoretical horizon at 7 p.m., suddenly all grid cells receive direct sunlight.

Later in the model script, direct potential radiation is multiplied by the measured sunshine duration, which has a scalar domain from 0 to 1. Therefore, the bug in the calculation of direct radiation only resulted in mistakes when sunshine duration was measured due to diffuse radiation, even though the sun was hidden by obstacles. This is only the case during dawns and dusks. Therefore, values that were calculated with the

prior version of the potential evapotranspiration model were slightly overestimated. In the present model version, the angle between the sun and the horizon is set to zero when its value exceeds 90 degrees. The multiplication of potential direct radiation with measured sunshine duration can be seen as a check for the correctness of sunshine duration data.

Hereupon, another bug was detected in the calculation of mean daily sunshine duration (*sSSD_night*). Mean sunshine duration is used as a measure of cloudiness at nighttime, where obviously no direct sunshine can be observed. This cloudiness factor is used to calculate emission of long wave radiation during nights. For mean values of sunshine duration the sum of those hours has to be determined, during which a cell potentially receives direct sunlight. This sum depends on the sun position and the topographic location of a cell. For the identification of hours with direct sunlight, the *SHADE*-function was used again. Whenever no direct sunlight was determined after a period of sunshine, daytime was considered to be over in the former model version. In addition to calculation of sunshine during nighttime, obstacle in the direction of sunlight may result in wrong values for mean sunshine duration, if the sun is only temporarily hidden. In the actual model, sunshine duration was averaged over the period that was not interrupted by more than two shaded hours.

4.3 Modification of slope factor

The slope factor, combined with the storage coefficient, determines the outflow of storages from the runoff generation routine. It occurs in isolated cells that this combination exceeds one, so that more water leaves a cell, than it contains. A creation of water and therefore, a negative water balance was the result in the previous model version. In the reviewed version, outflows are limited to actual storage levels.

Another problem is caused by very low slope factors. Small storage coefficients are intended to represent good storage characteristics. In combination with very low slope factors, the contrary effect is obtained, because no important outflow is produced until overflows are activated. Once the maximum storage capacity is reached, retention of water within the cell is negligible. Therefore, slope factors were limited to a minimum of 0.3 in the revised model version.

4.4 Modification of snow routine

In prior model versions, the outflow of the snow-routine was set to zero for air temperatures lower than the threshold-temperature. Nevertheless, water content (*sWaterContent*) was limited to a fraction of snow pack (*sSnowPack*):

*sWaterContent = cCWH * sSnowPack;* **Eq. 4.2**

cCWH:	water-holding capacity [-]
sWaterContent	water content [mm]
sSnowPack	snow pack [mm water equivalent]

This was done, assuming that the amount of snow and the water content do not change during low temperatures. The outflow of the snow layer was set to zero, because no melting occurs. However, because snow pack is reduced by the temperature independent snow evaporation (*sSnowET*), water-holding capacity is reduced as well. In case of previously full water content, the snow routine looses the amount of unconsidered water, which equals the reduction of water holding capacity. Therefore, the result is a positive internal water balance. In order to correct this mistake either the water content must not be limited to the water-holding capacity at temperatures below threshold or the overflow of the water content has to be added to the outflow of the snow-routine. The latter was performed in the recent model version.

In prior model versions, it was taken for granted that there can be no further evapotranspiration from underlying interception or soil storages if a snow cover exists. Hence, the total evaporation was set to the value of the snow evaporation. This certainly holds true if there still exists a snow-cover when evaporation out of the interception and the soil storage is calculated. However, because the snow pack is reduced by melting (*sMeltWater*) after snow evaporation was subtracted, it might disappear and then further evapotranspiration takes place. In the total evapotranspiration, this additional loss of evaporation water was not accounted for, but it was still subtracted from the storage levels. Also here the result was a loss of water and consequently a positive internal water balance.
Other bugs concerning the integration of the snow routine into TAC^d are:

- The lump-sum parameterized snow evaporation has to be limited to the potential evapotranspiration.
- The sum of snow evaporation, evaporation out of the interception storage and evaporation out of the soil storage must not exceed the potential evaporation.

4.5 Modification of urban runoff routine

Because of a complete failure of the prior urban runoff module, a new routine had to be developed. The main mistake in the urban runoff routine of former model versions was the use of the *accufractionstate*-function. It was used to calculate the part of water that was not directed into the next downstream river cell, but remains as input for the soil routine. Since *accufractionstate* accumulates values of all upstream river cells, this mistake resulted in a creation of water and therefore, in a negative water balance. In the

present model version, the remaining input into the soil routine is simply the fraction of water, which does not take part in the urban runoff routine.

To make sure that only upstream urban runoff from non-stream cells is transformed into stream flow the variable for urban runoff (*sUrbanFlux*) has to change its name (*sUrbanFlux_*). Otherwise, the urban runoff from the entire upstream catchment area would be added to stream flow (*sIntoStream*), disregarding the fact that it might have already been added to the stream before. This mistake as well resulted in a creation of water.

Because of the small fraction of urban or sealed areas within the catchment, both mistakes only had a limited effect on hydrographs.

4.6 Modification of soil routine

Obviously, the actual evaporation from the soil routine (*sActET*) has to be limited to its water content (*sSoilMoisture*):

$$sActET = min\,(sActET, sSoilMoisture); \qquad \textit{Eq. 4.3}$$

This has been neglected in former model versions.

4.7 Modification of groundwater – surface water interaction

As recent investigations showed (*VAN DER PERCK 2004*), the *kinematic*-function can also handle negative input (*sIntoStream*) as long as outflow from the stream into the groundwater does not exceed the amount of water stored within the stream channel. This justifies the program script of prior *TAC*^{d} versions, where Infiltration (*sQ_inf*) is simply subtracted from *sIntoStream* and added to *sUS_box*. Nevertheless, there was no limit set for infiltration.

The reviesed version of *TAC*^{d} calculates the volume of water stored in the channel and subtracts infiltration directly from this volume. Afterwards the remainder is transformed back to the value (*sQ_step*) used by the *kinematic*. The minimum amount of water remaining in the channel system is set to the initial value (sQIni) (see chapter 3.13). Since the water for infiltration is taken from the kinematic, which has a different balancing routine (*sBalanceRouitng*) than the rest of the model, it has to be subtracted from this balancing routine and added as an input into the main balance check (*sBalance*).

4.8 Modification of balance check for the wave routing routine

In the prior version water, which is stored within the channel segments, was not included in the balancing module. This results in fluctuations of water balance, when water levels in the channel system change rapidly. Nevertheless, the balance has to be approximately zero at the beginning and end of runoff events. In the present version, the channel storage was included into balance calculations.

4.9 Modification of evaluation methods

In prior versions of *TAC*^{d,} three different measures for simulation accuracy were calculated:

- Model efficiency (*sEfficiency*) according to Nash & Sutcliff (1970)
- Logarithmic model efficiency (*slogEfficiency*)
- Volume error (*sVolumeError*)

For computation of model efficiency and logarithmic model efficiency, mean gauged runoff and mean gauged logarithmic runoff in respect to the whole simulation period are necessary (see equations chapter 3.12). The mean gauged runoff values, used in prior versions do not reflect the arithmetic means for the whole simulation period as only values up to the actual time step can be taken into account. Thus, an extra model for simulation evaluation had to be developed. For calculation of volume error a dubious scalar factor of 1/11.170139 was introduced, for which no justification could be found. Thus, this factor was eliminated from the recent model version.

4.10 Modification of initialization and calibration procedure

In most applications of *TAC*^{d}, one single run of initialization was carried out, to obtain starting values for calibration. This leads to inaccuracies during calibration, because a change in the parameter set would also result in different starting values for storage levels. If, for example, the recession constant of a storage is reduced during a calibration run, storage levels at the beginning of calibration are underestimated due to their computation with a larger recession constant in the initialization procedure. In general, calibration proved to be very sensitive to initial conditions. It has to be noted that the proposed initialization and calibration can only be performed with optimum data supply. In particular cases the initialization procedure has to be adjusted to data availability (see chapter 6.4).

4.11 Conclusion of model modification

Numerous modifications were carried out in order to eliminate logical mistakes from the model script. The conceptual ideas behind the scripts remained untouched as far as possible. The internal water balance was used as a diagnostic tool for violations of mass conservation. According to this indicator ca 400000 m^3 of water got lost in prior model versions during a simulation period of six months. In the present model script, significant violations of mass conservation could be eliminated.

Some of the corrections are irrelevant for simulation accuracies under the local climatic and topographic situation and the present degree of urbanization. However, in order to keep the model's universality it is essential to eliminate all logical errors. Fundamental mistakes in the urban runoff routine stayed without dramatic consequences because of the low fraction of sealed and urbanized areas in the catchments, to which the model was applied so far. When the model would have been applied to denser populated areas the mistakes would have become obvious. Also errors in the snow routine would lead to significant inaccuracies in areas with increased importance of snow precipitation.

Correct conceptionalization and formulation of water fluxes and volumes in water storages are the fundamental prerequisite for the development of a solute transport model, which is based on the coupling between water and solute fluxes.

5 The model extension for solute transport

The model for solute transport uses the water fluxes and storage levels calculated by *TAC*^{d} to route any kind of conservative solute through the routines of the catchment model. For this purpose, a parallel system of distributed storages for solute loads was established. With this conceptionalization, the model accounts for advective solute transport and mixing in all sections of the land phase hydrological cycle. The model can handle concentrated input from point sources as well as diffuse input from non-point sources, including mineralization. When timeseries of solute input are available, simulations are not only limited to single events but also continuous calculations of solute distributions within the catchment area can be performed.

Applications are:

- point source input
- non-point source input
- instantaneous input
- continuous input

So far, no further chemical reactions, such as retardation, absorption or decay, are included in the model. The present version is rather seen as a framework, where further solute reaction can be included with ease (see chapter 7.3)

5.1 Conceptualization of solute transport

The fundamental concept of solute transport in *TAC*^{d} is the interconnection of water fluxes and solute fluxes given by the following equation:

$$-\frac{\Delta N}{\Delta t} = \frac{Q^* \cdot N}{V} \qquad \textit{Eq. 5.1}$$

Q^*:	water flux [mm/time step]
V:	volume of water within the water storage [mm]
$-\Delta N/\Delta t$:	solute flux [see chapter 5.2]
N:	amount of solute within the solute storage [see chapter 5.2]

The implementation of this equation is performed by a system of storages in strict analogy to the *TAC*^{d} system for water fluxes. This system is referred to as solute model, whereas the original *TAC*^{d} is called water model in the following chapters. The parallel architecture of the solute transport model becomes more obvious, when the equation above together with

$$-\frac{\Delta V}{\Delta t} = Q^* \qquad \textit{Eq. 5.2}$$

is written in the form

$$\frac{\Delta N}{N \cdot \Delta t} = \frac{\Delta V}{V \cdot \Delta t} \qquad \textit{Eq. 5.3}$$

V:	volume of water within the water storage
-ΔV/Δt:	water flux
N:	amount of solute within the solute storage
-ΔN/Δt:	solute flux

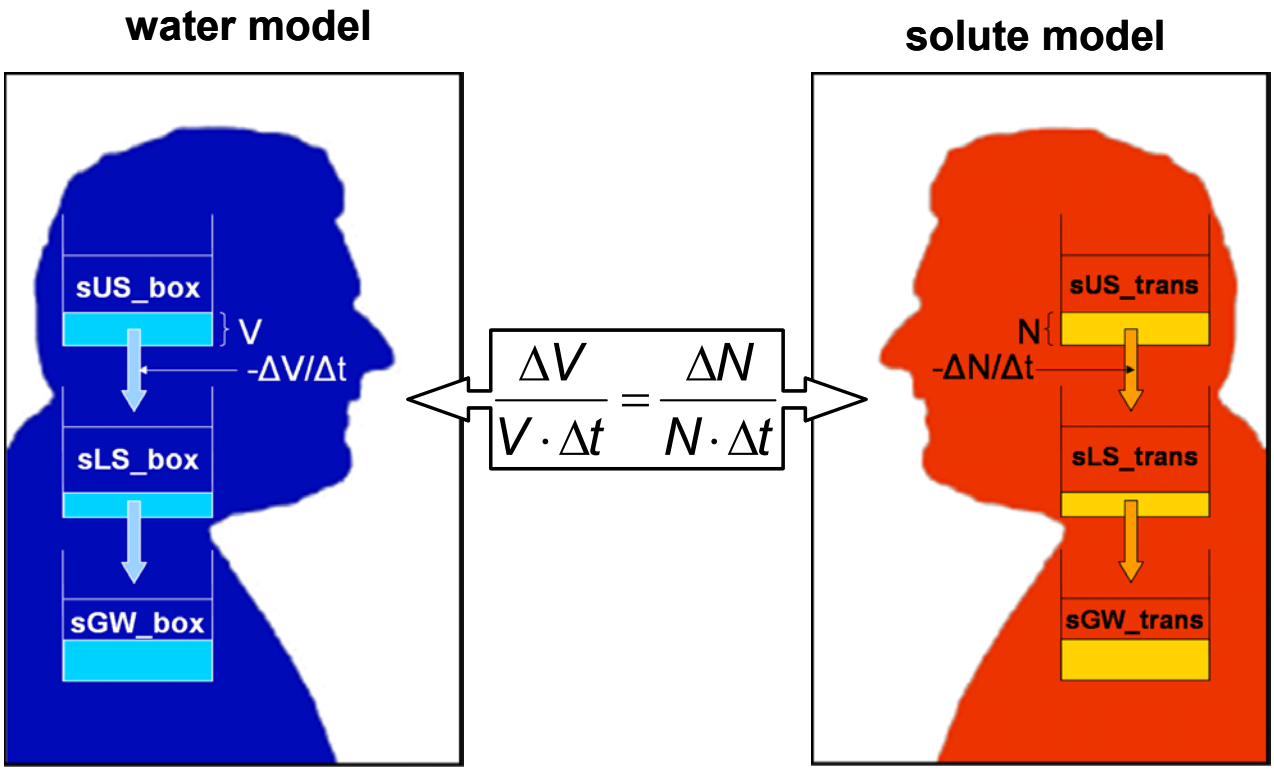

Figure 5.1: The parallel model architecture of solute transport

As Figure 5.1 illustrates, the conceptualization of storages and fluxes in the solute model is a mirror image of the water model. This means, that each storage and flux of the water model has its corresponding storage or flux of solute.

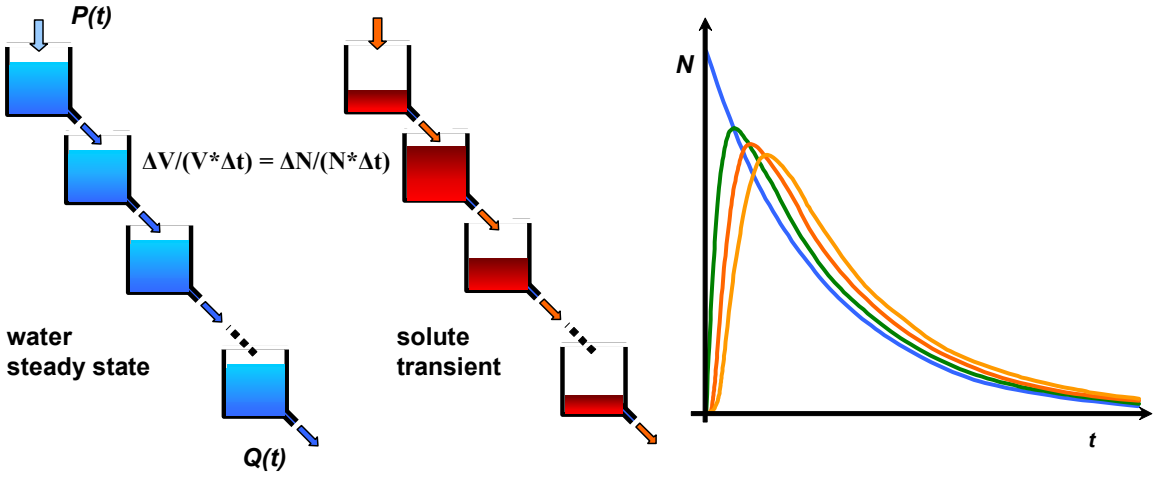

Figure 5.2: Instantaneous solute input in steady state water system

Since the linkage of storages by lateral fluxes results in a storage cascade, solute concentrations are subject to translation and dispersion (see Figure 5.2). The right side of Figure 5.2 gives an example of the breakthrough curves at different downstream locations, which result from an instantaneous solute input into a steady state water model.

The dynamics of processes within the solute model are fully dependent on the parameterization of the water model. As a result, no further calibration is necessary for solute transport. In fact, calibration of the water model determines the accuracy of solute simulations as long as the conceptualization of the water model represents the water fluxes in an appropriate way. Besides water fluxes, the solute model is also dependent on the correct representation of water volumes in the storages, because these volumes determine the degree of dilution of solute and therefore the shape of the output curve from storage cascades. Thus, solute simulations can help to detect inadequate conceptionalization of water fluxes and volumes, when data uncertainties are sufficiently small.

Wherever a different conceptionalization than stated above had to be established, it is noted in the following chapters. In general, variable names for the solute model are distinguished from the water model by the ending "*_trans*".

5.2 Units of solute transport

Input values for the solute transport model have to be provided in units of solute per volume of water. Accordingly, the amount of solute can be measured in units of mass, number of particles or other positive quantities. As the solute model calculates in units of loads, concentrations are converted to loads within the first modeling step. Fluxes of solutes such as nitrate or sulfate are calculated in units of mass per time step as their concentration is usually given in mass per volume of water. For simulations of ^{18}O a unit conversion from negative δ-values to positive ^{18}O concentrations has to be performed (see chapter 6.2.3), because some functions within the model for solute transport can not handle negative input.

5.3 Example code

As an example, part of the runoff generation routine is shown in the original *PCRaster* code. Comments are written in green and functions in blue. Parts, which are only relevant for solute transport, are marked by comment lines “TRANSPORT” at the beginning and end.

```
#************************************************
# Runoff Generation Routine - Upper storage (US)
#************************************************

# Input of percolated water to upper storage (mm)
sUS_box = sUS_box + sToRunoffGeneration;

#TRANSPORT TRANSPORT TRANSPORT TRANSPORT TRANSPORT TRANSPORT
sUS_trans = sUS_trans + sToRunoffGeneration_trans;
sUS_konz_mix = if (sUS_box > 0, sUS_trans/ sUS_box, 0);
#TRANSPORT TRANSPORT TRANSPORT TRANSPORT TRANSPORT TRANSPORT

# Runoff out of upper storage, modified by slope (mm/d)
sQ_US = min((sUS_box * cUS_K) * cSlopeFactor, sUS_box);
sUS_box = max(sUS_box - sQ_US,0);

#----------------------------------------
#TEST plus runoff over limit of cells (mm/d)
sQ_US = sQ_US + max (sUS_box - cUS_H, 0);

#TRANSPORT TRANSPORT TRANSPORT TRANSPORT TRANSPORT TRANSPORT
sQ_US_trans = sQ_US * sUS_konz_mix;
#TRANSPORT TRANSPORT TRANSPORT TRANSPORT TRANSPORT TRANSPORT

# Check that storage is not above limit
sUS_box = min (sUS_box, cUS_H);
#----------------------------------------

#TRANSPORT TRANSPORT TRANSPORT TRANSPORT TRANSPORT TRANSPORT
sUS_trans = max (sUS_trans - sQ_US_trans, 0);
#TRANSPORT TRANSPORT TRANSPORT TRANSPORT TRANSPORT TRANSPORT

# If upper and lower storage exist, then percolation into lower storage, else into
groundwater (mm/d)
sStorageLeak = if (defined(cUS_T), min (sUS_box, cUS_T), min (sUS_box, cAll_P));

#TRANSPORT TRANSPORT TRANSPORT TRANSPORT TRANSPORT TRANSPORT
sStorageLeak_trans = sStorageLeak * sUS_konz_mix;
#TRANSPORT TRANSPORT TRANSPORT TRANSPORT TRANSPORT TRANSPORT

# Remaining water in upper storage
sUS_box = sUS_box - sStorageLeak;

#TRANSPORT TRANSPORT TRANSPORT TRANSPORT TRANSPORT TRANSPORT
sUS_trans = max (sUS_trans - sStorageLeak_trans, 0);
#TRANSPORT TRANSPORT TRANSPORT TRANSPORT TRANSPORT TRANSPORT
```

The concrete implementation of equation 5.3 is performed by the two lines highlighted in yellow. In the first line, concentration (N/V: *sUS_trans/sUS_box*) within the upper storage is calculated. The second line calculates the solute flux (dN/dt: *sQ_US_trans*) in dependency of the corresponding water flux (Q: *sQ_US*). Because of the strong linkage between the water model and the solute model, the latter has to be patched into the program code of the water model whenever corresponding calculations are performed.

5.4 Solute input scenarios

Depending on the problem set, different ways of solute input can be selected. In general, natural solutes enter the catchment either via precipitation, or via dry deposition, or they are mineralized from catchment inherent substances (e.g. silicate). For both, simulation of single events or continuous simulations, initialization is necessary.

5.4.1 Input via precipitation

When solute enters the catchment via precipitation, input is usually measured in units of concentration. In order to obtain solute loads, concentrations have to be regionalized, for example by inverse distance weighting, and then multiplied by regionalized precipitation.

5.4.2 Input via dry deposition

In case of dry deposition, inputs can be provided as maps or time series for selected cells or areas. Depending on the temperature and the existence of a snow layer, input loads enter either the snow storage (*sSnowPack_trans*), the water content of snow (*sWaterContent_trans*) or the interception storage (*sIntPrec_trans*). If the fluxes out of the corresponding water storages (*sSnowPack, sWaterContent, sIntPrec, sSoilMoisture*) are zero, solutes loads are trapped until water fluxes, induced by precipitation, mobilize these loads (“first-flush” effect).

5.4.3 Input via mineralization

Depending on a mineralization rate and water volume in storages, mineralization can be calculated. The mineralized solutes then enter the corresponding solute storage. Afterwards, they are treated like any external solute. Mineralization rates can be dependent on storage type, temperature or any other kind of spatial catchment information. They have to be provided in units of $\frac{mass}{volume\ of\ water * time\ step}$.

5.4.4 Human input

As it is also possible to model input from human sources, substances can be treated the same way as precipitation input, if they enter the system as an aqueous solution. Human input of dissolvable solids is treated as dry deposits.

All types of solute input can be spatially distributed or concentrated in one single cell within the catchment. This cell is then considered to be a point source.

5.5 Interception routine of solute transport

The interception routine has a slightly different structure as generally stated in chapter 5.1. In the case of dry deposition, where no water enters the interception routine at all, solute input is added to the interception storage of solute transport (*sIntPrec_trans*). Otherwise (input via precipitation), the ratio of solute entering the interception equals the corresponding ratio of water, in order to obtain same concentrations in bypassing as in intercepted water.

5.6 Solute translation within the river network

As shown in chapter 0, water is directed through the river network by the kinematic wave routing method. So far, it was not possible to include an equivalent routing scheme for solutes in a manner that concentrations are unaffected by the transportation processes. In other words, when water enters the river network with a constant concentration the solute loads have to be transformed in the same way as water, so that the discharge at the catchment outlet still has the original concentration.

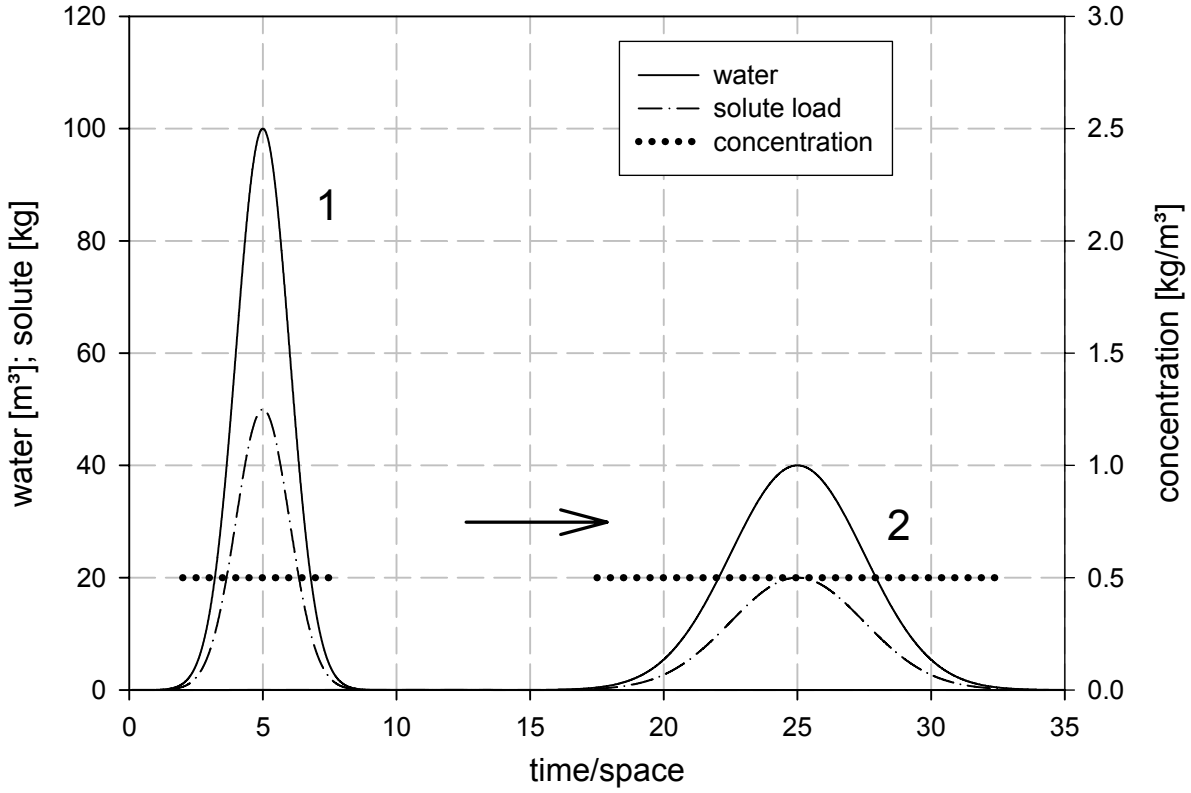

Figure 5.3: Channel routing of solute

Figure 5.3 shows the channel routing for solute as it was originally intended. Curves (1) represent water in m³ and solute load in kg in the stream channel at a certain location.

Curves (2) reflect the same waves later in a downstream location. The arrow indicates the direction of wave propagation. As can be clearly seen, the kinematic wave routine alters the form of the water wave as it moves downstream. The problem for solute transport results from the fact that the solute loads have to be altered in the same way as water to obtain true concentrations, in the example of Figure 5.3 0.5 kg /m³. Unfortunately, the kinematic wave routing scheme cannot be directly accessed for the implementation of solute transport, as it is encapsulated in a predefined PCRaster function

In order to account for translation of solutes in a simplified way, a mean translation time was calculated. For this purpose, flow velocities (an output of the kinematic wave routing routine), were averaged whenever the discharge at the channel outlet was within a specified range. This was done to account for different flow velocities during floods or low water. With those mean velocities, translation times to the channel outlets were calculated for each channel cell. In order to obtain one single translation time for each subcatchment, a spatial average was calculated by weighting all translation times with the amount of stream input (*sIntoStream*). It has to be noted here that the same translation time is assigned to all lateral stream inputs of solute disregarding their distance to the catchment outlet.

It was proven by numerous authors (*FRITZ 2001, NOLAN & HILL 1990, DINGMAN 1984, GLOVER & JOHNSON 1974*) that flow velocity of water particles in a steam is about a factor 3/5 slower than the kinematic water wave (wave celerity) in an idealized rectangular channel. This could also be proofed for stream sections at the Zastler Talbach in the Black Forest Mountains (*FRITZ 2001*). Therefore, the factor of 3/5 was used to modify flow velocities of solute, before calculating translation times. As this method of solute translation is considered a simplified workaround, the factor was not calibrated in order to achieve a better simulation of solute dynamics.

5.7 Groundwater – surface water interaction of solute transport

This module for groundwater- surface water interaction was eliminated from the recent model of solute transport, because exact concentrations within cells of the river network could not be calculated, and therefore loads of infiltrating solute are unknown. In order to avoid further mistakes it also had to be deleted from the water model.

5.8 Code verification

Together with the obligatory solute balance, four fundamental tests were accomplished to evaluate the model's accuracy and plausibility. In order to gain a better understanding of the complexity and interaction of different processes synthetic data sets for solute input were used for those tests. For tests of point source and area-wide input, also climatic data input was modified. The tests were carried out in the Dreisam catchment, where the model also was applied to gauged events and therefore spatial GIS data was available. Since solute input is synthetic data in the first place, units of solute can be any arbitrary positive quantity such as mass or number of particles.

5.8.1 Internal solute balance

The solute balance is the equivalent of the water balance, and therefore it is calculated by the corresponding equation.

$$sBalance\_trans = \sum_{i=1}^{n}\left(\sum_{j=1}^{k} Input\_trans_{i,j} - \sum_{j=1}^{k} Output\_trans_{i,j} + \sum_{j=1}^{k} Storages\_trans_{i,j} - \sum_{j=1}^{k} Storages\_trans_{i,j}\right)$$

Eq. 5.4

sBalance_trans:	sum of balance errors for evaluation period
Input_trans:	input of solute
Output_trans:	output of solute fluxes
Storages_trans $_{1,j}$:	sum of storage levels of all storages at first time step of simulation period
Storages_trans $_{i,j}$:	sum of storage levels of all storages at actual time step
n:	number of time steps
k:	number of grid cells

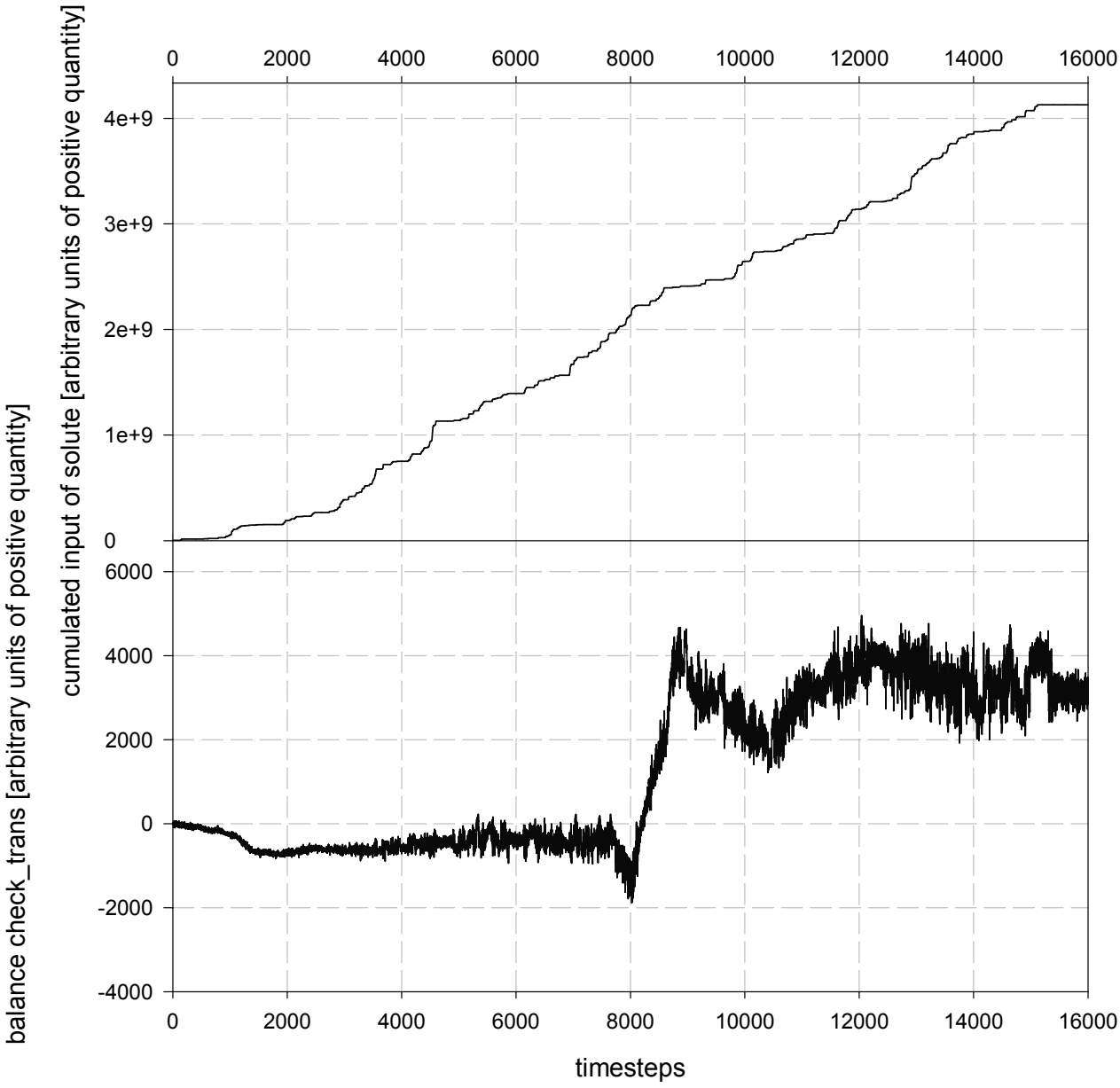

Figure 5.4: Solute balance and cumulated solute input for 16000 time steps

Figure 5.4 shows the solute balance for an input of constant concentration into the same natural data set, which was used for the calculation of the water balance (Figure 4.2). The cumulated amount of solute input is displayed in the upper part and the internal solute balance in the lower part, both in arbitrary units of positive quantity. When comparing the solute balance of about 3000 to the total solute input of about 4 billion computation errors are in the range of 0.0001% for 16000 time steps. Therefore, computation errors are irrelevant for modeling accuracy. Furthermore, it can be seen from the graph that amplitudes react in the opposite directions of the internal water balance (Figure 4.2) until the rise at time step 8000 stops this tendency. The reason for this can be seen in the strong linkage of the water model and solute transport. Thus, a loss of water results in a gain of solute.

5.8.2 Steady state water flow

To gain a clearly interpretable output signal the model tests for point source input (5.8.3) and area-wide input (5.8.4) were conducted under steady state water flow conditions (Q = constant). Steady state fluxes are produced by adding 0.1 mm of precipitation to each cell at each time step and waiting until output fluxes stay at a plateau that equals the amount of input. This can only be achieved, if the storage capacity of the entire catchment is constant in time. Therefore, the evapotranspiration model as well as the snow routine has to be turned off. This was done by setting the evapotranspiration to zero and air-temperature to 10 °C for the entire catchment. For steady state water flow conditions, it is also necessary to set the maximum interception storage (*sStorageMax*) to a fixed value. In *TAC*[d] *sStorageMax* normally changes monthly due to different leaf area indices and values of vegetation coverage. A sudden change in *sStorageMax* at full interception storages leads to a discharge amplitude in all subsequent modules. For the tests in chapter 5.8.3 and 5.8.4 solute was supplied at a time when water fluxes had reached steady state.

5.8.3 Instantaneous point source input

The test of an instantaneous input of solute at a single cell was performed in order to examine the model's response to point source contamination. For the location of input, a cell at the catchment boundary with a long distance to the next river channel was chosen, so that lateral subsurface flows could be observed. A solute load of 400 was added to this cell via 0.1 mm of precipitation with a concentration of 100 solute units/m³ at time step 20000.

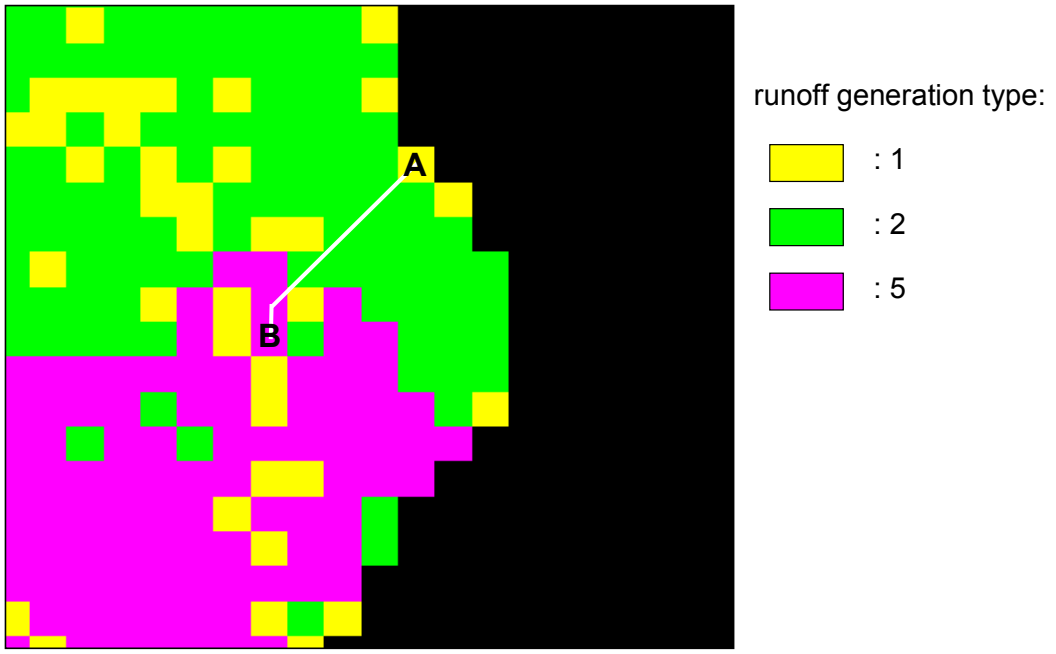

Figure 5.5: Small section of the runoff generation map of the Dreisam catchment; location of solute input into catchment (A); location of solute input into stream (B); flow path (white line)

The solute enters the catchment in a cell with runoff generation type (*nRGType*) 1, marked by 'A' in Figure 5.5. Before entering the stream channel in cell 'B' with *nRGType* 5, the

solute flows through four cells with runoff generation type 2 and two cells with runoff generation type 5. As cell 'B' only consists of upper storage (US) and groundwater storage (GW), stream input from the lower storage (LS) and saturated overflow (SOF) do not exist. In addition, no solute input from direct runoff components exists.

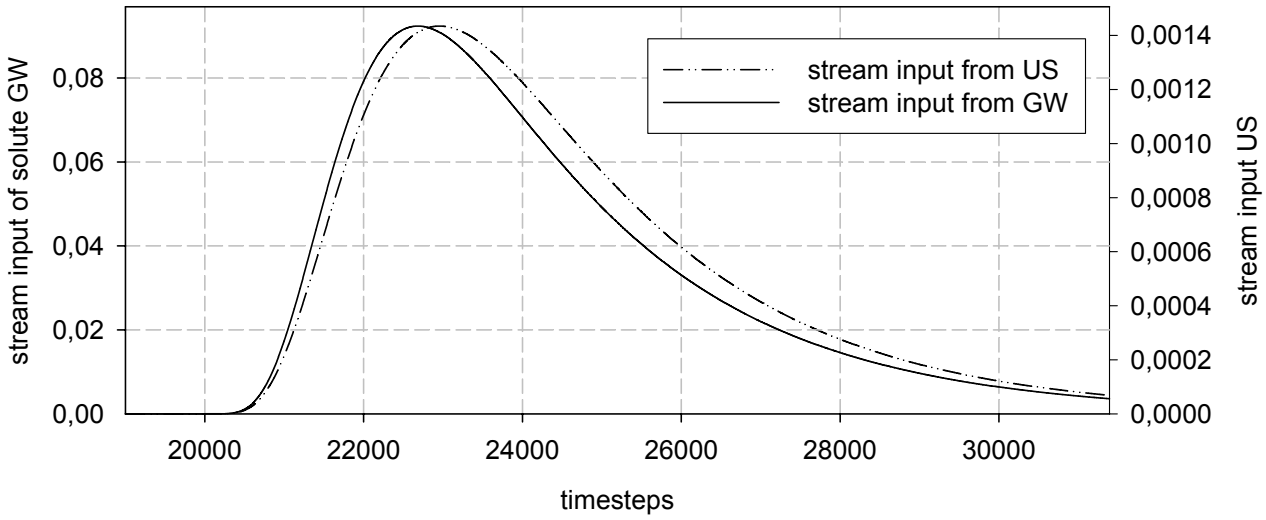

Figure 5.6: Stream input from upper storage (US) and groundwater storage (GW); point source test

Figure 5.6 shows the input of solute load (*sIntoStream_trans*) from different storage types into the river network at the first downstream river cell. In order to compare their dynamics, the breakthrough curves from upper storage and groundwater storage are plotted on different y-axis. Note that the peak input from the upper storage is about 60 times smaller than from the groundwater storage. The integrated input of solute loads from the upper storage adds up to only 1.6% of the input from the groundwater storage. As can be seen from the graph, both curves show the typical translation-dispersion shape of a storage cascade. Higher flow velocities caused by larger storage coefficients are observed for groundwater solute flux. The multitude of vertical and lateral interconnection between storages impedes a closer interpretation of flow dynamics even with the eight participating cells. Dispersion results from mixing of solute and water before solute fluxes are calculated cell by cell.

5.8.4 Instantaneous area-wide input

With this test, the catchment's reaction to an area wide input of solute could be observed. The solute was added to the entire catchment area with the same concentration in precipitation (100). Therefore, 400 solute units entered each cell of the system at time step 20000 (*sPrec_trans*). With 6437 cells, the total amount of solute entering the Dreisam catchment adds up to 2574800.

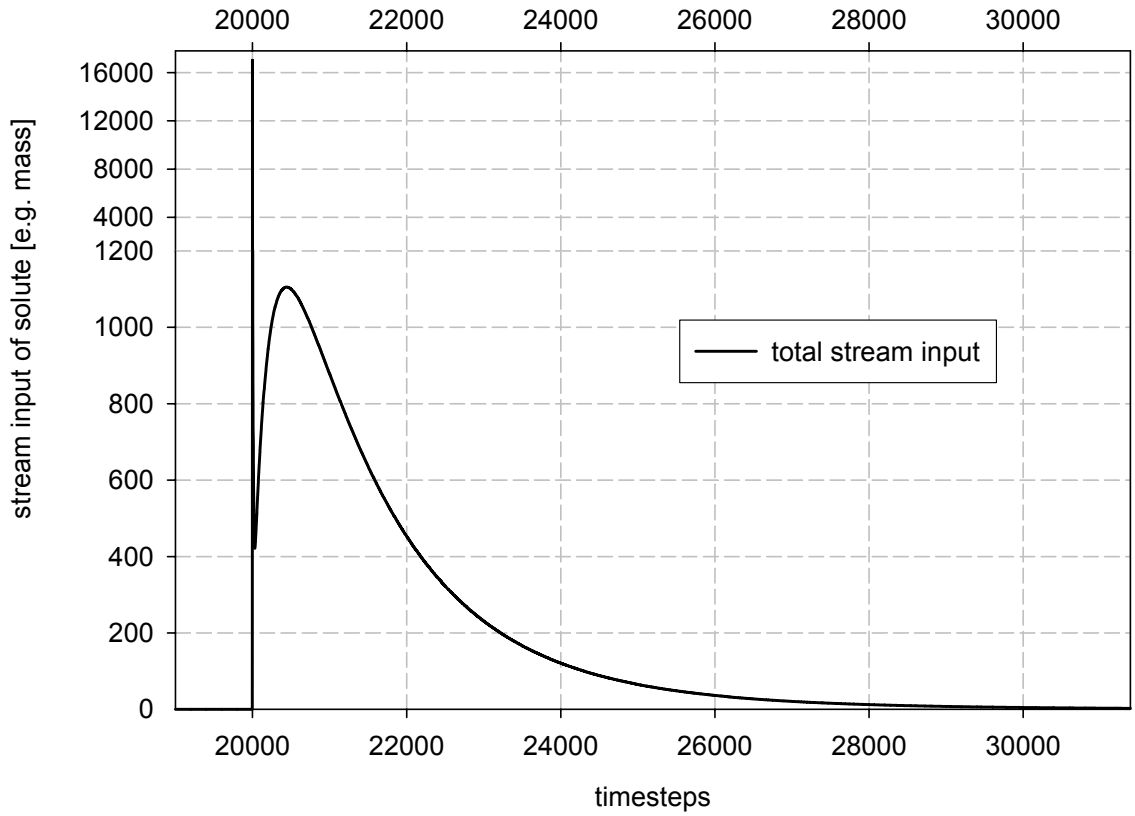

Figure 5.7: Total stream input*; *area-wide input

The total amount of solute entering the stream channels (*sIntoStream_trans*) is shown in Figure 5.7. Note that the y-axis has a break at 1200. Total solute entering the streams is less than total catchment input, because a significant amount of solute bypasses surface runoff across the watershed via underground flow in a porous aquifer. Integrated over the whole simulation period an amount of 2326177.6 solute units enters the streams, which is about 90.3% of total catchment input.

An extremely high peak of nearly 18000 at time step 20000 is caused by solute in direct runoff components from sealed or open-water areas. Those components enter the stream channel within the same time step of their release from the interception routine.

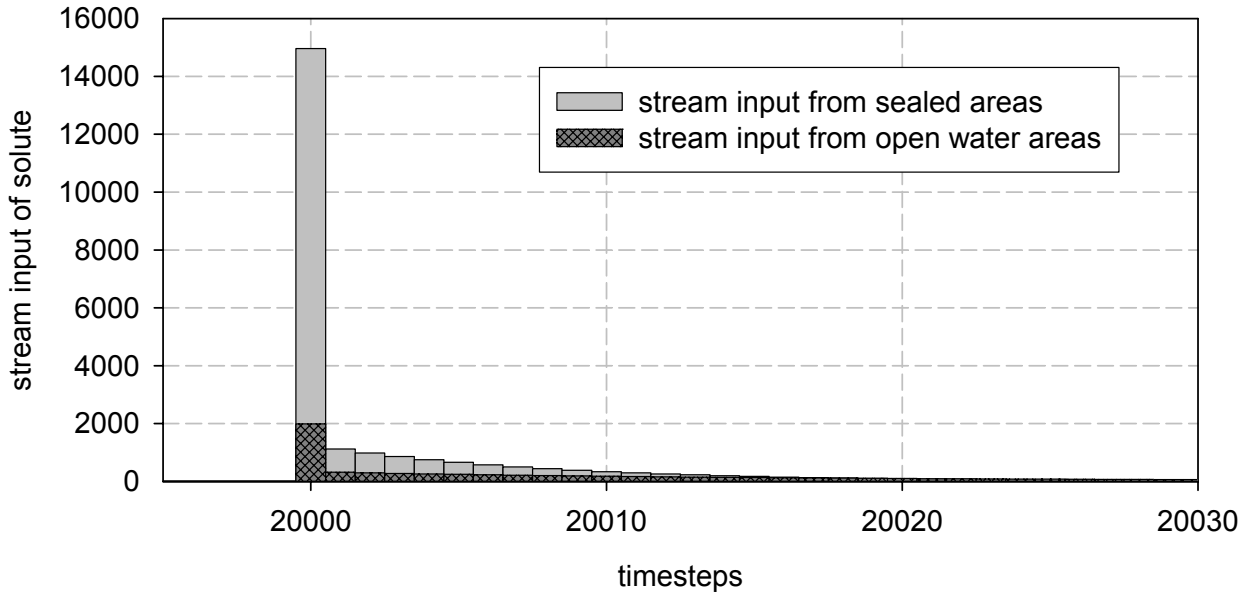

Figure 5.8: Solute in direct runoff components; area-wide input

In Figure 5.8 solute load in direct runoff components is displayed for the first 30 time steps after solute input into the catchment area (*sPrec_trans*). Due to the small part of water that enters the interception storage and its small storage capacity, dilution within the interception routine is minimal. Therefore, the input impulse of solute is barely transformed. As the following routine (solute transport of direct runoff components) directs a certain fraction of solute input into the stream without retention, Figure 5.8 reflects the dynamics of solute output from the interception routine. Despite the exclusive contribution during the first time steps, only 1.38% of total solute enters the stream via direct runoff components during the entire simulation period.

In the time steps after the first peak, the amount of stream input (*sIntoStream_trans*) drops down to values of about 440. At that time, further outflow from the interception storages in urban areas and storages from those cells contributes to stream input, which are located close to the channel. Little by little, solute fluxes from more distant cells reach the river network and a second peak around time step 20450 is produced.

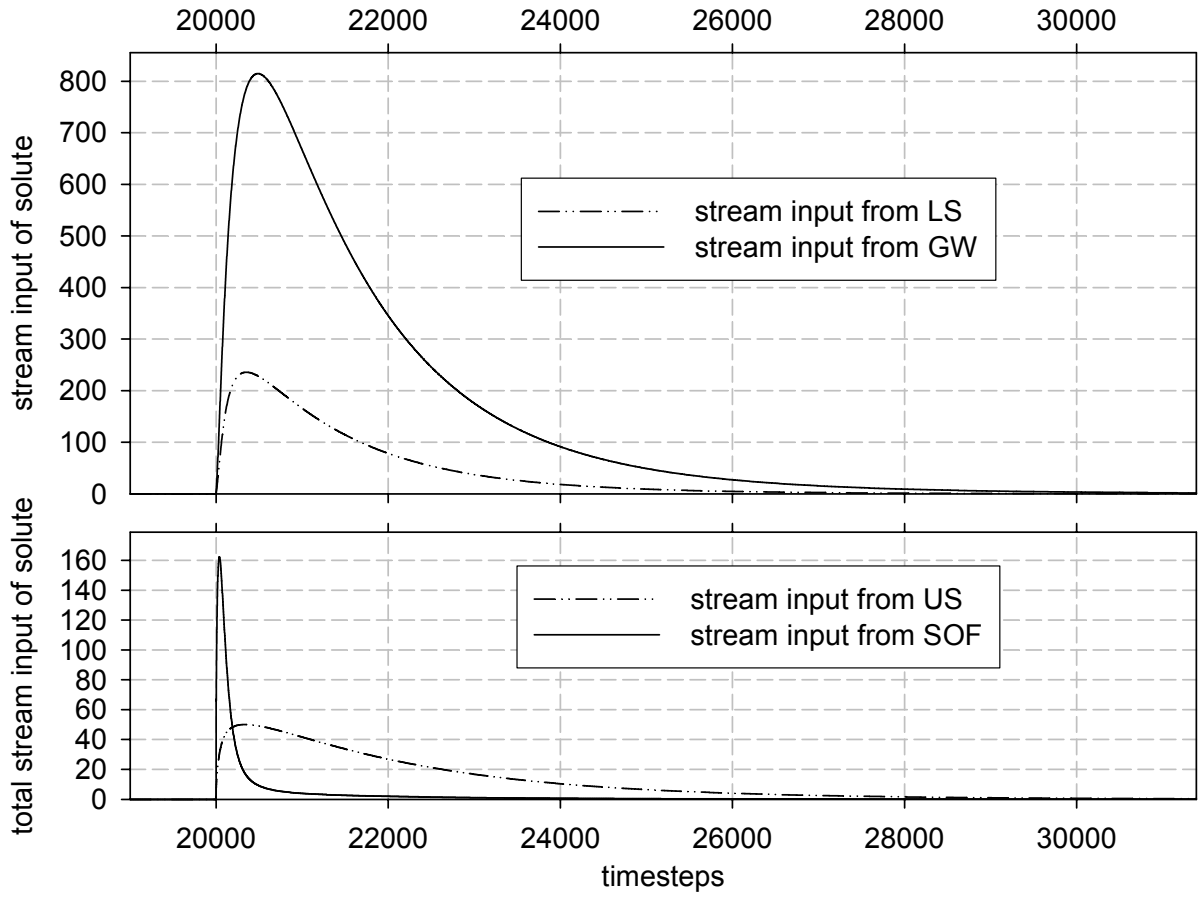

Figure 5.9: Stream input from different storage types; area-wide input

Figure 5.9 shows solute input into stream channels for different storage types. The main part of solute stream input (*sIntoStream_trans*) obviously originates from groundwater storages. They provide about 73.2% of total solute input, followed by 18.1% from lower storages. Only 5.8% of total stream input stem from upper storages and 1.6% from saturated overland flow (SOF). As expected, the component from saturated overland flow has very fast runoff dynamics, compared to subsurface components.

Again, it has to be noted that the presented results are only valid for a water model in steady state.

5.8.5 Input of constant concentration

For this test, measured timeseries of climatic input were used. At each time step, regionalized precipitation was loaded with the same concentration of solute. In addition, it was stated that concentrations within the storage system are not effected by evapotranspiration. Thus, evapotranspiration was considered a water flux that reduces storage levels of solute in the same ratio as storage levels of water. As a result, the quotient of solute and corresponding water, whether flux or storage level always has to reflect the original concentration of precipitation input.

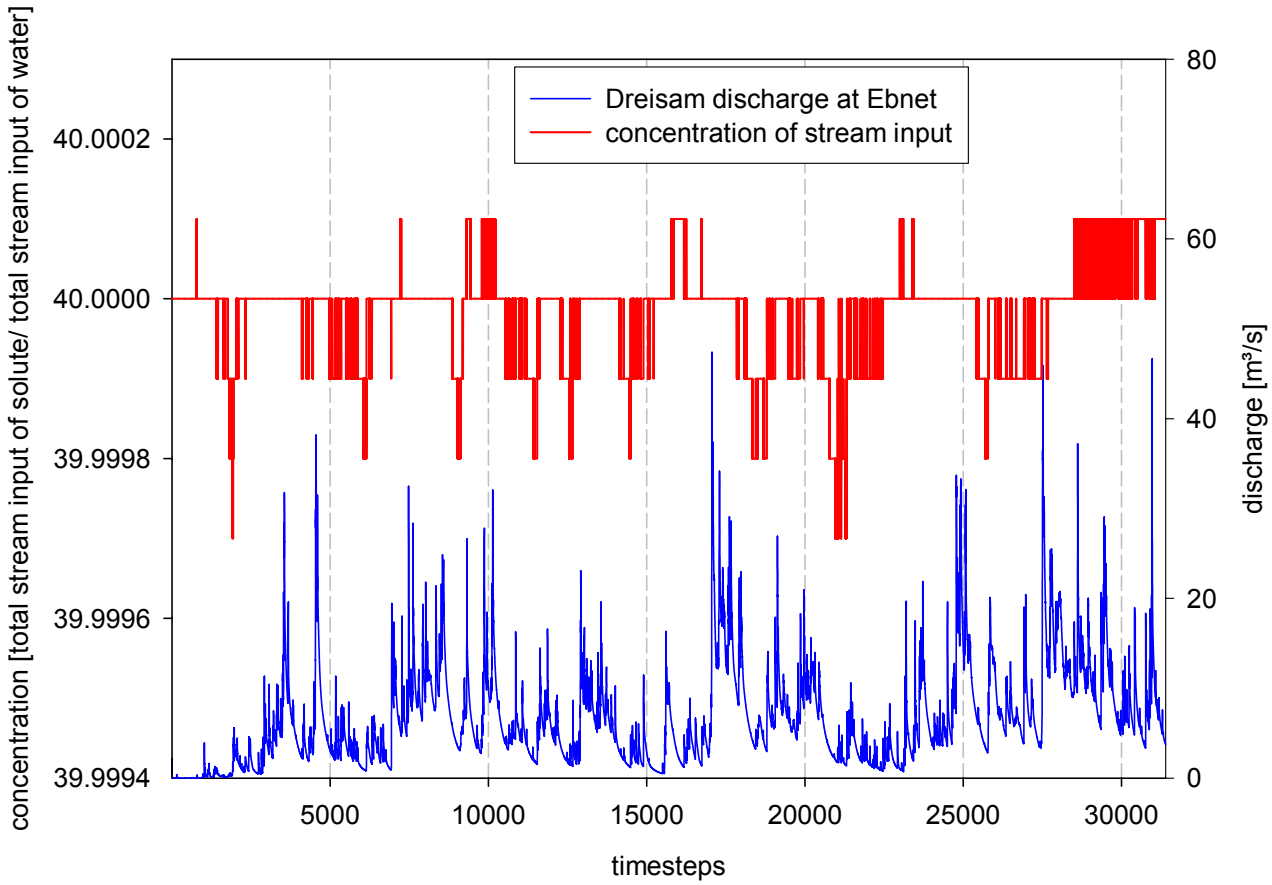

Figure 5.10: Concentration of stream input and Dreisam discharge; constant concentration test

Figure 5.10 shows the simulated Dreisam discharge (blue) and simulated concentration of stream input (red). Although the model calculates fluxes of solute loads, concentrations (total stream input of solute / total stream input of water) stay within 0.00075% of the expected value (40). In some cells the concentration of stream input deviates some more from the expected value, but because the amount of water (and solute) in those cells is very small their concentrations are unimportant for total stream input.

This test is a proof of the correct conceptualization and programming of the solute transport model.

5.9 Conclusions on model development

Continuous simulations of solute distributions within mountainous, snow influenced, meso-scale catchments can be performed with the presented model of solute transport. Solute concentrations can be reported in stream discharges at the catchment outlet as well as in the different storages at arbitrary locations within the catchment.

Based on the revised water model TAC^d, the solute model is reflected by a system of solute storages and fluxes. This system is in full analogy to the water model, so that each water storage and flux is represented by a solute storage and flux. The connection between the water model and the solute model is given by equation 5.3.
Without including further solute reactions the model can be used for the transport of any conservative substances such as ^{18}O or deuterium. The flexibility of the model structure allows area wide solute input as well as input from point sources. Both, instantaneous and continuous input can be simulated. In addition, the solute can be introduced via precipitation or directly into each section of the land phase hydrological water cycle.

During model tests, the solute balance showed no violation of the mass conservation law. In addition, the solute model proofed its applicability in tests of point source and area wide solute input with synthetic data as well as for constant concentration solute input via precipitation under natural climatic conditions. For solute transport, no further calibration is necessary because the dynamics of processes within the solute model are fully dependent on the parameterization of the water model. Thus, solute simulations can help to detect inadequate conceptionalization of water fluxes, when data uncertainties are sufficiently small.

It has to be noted here that within the scope of this thesis only the first steps towards a general description of solute transport model could be made.

6 Model applications

The model of solute transport was applied to three different precipitation events. They are named DS 07_03, DS 05_02 and BRU 06_01. Both events named with 'DS' were simulated for the whole Dreisam catchment and its subcatchments, whereas in 'BRU' the model was only applied to the Brugga subcatchment. The numbers indicate the month and year of the event. In addition, simulations were accomplished for different antecedent moisture conditions. Selected results from subcatchments are examined after the results from the entire Dreisam catchment for DS 05_02 and DS 07_03. Area precipitation refers to the catchment or subcatchment under consideration. The units of stream input of water from different storage types [mm/ time step] always refer to one single cell. Hence, with a cellarea of 200*200 m² and a time step discretization of one hour, the total volume of stream input [m³/s] from the entire catchment can be calculated by multiplying the millimeter notation by 1/90.

$$stream\ input\left[\frac{m^3}{s}\right] = \frac{cellarea\left[m^2\right]\cdot 0.001}{3600\left[s\right]}\cdot stream\ input\left[\frac{mm}{h}\right] \qquad \textit{Eq. 6.1}$$

6.1 Area of investigation

The Dreisam catchment was chosen for real-life model applications because of the numerous previous studies that were already accomplished throughout this site. A calibrated version of TAC^d with all spatial and climatic input data was available for the period 1994 until 1999 (*OTT 2002*). Thus, time-consuming data preparation, especially for GIS input maps could be avoided. In addition, ^{18}O-data for precipitation and runoff was available for selected events from the dissertation of *DIDSZUM* (*2004*).

This chapter wants to give a brief review of the catchment characteristics in the area of investigation. For a more detailed description, see *OTT* (*2002*), *UHLENBROOK* (*1999*), *HÄDRICH & STAHR* (*1997*), *BECKER* (*1992*), *TRENKLE & RUDLOFF* (*1989*).

6.1.1 Morphology

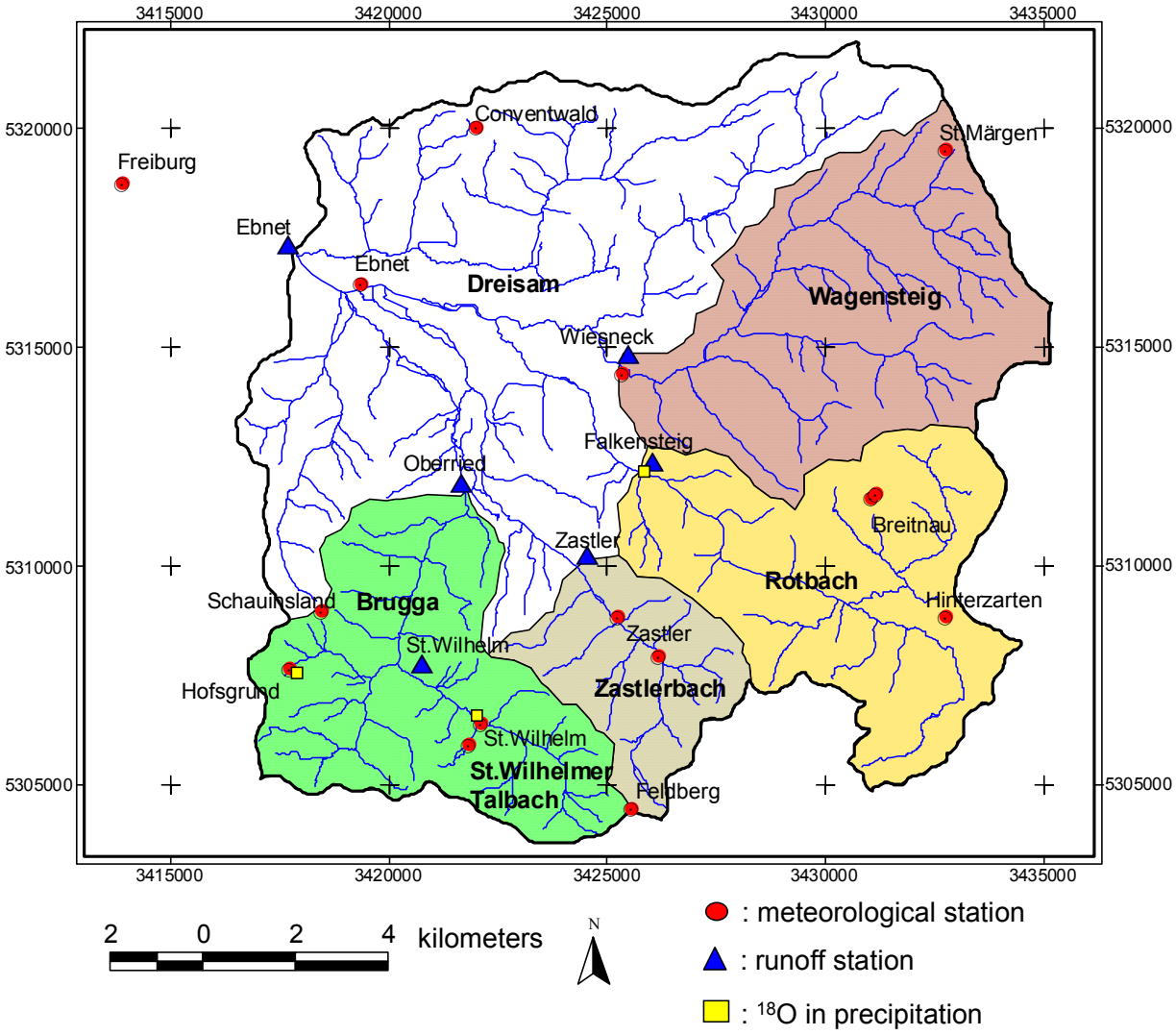

Map 6.1: The Dreisam catchment and its subcatchments (Brugga in green)

The Dreisam catchment, shown in Map 6.1, is located in the southwest of Germany in the southern Black Forest region. Westward, it borders on the Upper Rhine Valley at the catchment's outlet in Ebnet (316 m above sea level, a.s.l.). To the south, east and north, it is surrounded by the plateaus and mountains of the Black Forest. The catchment's highest elevations are located in the south with the peaks of Schauinsland (1284 m a.s.l.) and Feldberg (1493 m a.s.l.). The latter is also the Black Forest's highest peak. With a total area of 257.5 km² the catchment belongs to the upper meso-scale (*BECKER 1992*).

The Brugga subcatchment (green in Map 6.1), with an area of 40.2 km² and a mean hill slope of 17.5° covers the most elevated regions of the Dreisam catchment. From all subcatchments, it is the one with the highest difference in elevation (more than 1000 m from the Feldberg summit to the outlet in Oberried).

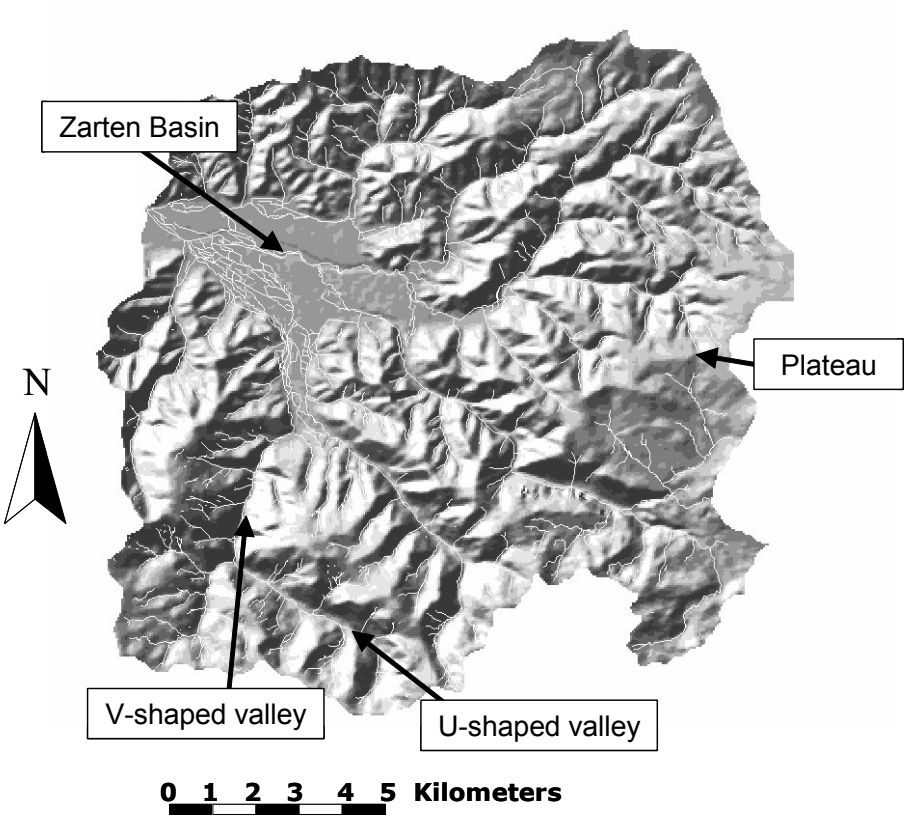

Figure 6.1: Topography of the Dreisam catchment

The shade plot of Figure 6.1 pictures well the trisection of the Dreisam catchment. The three dominating morphological units can be described as follows:

- The **PLATEAU BLACK FOREST** in the east and northeast shows characteristics of a peneplain that existed before the Black Forest was created.
- The **ZARTEN BASIN** in the center is part of the Dreisam fault. It was created by crustal movements associated with the creation of the Rhine Valley. Its actual appearance originates from alluvial deposition of large Pleistocene and Holocene topset beds.
- The **LOW MOUNTAIN RANGES** in the south and north are dominated by steep slopes with rock escarpments, scree and talus fields. Headwater valleys in the south show clear signs of glacial erosion (U-shaped valleys, moraines, cirques) (*METZ 1997*). The lower valleys are subject to recent alluvial erosion (V-shaped valleys, gullying) (*LIEHL 1988*). Geographically the northern part, which is lower in elevation, is also called **MIDDLE VALLEY BLACK FOREST**. The southern, more rugged part is named **CREST BLACK FOREST**.

6.1.2 Climate

The catchment is located in the temperate zone of the so-called west wind drift. This zone is characterized by fast changes of weather situations with alternating subtropical and polar air currents. Due to the mountainous relief, general climatic situations are considerably altered in the small scale (*TRENKLE & RUDLOFF 1989*). Therefore, regional climatic distinctions have to be taken into account.

AIR TEMPERATURE shows a pronounced altitude dependency. The mean annual temperatures of 10.3°C in Freiburg (269 m a.s.l.) and 3.2°C at the Feldberg (1486 m a.s.l.) prove this fact. During the winter months, inversion weather situations with an upper boundary at 500 to 800 m a.s.l. are frequent. As inversions prevent vertical circulation and therefore high fog is common, a reversed altitude dependency can be the result. Thus, air temperatures in elevated areas can even exceed those of lower regions (*TRENKLE & RUDLOFF 1989*).

The general **WIND** direction in the high regions of the Black Forest is ruled by the west wind drift. However, local wind systems with different directions evolve due to the mountainous terrain (e.g. ridge turbulences, katabatic winds) (*TRENKLE & RUDLOFF 1989*).

The spatial distribution of annual **PRECIPITATION** is mainly ruled by area topography. Precipitation also shows an altitude dependency, which is modified by local wind systems. Luff-lee-effects are evident at ridges transverse to the main wind direction (*PARLOW & ROSNER 1997*). An annual precipitation of 955 mm for the period 1961-90 was gauged in Freiburg, near the catchment outlet, whereas 1909 mm were gauged for the same period at the Feldberg (*FUCHS ET. AL. 2001*). The precipitation regime for the lower elevations shows a single maximum during the summer months caused by convective events. For elevations above 900 m a.s.l., even larger amounts of precipitation are recorded in summer due to a higher frequency of convective cells and thunderstorms. Nevertheless, in those altitudes the ratio of summer precipitation to total precipitation is smaller compared to lower elevations (*PARLOW & ROSNER 1992*). This is due to a secondary maximum during winter months that even exceeds summer precipitation at times. It is caused by advective precipitation that results in a continuous snow layer of more than 30 cm during an average of 60 days (*RIES 1992*). Therefore, snow precipitation adds up to two thirds of total precipitation in the elevated areas of the Black Forest (*PARLOW & ROSNER 1997*).

Mean annual **SUNSHINE DURATION** varies from 1800 hours in Freiburg at the border to the Rhine Valley to merely 1400 hours in the deep valleys of the Black Forest. Next to topography, sunshine duration is also dependent on predominant weather situations. Therefore, sunshine at the Feldberg summit is reduced by convective cloudiness in summer. In Freiburg, it is reduced by winter inversions with high fog. Thus, sunshine duration in winter is higher in elevated areas, whereas in summer it falls behind those of lower regions (*PARLOW & ROSNER 1997*).

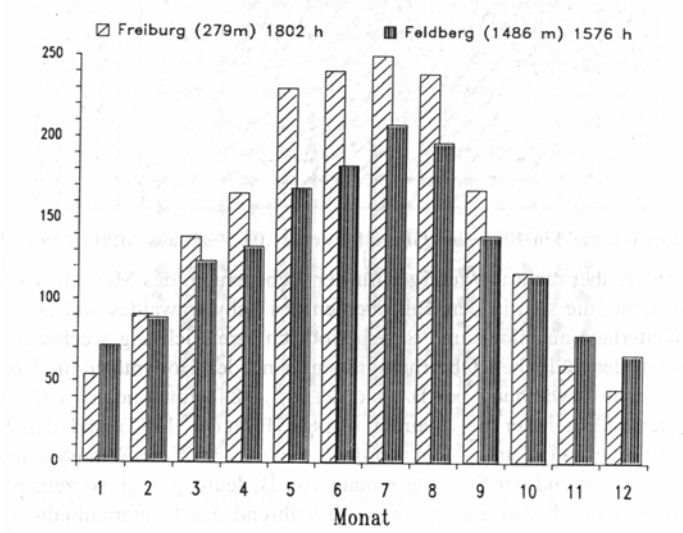

Figure 6.2: Seasonal vaiation of sunshine duration at the stations Feldberg and Freiburg (from Parlow & Rosner 1997)

The seasonal variation of sunshine duration at the stations Feldberg and Freiburg is displayed in Figure 6.3.

ATMOSPHERIC HUMIDITY shows a general increase with altitude. Inverse to air temperature, water vapor content shows a maximum in the morning at low temperatures and decreases towards the temperature maximum at noon. In addition, its daily periodicity is modified by topography.

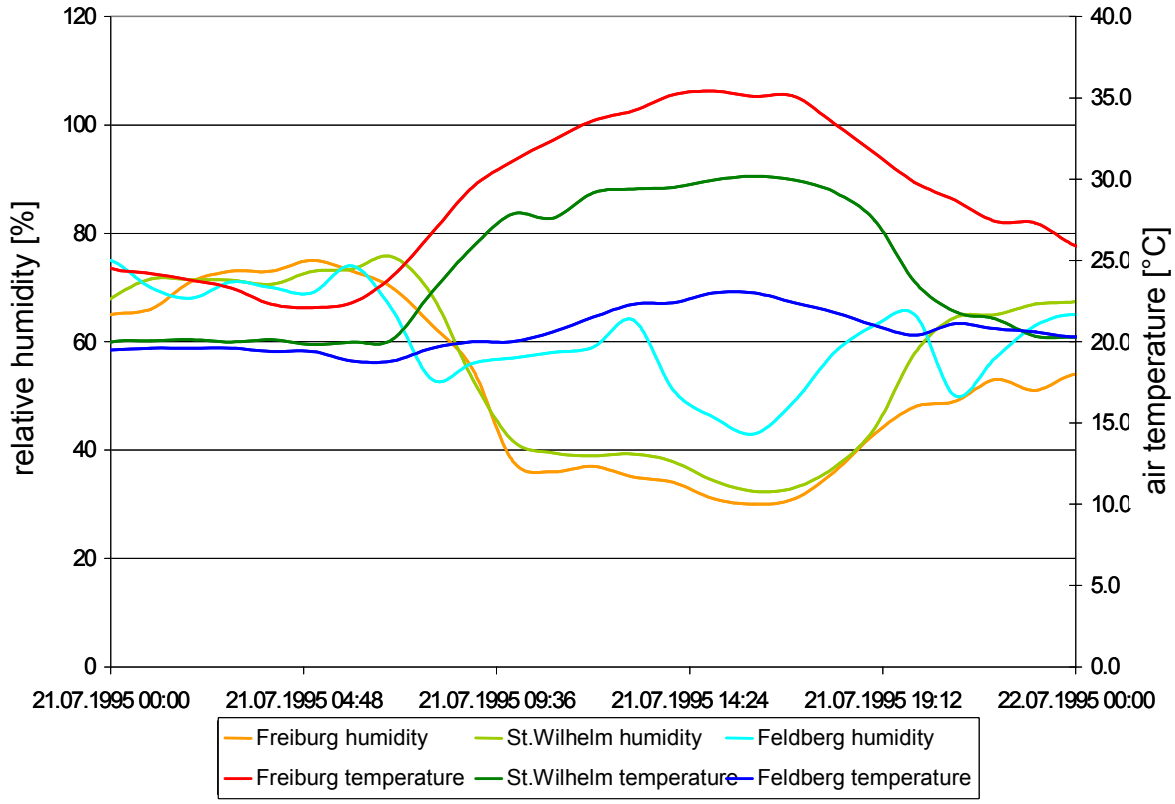

Figure 6.3: Air temperature and humidity for a representative summer day at the stations Freiburg (269 m a.s.l.), St.Wilhelm (765 m a.s.l.) and Feldberg (1486 m a.s.l.) (from Ott 2002)

6.1.3 Hydrogeology

The area of investigation can be divided into two major units:
The **BLACK FOREST BASEMENT** consisting of gneiss, anatexites, metatexites and diatexites. Because of their similar mineralogical composition, they are sometimes only specifiable by their genesis (*SAUER 1988*). A more or less homogeneous system of fractures, which is responsible for water transport, is assumed for all sorts of rock. With a void ratio of 0.1% to 2.1% hydraulic conductivity ranges from 10^{-10} to 10^{-5} m/s. As the extreme values equal those of a sandy aquifer and solid rock, this range indicates the great subsurface heterogeneity within the basement (*STOBER 1995*). In general, hydraulic conductivity is decreasing with depth. The crystal basement is covered by Quaternary sediments, predominantly consisting of rock debris and scree material. Three different layers can be distinct: A **BASE LAYER** with aligned rocks in a dense matrix, a **MAIN LAYER** with non-uniform embedding of rocks, and a **TOPSET LAYER** with spatially variable properties. For further reading cosult *UHLENBROOK* (*1999*), *REHFUSS* (*1990*) and *STAHR* (*1979*). In the topset layers, a high proportion of incoming precipitation is transferred to runoff components of different dynamics. Their hydraulic conductivity highly depends on grain size distribution and density within the layer. **HOLOCENE ALLUVIUM** of different composition and thickness can be found throughout the valley bottoms (*UHENBROOK 1999*).

The second hydrogeological unit is the **ZARTEN BASIN**. An important aquifer has developed in its Pleistocene and Holocene gravels. The Zarten Basin consists of a less permeable lower layer and an upper layer, where hydraulic conductivities range from $0.5 \cdot 10^{-4}$ to $40 \cdot 10^{-4}$ m/s. Losses from the rivers contribute 73% of groundwater recharge. 0.35 m^3/s of water is withdrawn from the groundwater for local water supply (*SCHREMPP 2004*). Another 0.46 m^3/s leave the catchment via underground flow across the watershed (*BOLD 2000*).

6.1.4 Landuse

More than 60% of the Dreisam catchment is covered with forests. Only 24% of the total catchment area is used for agricultural purposes, mostly intensive grassland farming. Less than 3% is covered with settlements, which are scattered in rural areas (*OTT 2002*).

6.1.5 Hydrology

Table 6.1: Runoff characteristics (from Ott 2002 after LfU 2000)

	Dreisam	Brugga	St.Wilhelmer Talbach	Zastlerbach	Rotbach	Wagensteig-bach
Easting	3417831	3421750	3420342	3424308	3425850	3425304
Northing	5317258	5311663	5307598	5310010	5312113	5314643
Time serie	1941-1996	1934-1994	1955-1994	1955-1994	1979-1992	1946-1994
HQ [m³/s]	155,28	33,61	11,6	24,37	45,0	24,6
MHQ [m³/s]	60,99	15,75	6,6	6,86	22,19	13,27
MQ [m³/s]	5,87	1,54	0,66	0,63	1,12	1,17
MNQ [m³/s]	0,45	0,37	0,13	0,13	0,15	0.11
NQ [m³/s]	0,025	0,19	0,07	0,06	0,09	0.01
MHQ [l/s·km²]	250	442	390	385	551	263
MQ [l/s·km²]	21,9	39,1	41,3	35	27	23
MNQ [l/s·km²]	2,07	9,03	7,92	7,3	2,2	2,2

Table 6.1 show the main values of hydrological statistics for gauging stations within the Dreisam catchment.

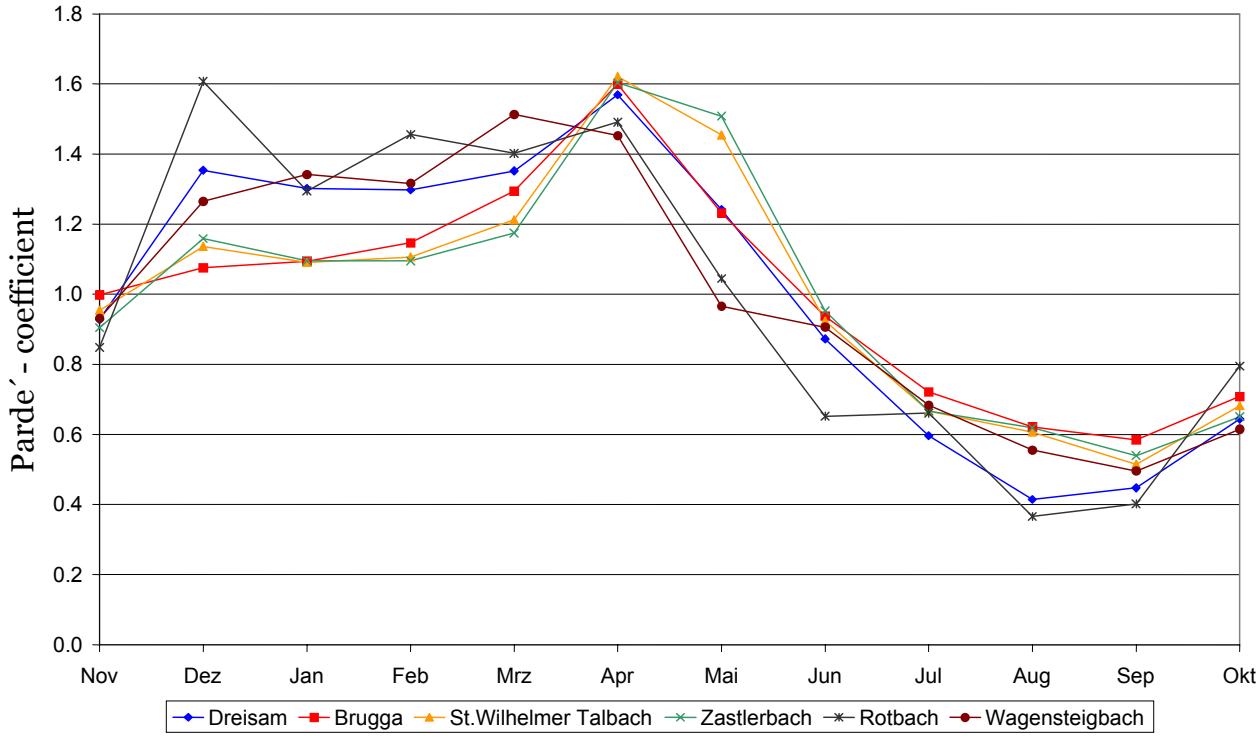

Figure 6.4: Runoff regimes of the Dreisam and its contributing streams (from Ott 2002)

The runoff regimes of the Dreisam and its contributing streams presented in Figure 6.4 show a clear minimum during the months August and September, caused by high evapotranspiration values. Besides the Rotbach, all streams show a runoff maximum in April and another lower peak in December. Therefore, these subcatchments can be classified by the nivo-pluvial regime type. Due to its runoff maximum in December and the lower peak in April, the Rotbach is better described by a pluvio-nival regime. In general, runoff maxima in spring can be explained by snowmelt, whereas the December maxima are caused by intrusions of warm air. These weather situations are often accompanied by steady rain also in elevated areas. Because of high soil moisture contents and rain-on-snow effects, these precipitation events can lead to serious floods (*UHLENBROOK ET AL. 2001*).

6.2 Methodology of oxygen-18 simulation

Since the model of solute transport was not designed for ^{18}O simulations in the first place, some considerations and modifications were necessary.

6.2.1 Basics

The model was applied to event-based simulation of the stable isotope oxygen-18 (^{18}O) in the Dreisam catchment. This natural tracer was used, because it can be considered a conservative substance by good approximation. Thus, no further chemical reactions had to be incorporated in the model. For the simulations of ^{18}O, data from selected events during the period 2001 until 2003 was used. This data was collected by *DIDSZUN* (*2004*) within

the scope of his Ph.D. thesis. Although the model itself calculates with different units (see chapter 6.2.3), all results are presented in the common δ-notation:

$$\delta^{18}O = \left(\frac{R - R_{St}}{R_{St}} \right) \cdot 1000 \qquad \textit{Eq. 6.2}$$

(*MOSER & RAUERT 1980*)

$\delta^{18}O$ [‰]
R: $^{18}O/^{16}O$ ratio in sample [-]
R_{St}: $^{18}O/^{16}O$ ratio in standard (V-SMOW) [-]

A standard deviation of 0.2‰ for the analysis with an isotope ratio mass spectrometer was determined by *DIDSZUN* (*2004*). For more details on sample analysis, see *DIDSZUN* (*2004*).

Even tough ^{18}O is identical to ^{16}O in its chemical behavior some distinctions have to be considered due to their different physical properties. Because of their different relative atomic masses, the isotopes are subject to fractionation processes during phase transitions. According to *KENDALL & MCDONNEL* (*1998*), fractioning leads to numerous general patterns in the spatial and temporal $\delta^{18}O$ -distribution of precipitation events. The main effects of fractionation are:

- Continental effect
- Elevation effect
- Latitude effect
- Amount effect
- Temperature effect
- Season effect

A general altitude dependency is the most prominent effect on the distribution of $\delta^{18}O$-values within a meso-scale river basin (*MOSER & RAUERT 1980*). Nevertheless, altitude dependency is only well observed at the windward sides of mountain ranges (*KENDALL & MCDONNEL 1998*). On a single-event basis however, those effects are often superimposed by unique event characteristics. *"Extreme differences have been observed in the stable isotopic composition of precipitation both during the course of a single storm and between storms."* (*KENDALL & MCDONNEL 1998, P.103*) On this account, no general elevation gradient was added to the regionalization of $\delta^{18}O$-values. The temporal variability (intra-storm-variability) was captured by high-resolution data sampling.

6.2.2 Data sampling

As can be seen from Map 6.1 three observation stations for precipitation input were established throughout the catchment. For each event, $\delta^{18}O$ was measured in two of these locations. The arithmetic average of their measurements was transferred to the whole catchment input (red dots in Figure 6.5). Samples were accumulated up to a certain level and then bottled. Thus, measurements represent bulk mean values for the preceding time intervals (light blue bars in Figure 6.5). Because sampling was carried out in different irregular intervals, values in between those intervals were linearly interpolated before averaging.

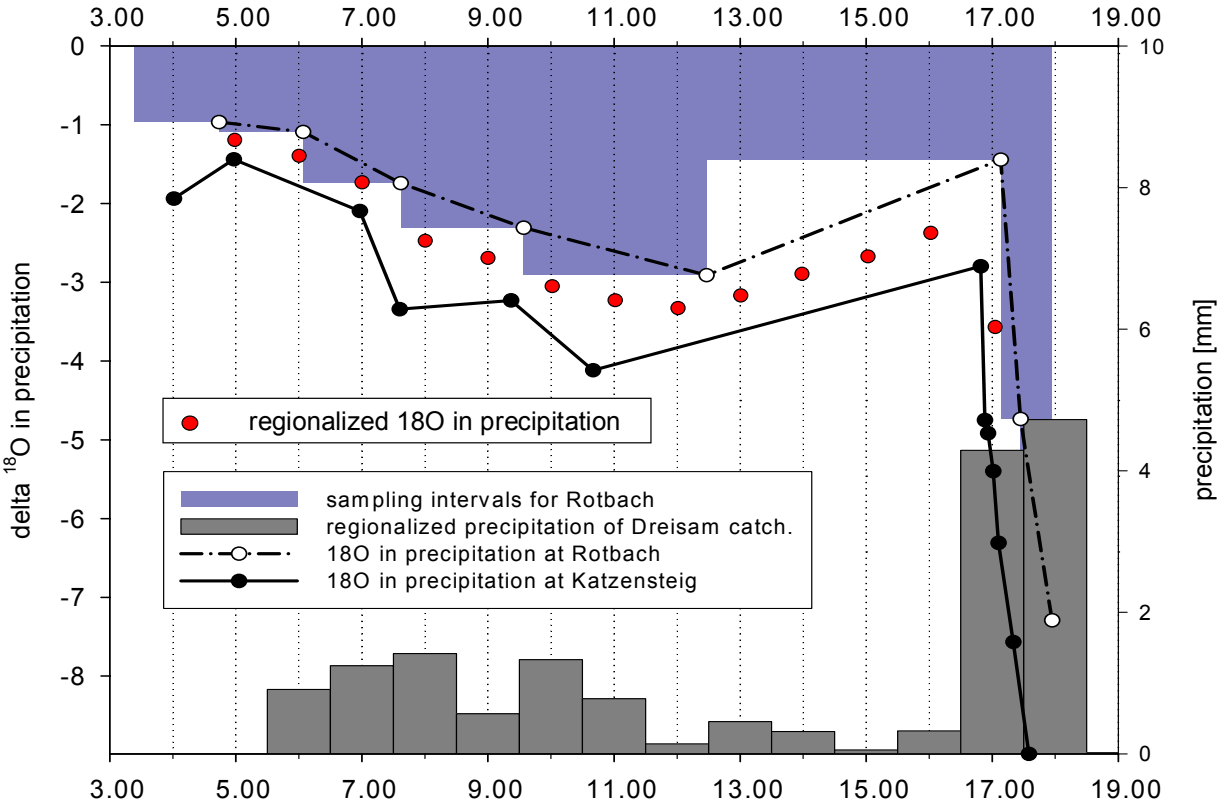

Figure 6.5: Input regionalization for ^{18}O (exemplary)

6.2.3 Unit conversion

Due to model limitations, a unit conversion from the δ-notation to number of ^{18}O molecules per m³ of water had to be performed for the processing of ^{18}O data. Since the water volume itself consists to a considerable extent of ^{18}O, this fact has to be regarded in the conversion calculations. In natural waters, the ratio of ^{18}O /^{16}O is in the range of 1:500 (*MOSER & RAUERT 1980*). This ration can be calculated from the $\delta^{18}O$-value using the following formula:

$$R = 1 + \frac{1}{\frac{\delta O_{18} \cdot R_{St}}{1000} + R_{St}} \qquad \textit{Eq. 6.3}$$

(after *MOSER & RAUERT 1980*)

R: ^{18}O /^{16}O ratio in sample [-]
$\delta^{18}O$: delta ^{18}O notation [‰]
R_{St}: ^{18}O /^{16}O ratio in standard [-]

The total number of ^{18}O molecules per m³ water can be calculated with:

$$N_i = \left(\frac{\frac{N_A}{R}}{20{,}016 \cdot \left(\frac{1}{R}\right) + 18{,}016 \cdot \left(1 - \frac{1}{R}\right)} \right) \cdot \frac{\rho \cdot 1000000}{10^{25}} \qquad \textit{Eq. 6.4}$$

N_i: number of particles per m³ [10^{25}/m³ of water]
N_A: Avogadro's number [-]
R: ^{18}O /^{16}O ratio in sample [-]
ρ*: density of water at 10°C (0.997 kg/l)
20.016: average molecular mass of $H_2{}^{18}O$ [g/mol]
18.016: average molecular mass of $H_2{}^{16}O$ [g/mol]

In the equation above the total number of molecules was divided by 10^{25}, in order to obtain numbers that are more manageable. After simulations, all results were transferred back to the $\delta^{18}O$-notation.

6.2.4 Evapotranspiration of ^{18}O

Common solutes such as salts or artificial tracers are unaffected by evaporation and transpiration. Because water is reduced, those solutes are enriched in the fluid phase, and therefore concentrations rise. However, volatile solutes such as ^{18}O are subject to evapotranspiration. Thus, ^{18}O loads are reduced by evapotranspiration even tough to a minor degree as ^{16}O. This leads to an enrichment of ^{18}O in the fluid phase (see chapter 6.2.1). Since event-based simulations evapotranspiration plays a secondary role, the solute model was simplified by neglecting fractionation. A proportionate amount of ^{18}O was subtracted from the solute storages in full accordance to equation 5.3. As a result, loads of ^{18}O within the solute model were reduced by evapotranspiration, but the ratio of ^{18}O /^{16}O and therefore δ-values remained unaffected.

6.2.5 Evaluation of ^{18}O simulations

Due to short simulation periods, little gauged data and large analytic uncertainties no statistical analysis with measures of goodness was accomplished for the simulated events. Thus, evaluation is restricted to a visual, qualitative assessment.

6.3 General comments on simulation uncertainties

The accuracy of the model results is determined by the accuracy of the input data and the degree to which the model structure correctly represents hydrologic processes (*DEVRIES & HROMADKA 1993*). *CHOW ET AL. (1988)* distinguish three categories of uncertainty in hydrologic modeling:

NATURAL UNCERTAINTY arises from the random variability, which is inherent in natural hydrologic systems. This variability cannot be captured by deterministic models (butterfly effect).

MODEL UNCERTAINTY describes how accurately the natural processes are represented by equations in the mathematical model.

PARAMETER UNCERTAINTY reflects inaccuracies of model parameters. As most parameters are determined by calibration, calibration and parameter estimating methods are crucial for parameter uncertainties.

MELCHING (1995) describes a fourth source of model uncertainty:

DATA UNCERTAINTY includes systematic and random errors inherent in the input data. Because regionalization methods fail with insufficient or non-representative input data, this uncertainty is assigned to data uncertainties.

Natural uncertainties influence all aspects of hydrologic modeling since they affect the input data, model parameters and model structure (*MELCHING 1995*). Therefore, no distinction can be made between natural uncertainties and other kinds of simulation uncertainties. The intended purpose of model applications was the assessment of model uncertainties. Since a clear distinction between the different kinds of uncertainties is impossible, this goal can only be achieved with a limited data- and parameter uncertainty. A discussion of parameter uncertainty is given in chapter 6.5.2. Data uncertainty and model uncertainty are discussed in the corresponding chapters of simulated events.

6.4 Initialization procedure for event-based simulations

In order to yield realistic storage levels in the water system and the solute model initialization is of great importance. During an initialization run, the model's storages are adjusted to pre-event conditions of moisture and solute content. Therefore, continuous timeseries prior to the simulation periods would have been highly desirable. Since only short data windows for solute and climatic input were available, the generally suggested initialization procedure (see chapter 3.13) had to be modified. Due to the special data structure with short simulation windows, initialization was performed prior to the actual simulation in the same model run.

6.4.1 Initialization of water storages

For the initialization of water storages, the climatic data windows were inserted into existing timeseries that have been processed in a former application of *TAC*[d] (see Figure 6.6).

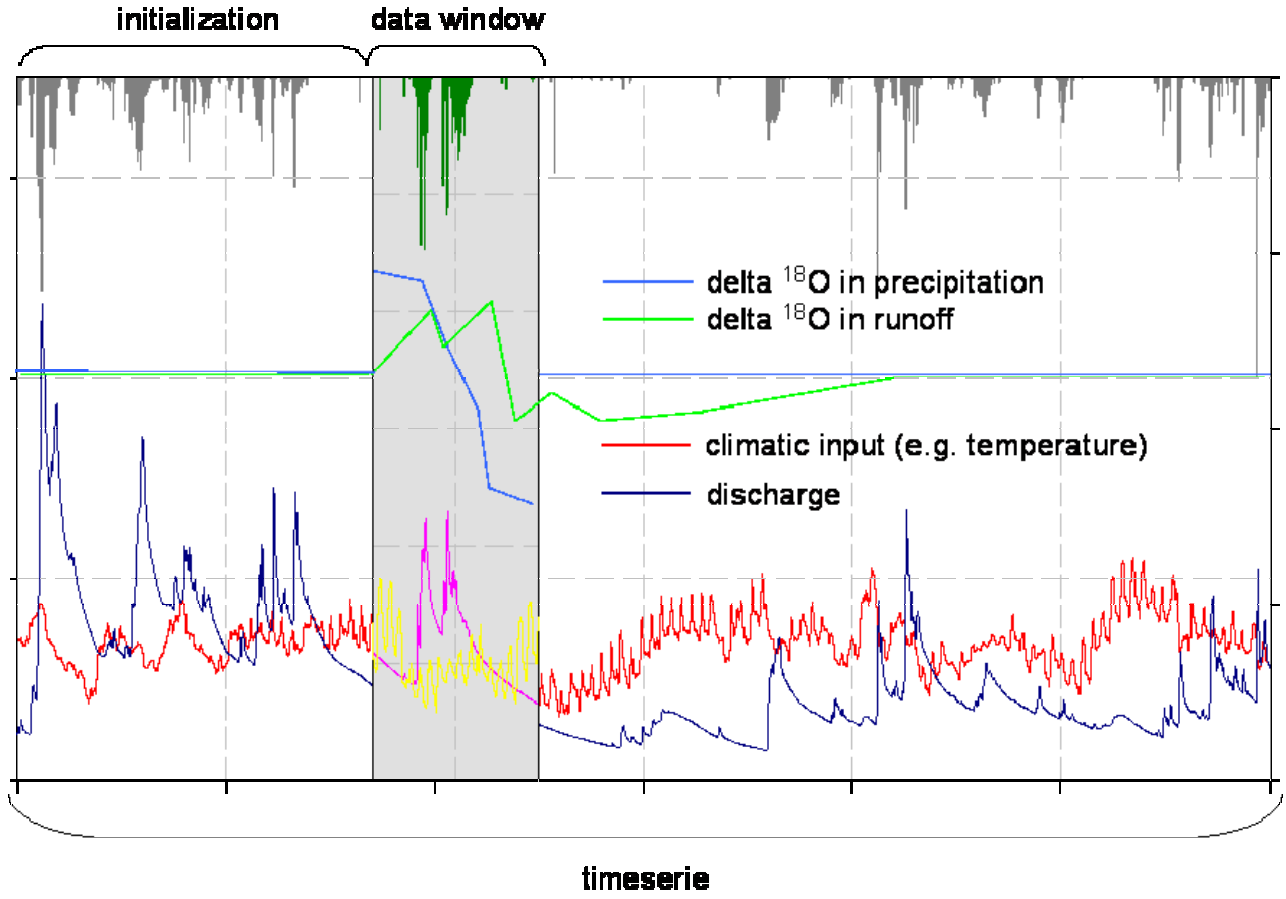

Figure 6.6: Insertion of data window

The time step of insertion was selected regarding the following criteria:

- Runoff:
  The data windows were inserted at a time when discharges of the timeserie matched the discharge at the beginning of the data window.
- Season:
  The time of data insertion was chosen in accordance to the season of the events (early summer).
- Runoff of subcatchments:
  For the simulations of the Dreisam catchment, also runoff of the subcatchments was regarded, as far as possible
- Pre-event situation:
  The general state of the catchment prior to the event was examined, e.g. whether the event took place after a recession or wetting phase.

The used timeseries cover a period from 1994 until 1999. With this procedure, initial water storages are not filled by the preceding climatic input. In fact, they are transferred from weather situations, which have produced a similar discharge in the past. This workaround can be justified by regarding the discharge as an integrative piece of information for moisture conditions within a catchment.

For all event simulations, the data windows were inserted at several different spots of the timeserie. Thus, simulations were accomplished under different antecedent moisture conditions within the catchment. Hence, it was possible to evaluate the effect of moisture conditions on solute transport. The different simulation runs are identified by a capital letter after the simulation name.

6.4.2 Initialization of solute storages

In addition to water storages, also solute storages have to be initialized. For this purpose, during the initialization period $\delta^{18}O$-values in precipitation were set to the first measured value in runoff (see Figure 6.6). This was done for each subcatchment individually. As a result, all water within a subcatchment has the same $\delta^{18}O$-value at the start of the actual simulation. The $\delta^{18}O$-value in Ebnet results from a combination of all subcatchment runoffs and the stream input from the residual Dreisam catchment (white in Map 6.1). Therefore, $\delta^{18}O$-values in precipitation of the residual Dreisam catchment had to be estimated in order to obtain the first measured value in Dreisam runoff.

6.4.3 Discussion of initialization

As mentioned before the applied initialization procedures are only a necessary makeshift in order to cope with the unsatisfactory data situation. For a correct initialization of both, the water and the solute model, continuous timeseries for climatic input data as for ^{18}O input with a high spatial resolution would be necessary. Because it is almost illusionary to fulfill these demands, it makes sense to test the model with the described workaround. The initialization method leads to a hydrological situation at the start of simulations that is similar to the one of the simulated period. Nevertheless, it is only an estimation for water contents and does not take the singularity of events into account. To choose an appropriate time for inserting the data window into the existing timeserie lies within the responsibility of the modeler.

The initialization of solute storages with constant concentrations in precipitation leads to a homogenization of vertical and horizontal solute concentrations within subcatchments. As storage contents are composed of waters of different age resulting from precipitation with varying ^{18}O concentrations, a very inhomogeneous spatial distribution of ^{18}O concentrations has to be expected in a natural system. The consequence of simplified initialization procedures on simulation results are very hard to assess.

6.5 Calibration of water fluxes

Little effort was put in the calibration of water fluxes. Despite the modifications, only about 10 additional runs were carried out for recalibrating the water model. Starting from the parameter table used by a previous model application (*OTT 2002*), only those parameters were varied, which proved sensitive in the diploma thesis from *SIEBER* (*2003*). The selected parameters were varied manually in a plausible range. The model was calibrated to the same period of 4560 time steps (7.2.1997 1:00 until 16.8.1997 1:00) that was used by *OTT* (*2002*). Therefore, a direct comparability of measurements of goodness was guaranteed. Automated evaluation was carried out using the new evaluation model. Prior to each calibration run, the model was initialized with the preceding year of climatic input and the modified parameter table.

6.5.1 Results of Recalibration

Table 6.2 lists the parameters that were varied during recalibration as well as their model efficiency and logarithmic model efficiency for discharge simulations of the Dreisam.

Table 6.2: Results of model recalibration

PARAMETER	ORIGINAL VALUE	VARIED VALUE	R_{EFF}	$R_{LOG\ EFF}$	R^2
pGW_K	0.002	0.005	0.865	0.821	0.880
pMTD	30	20	0.849	0.801	0.866
pDI_K_u	0.017	0.02	0.861	0.813	0.874
pDI_K_l	0.0025	0.008	0.792	0.772	0.834
pCFMAX	0.15	0.1	0.847	0.804	0.865
pFLI_K_u	0.2	0.1	0.853	0.801	0.876
Original parameter set from prior application			0.852	0.807	0.871
Original model and parameter set from prior application			0.874	0.748	0.864

The modification of the pGW_K parameter shows the best evaluation results. Thus, *pGW_K* was modified for the recent applications. This parameter determines the storage coefficient of the groundwater storages. The complete parameter table is shown in Appendix A.

6.5.2 Discussion of recalibration

As the parameter uncertainty is mainly determined by the applied calibration procedure, calibration plays a main role in the uncertainty assessment of model. An item of review is the fact that calibration was only carried out for 4560 time steps. Thus, it may be doubted that the achieved parameter set yields representative values for the following 31391 time steps. Nevertheless, the applied approach can be justified as follows:

- Calibration was carried out in a period from February until August. All events took place between Mai and July. Therefore, the calibration period covers the most

important runoff situations during spring and early summer, even tough it cannot be guaranteed that this calibration period is also representative for the simulation periods.
- Due to long computation times, it was impossible to calibrate the model to the full period of 31391 time steps.
- It could be shown that acceptable results are achieved also with a not extensively calibrated model.
- The model was applied to comparatively small runoff events. A logarithmic model efficiency of 0.821 proves good results in low water conditions.

As can be seen from Table 6.2, model efficiency (R_{eff}) is slightly worse for the revised model version, than for the model applied by *OTT* (*2002*), although the same parameter table was used. This can be explained by the modifications that were carried out in the revised version.

Already by manually calibrating in view runs, it was possible to find a parameter set with improved logarithmic model efficiency (R_{logeff}) and coefficient of determination (R^2). With extensive, automated calibration, better values for the measures of goodness can be expected.

6.6 Solute translation in the river network

6.6.1 Results of solute translation

In the following, solute translation means translation within the river network only. Mean solute translation times are listed below for two different runoff situations at the gauging station Ebnet. Translation times reflect the mean time between solute entry into the river network of a subcatchment and its arrival at the associated gauging station.

Table 6.3: Solute translation times

CATCHMENT	DISCHARGE OF DREISAM IN EBNET	NUMBER OF STREAM CELLS	SOLUTE TRANSLATION TIMES	
Dreisam	0-5 m³/s	2769	29244 s	8.12 h
	2-8 m³/s	2769	23501 s	6.53 h
Brugga	0-5 m³/s	477	5275 s	1.47 h
	2-8 m³/s	477	4421 s	1.23 h
Rotbach	0-5 m³/s	367	7441 s	2.07 h
	2-8 m³/s	367	5631 s	1.56 h
St. Willhelmer TB	0-5 m³/s	164	2166 s	0.60 h
	2-8 m³/s	164	1852 s	0.51 h
Zastler TB	0-5 m³/s	186	1727 s	0.48 h
	2-8 m³/s	186	1453 s	0.40 h
Wagensteigbach	0-5 m³/s	487	7218 s	2.01 h
	2-8 m³/s	487	5685 s	1.58 h

6.6.2 Discussion of solute translation

As described in chapter 5.6 the implementation of the *kinematic*-function into solute transport has yet not been realized. Thus, the present module can only be regarded as a tool for estimating mean solute translation times. A better estimation would be achieved by calculating the spatial average of translation times with weighted inputs of solute into the stream channels during the events. The spatial distribution of input signals into the river network and their superposition at the outlet is disregarded in this method.

However, it has been decided not to put further effort in a more sophisticated workaround. Instead, investigations were pushed towards a satisfactory implementation of the *kinematic*-function. The achieved translation times are well within the expected range for the Dreisam catchment under low-water conditions.

6.7 DS 05_02

6.7.1 Characterization of DS 05_02

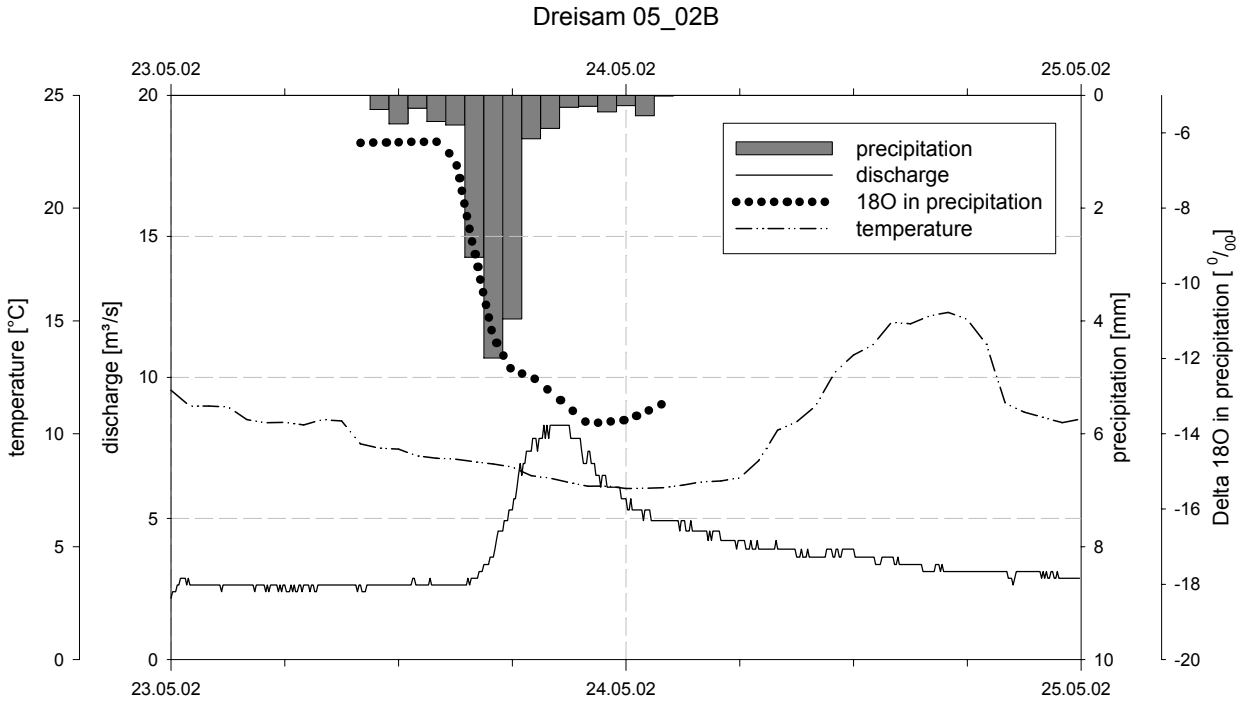

Figure 6.7: Event characteristics DS 05_02

Figure 6.7 shows the main characteristics of the event in May 2002. The storm is characterized by one distinct maximum in precipitation intensity of 4.6 mm/h and only three hours of more than 2.5 mm/h. It produces an increase in discharge at the gauging station Ebnet of about 6 m³/s up to a maximum of 8.3 m³/s. The $\delta^{18}O$-values in precipitation show a decrease at the time of maximum intensities from -6‰ to about -14‰. Therefore, precipitation produces clear input signals for the solute model.

PRECIPITATION data was available from the stations Freiburg, Zastler, Conventwald, Breitnau, Hofsgrund, Schauinsland and Rotbach (Falkensteig). **TEMPERATURE** gradients were calculated by least square fitting from the stations Zastler, St.Wilhelm and Schauinsland. Thus, no inversion weather situations could be considered. **WIND** data was available from Schauinsland and St.Wilhelm. The average of those two stations was transferred to all other stations before regionalization. No data for **SUNSHINE DURATION** was available. Therefore, this data was created artificially by setting sunshine duration to 0.5 at daytime if no precipitation was measured at the station. In case of precipitation, it was set to zero. **ATMOSPHERIC HUMIDITY** was calculated from the three stations St.Wilhelm, Zastler and Schauinsland. The average of these stations was assigned to all other humidity stations throughout the catchment. $\delta^{18}O$ was measured in the two stations Hofsgrund and Katzensteig, near St.Wilhelm and then regionalize with the procedure described in 6.2.

6.7.2 Results of DS 05_02

DREISAM:

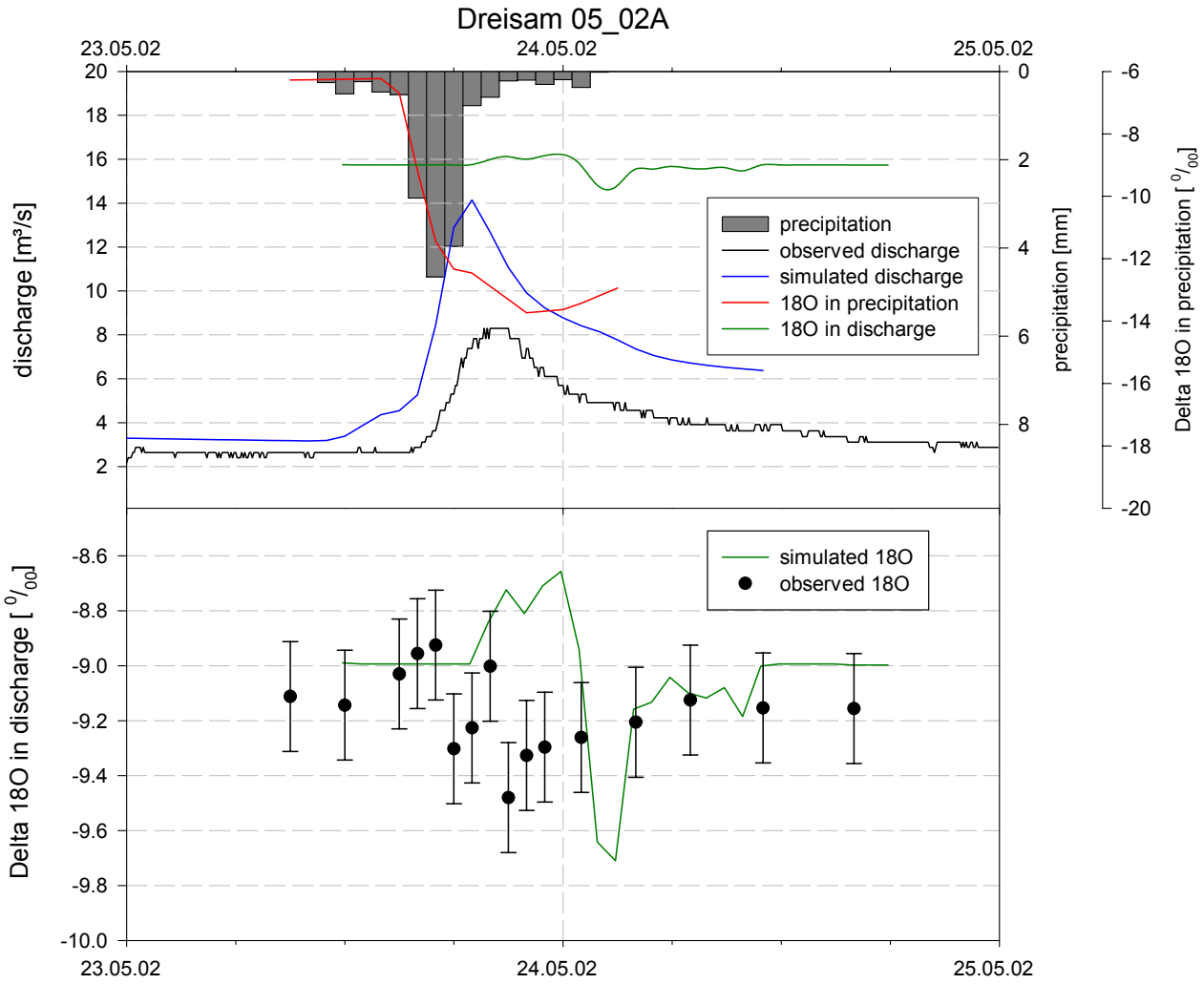

Figure 6.8: Results of DS 05_02 A; Dreisam

In simulation 'A' the modeled runoff (blue) was significantly overestimated (ca. one and a half times the measured runoff). The regionalized $\delta^{18}O$-values in precipitation (red) show a decline from -6.2‰ to -13.4‰ in the middle of the precipitation event. The simulated δ-values in the Dreisam discharge are shown in green. As can be seen from the upper part of Figure 6.8, the δ-values in precipitation cross the values in discharge. Consequently, the δ-values in discharge first rise to a maximum of -8.66‰ and then decline down to -9.71‰ before they level off at about -9‰ (lower part of Figure 6.8). The measured δ-values in the Dreisam discharge with their estimated standard deviation of analytical accuracy (error bars) are shown as black dots on the lower part of Figure 6.8. These values range from -8.92‰ to -9.48‰.

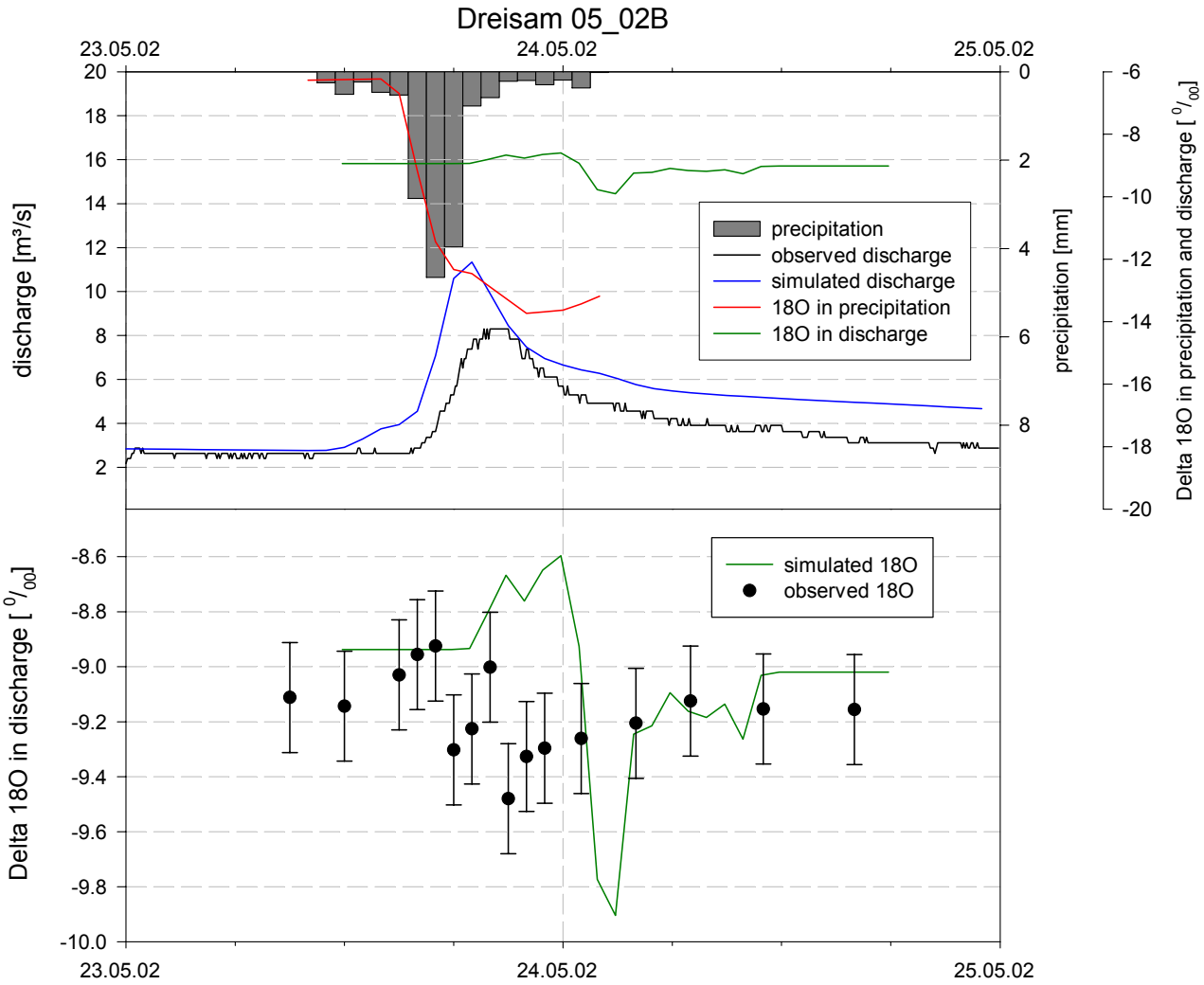

Figure 6.9: Result of DS 05_03 B; Dreisam

Figure 6.9 (simulation 'B') shows the same simulation as DS 05_02 A with a different initial moisture content. The difference between modeled and measured Dreisam discharge is not as eminent as in simulation 'A'. The simulated $\delta^{18}O$-values range from -8.60‰ to -9.90‰.

In both simulations, the modeled fluctuations of $\delta^{18}O$ exceed the variability of measurements. In addition, the general dynamics of modeled values are delayed for about three hours in respect to the observed dynamics. Comparing the $\delta^{18}O$ -values of both simulations, their general dynamics are the same with more pronounced fluctuations in run 'B'.

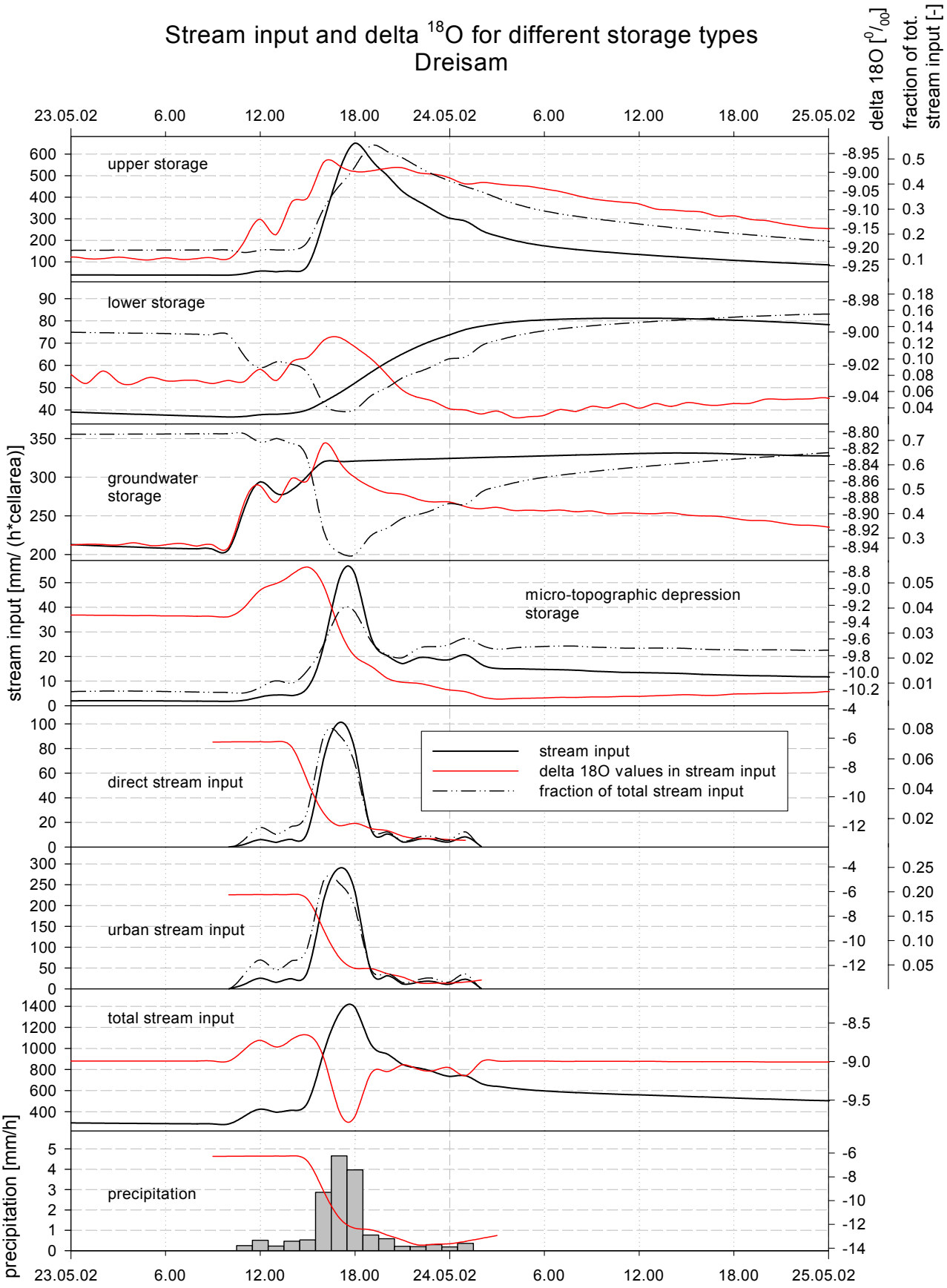

Figure 6.10: Stream input (black), fraction of total stream input (dash-dotted) and $\delta^{18}O$-values (red) from different storage types; DS 05_02 A; Dreisam catchment

Figure 6.10 shows the amount of water entering the stream channel (*sIntoStream*) from different storage types in millimeters per cellarea and their $\delta^{18}O$-values for the simulation DS 05_02 A. In order to assess the relevance of storages types to total stream input, their weight was plotted in addition to absolute input and $\delta^{18}O$-values. The weight of a storage type is determined by its contributing fraction of total stream input.

A major part of stream input during the event originates from upper storage boxes (*sUS_box*, ca. 650 mm). It has the typical shape of a Weibull curve. $\delta^{18}O$-values show one rise towards values of -8.96‰ before declining smoothly towards initial values (-9.23‰).

The stream input from lower storages (*sLS_box*) contributes at the most 80 mm to total stream input. Thus, they are comparatively insignificant for the over-all catchment reaction. Compared to the upper storage their reaction is strongly damped. $\delta^{18}O$ shows again a peak at the same time as for the upper storage but then values decline beyond initial values. Their range is from -9.0‰ to -9.6‰.

Groundwater storages (*sGW_box*) deliver the second larges part of total stream input during the event. It rises from 210 mm to a plateau of up to 330 mm were it remains for the rest of the simulation. Before and after the event groundwater storages supply 60 to 70% of stream input. $\delta^{18}O$-values follow the first rise in stream input by forming a pointed peak before they slowly decline towards their initial values.

Storages of micro-topographic depressions (*sMTD_box*) in areas with saturated overland flow, deliver a maximum of 57 mm to total stream input. Their maximum contribution ranges at about 4% of total stream input. The input curve reflects the dynamics of precipitation input with only little retention. After the event, stream input remains at a plateau of about 10 mm for the rest of the simulation period. $\delta^{18}O$-values follow closely the dynamics of ^{18}O signature in precipitation input. This results in a first peak of -8.8‰ and a following decline to -10.3‰.

As runoff components from urban (*sUrbanIntoStream*) and open water (*sDirectIntoStream*) areas are a certain fraction of precipitation with only minimal dilution and retention in the interception storages, those components follow precipitation input in discharge as in $\delta^{18}O$-values. Both components together (in the following called “direct runoff components”) contribute at the most 400 mm to stream input. This is about 3% of total stream input.

Total stream input (*sIntoStream*) results from a superposition of runoff curves from all participating storage types. Thus, $\delta^{18}O$-values in total stream input reflect an average value over all storage types.

BRUGGA:

Figure 6.11 shows the results of the simulation run DS 05_02 A for the Brugga subcatchment.

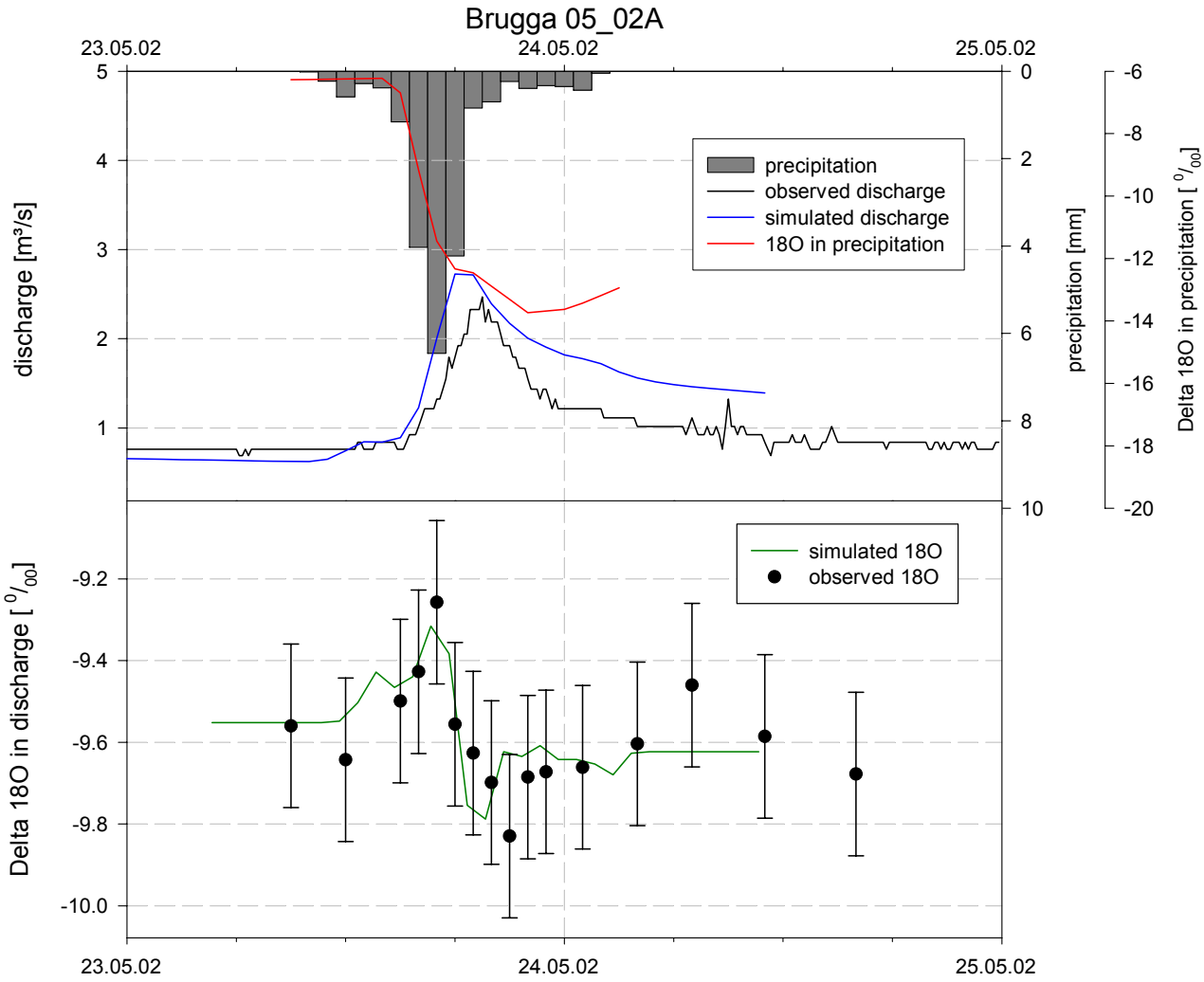

Figure 6.11: Result of DS 05_03 A; Brugga

The discharge is only slightly overestimated. Precipitation regionalization leads to maximum intensities of about 6.5 mm/h. Simulated $\delta^{18}O$-values ranging from -9.32‰ to -9.79‰ are well within the analytic accuracy for all conducted point measurements.

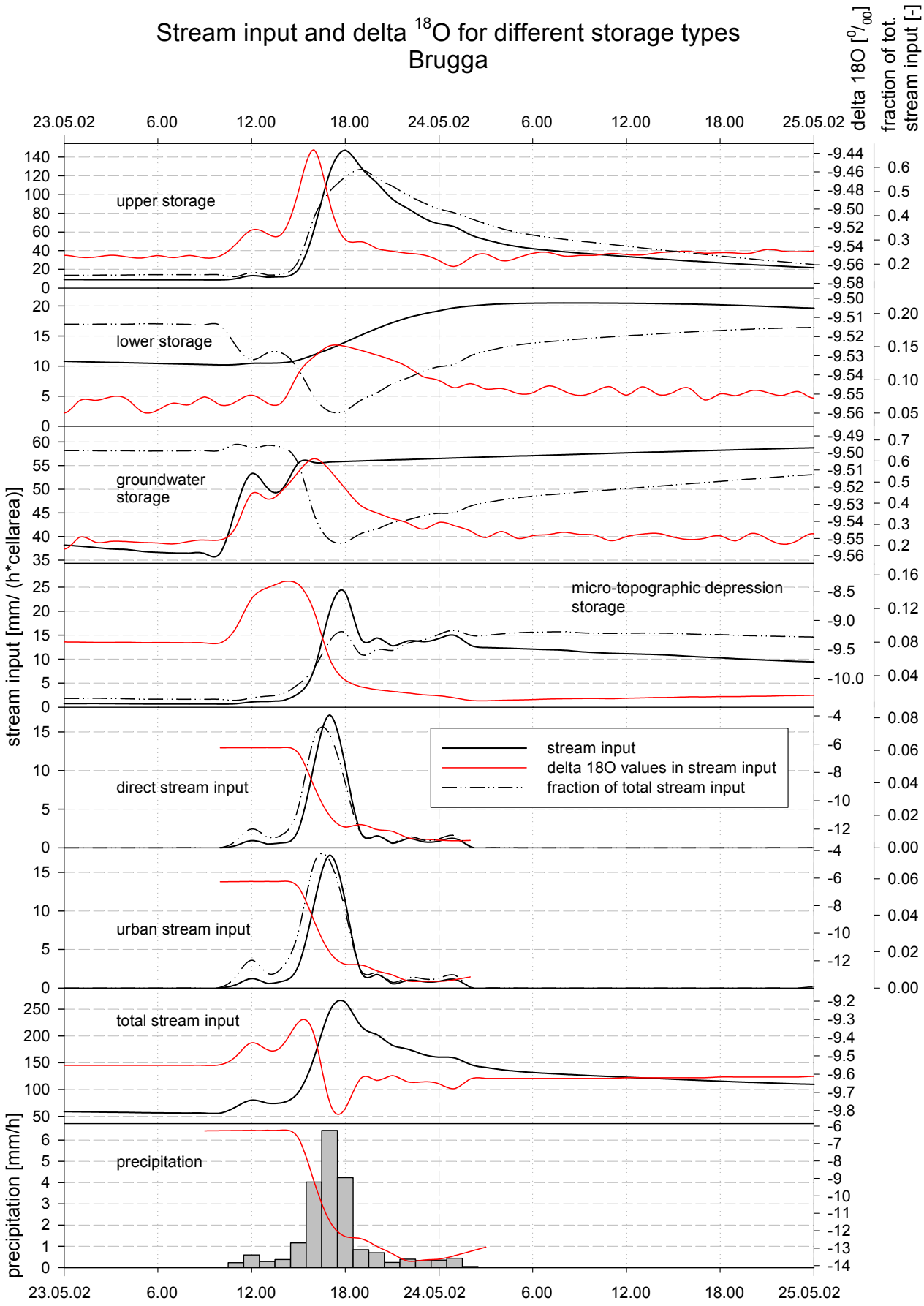

Figure 6.12: Stream input (black), fraction of total stream input (dash-dotted) and $\delta^{18}O$-values (red) from different storage types; DS 05_02 A; Brugga subcatchment

Figure 6.12 is equivalent to Figure 6.10 except that results are displayed for the Brugga subcatchment.

$\delta^{18}O$ in the upper storages shows only variations of 0.14‰. Their maximum (ca. -9.44‰) precedes the maximum contribution of water to stream input (ca. 60%).

$\delta^{18}O$-values of stream input from lower storages only varies in the range of 0.05‰. In addition, their contributing fraction never exceeds 20%.

At the beginning of the event contributions of groundwater storages range between 60% and 70% but decrease in the course of the event as runoff from upper storages rises. Also here variations in $\delta^{18}O$-values are small compared to fluctuations in total discharge.

$\delta^{18}O$ variations in input from micro-topographic depression storages are significantly higher (ca. -8.3‰ to -10.5‰). Nevertheless, their runoff contribution never exceeds 10%.

Direct stream input from open water areas together with urban runoff reach a maximum runoff fraction of 16‰. However, their isotope signature ranges from ca -6‰ at the beginning of the event to ca. -13‰ at the end.

6.7.3 Discussion of DS 05_02

DREISAM:

- Initialization (antecedent moisture condition):

The comparison of the two simulations with same data input but under different antecedent moisture conditions (DS 05_02 A, DS 05_02 B) demonstrates the importance of initialization. The significant overestimation of discharge in 05_02A indicates unrealistic high moisture contents in the initialization period prior to the event. Under wetter conditions (DS 05_02 A) mixture of event water with larger amounts of pre-event water takes place. Consequently, values of $\delta^{18}O$ in precipitation input produce are more damped output signal in runoff. As solute storages are initialized with constant concentrations of $\delta^{18}O$, the over-all reaction stays the same. Antecedent moisture conditions, of course also affect runoff simulations. The example shows that despite worse runoff simulations (overestimation), ^{18}O simulations are better (smaller fluctuations) in DS 05_02 A. Therefore, drier antecedent moisture conditions in 05_02B lead to smaller runoff with a higher contribution of event water. Therefore, variations in $\delta^{18}O$ are more accentuated.

- Precipitation regionalization:

Uncertainties in precipitation regionalization and $\delta^{18}O$ input regionalization also have to be considered. With only seven precipitation stations, regionalization using a wind and elevation corrected inverse distance method can lead to inaccurate area precipitation. An overestimated area precipitation would result in an overestimated fraction of event water

in stream discharge, which would then lead to the observed overestimated fluctuations of ^{18}O.

- $\delta^{18}O$ regionalization:

Due to the distinct heterogeneity of $\delta^{18}O$ in precipitation, it cannot be expected to cover its spatial distribution in the entire Dreisam catchment with only two measurement stations. Further uncertainties arise from the fact that these stations are located in similar altitudes and the same sector of the catchment. This impedes also analysis of a general altitude dependency. Hence, differences in measured and observed values of $\delta^{18}O$ in river discharges can also result from a failure of $\delta^{18}O$ regionalization.

- Model uncertainties (immobile phase, solute transport in the river network):

In addition, model uncertainties have to be considered.
First, equalization of solute concentrations between mobile and immobile domains is not implemented in the model. As these reactions lead to a damping effect on $\delta^{18}O$-values in discharge, their neglect results in an overestimated sensitivity towards variations in ^{18}O input (see chapter 6.8.3 Brugga).
Second, as solute concentrations within a natural river are subject to dispersion and diffusion, fluctuations of solute concentrations in stream input are damped by channel transport. In the presented procedure of solute transport, these effects are disregarded enhancing the overestimation of $\delta^{18}O$ fluctuations. The time lag of three hours between observed and measured dynamics can be assigned to the simplified routing of solute in the river network and the parameter, which accounts for wave celerity (solute velocity = 3/5 wave celerity from kinematic wave routing routine) .

Figure 6.10 can be interpreted in the following way:
During the event, the influence of upper storages rises until they supply more than 50% of total stream input. At that time, $\delta^{18}O$ ranges at values of about -9.0‰. Thus, $\delta^{18}O$ variations in total discharge are not mainly determined by the upper storages. Since lower storages never exceed a contribution of 16‰, and their $\delta^{18}O$ shows no dramatic variations they can be regarded as insignificant for fluctuations of $\delta^{18}O$ in total discharge. Groundwater storages show an approximately inverse contribution characteristic compared to the behavior of upper storages. At the beginning of the event, their contribution is still about 70%, although $\delta^{18}O$-values are already elevated to -8.85‰. Consequently, groundwater storages are involved in the rise of $\delta^{18}O$ in total stream input in the beginning of the event. In the further course of the event, the importance of groundwater storages is pushed back until they regain their rank after the event. When micro-topographic depressions reach their maximum fraction of about 5%, they have $\delta^{18}O$-values of about -9.8‰. Therefore, this component contributes mostly to the decline of $\delta^{18}O$ in total stream input.

Even though fractions of stream input from urban and open water areas are low (maxima of 25% and 8%), those components dominate fluctuations of $\delta^{18}O$ in stream input because

of their undiluted contribution of precipitation water. In the early stages of the event, they add high $\delta^{18}O$-values to the stream input from groundwater storages. When they reach their maximum contributions, those components supply water with $\delta^{18}O$-values of -10‰ to – 13‰. Therefore, the decline of $\delta^{18}O$ in total stream input can be nearly exclusively accredited to urban and direct runoff components.

BRUGGA:
Although slightly overestimated, the measured runoff dynamics are well reproduced by the simulated discharge. This indicates an adequate precipitation regionalization under realistic antecedent moisture conditions. With a comparatively good data basis for regionalization of climatic input and ^{18}O-values, data uncertainties for this subcatchment are small compared to the whole Dreisam catchment. As simulated $\delta^{18}O$ plots within the confidence interval of measurements, model uncertainties are not evident. Short distances from the catchment's boundaries to the outlet make solute translation within the river network less important.

The results of Figure 6.12 clearly indicate the dominance of direct runoff components on $\delta^{18}O$ signature in the Brugga discharge. Although their contribution to stream input is small, these components mainly consist of undiluted event water. Together with the micro-topographic depression storage, urban runoff and stream input from open water areas are responsible for fluctuations of ^{18}O in total stream input. The ^{18}O peak in stream input from upper storages can be explained by the initially high $\delta^{18}O$-values in precipitation. When this event water enters the storages, it leads to a strong increase in $\delta^{18}O$. This effect is amplified by low water contents within the upper storages and thus a high ratio of event water. In the course of the event $\delta^{18}O$-values in precipitations drop and more and more water with low $\delta^{18}O$ enters the upper storage system. When early and late precipitation components mix, they compensate their different $\delta^{18}O$-values. Consequently, $\delta^{18}O$ is decreasing towards its initial values during the second half of the precipitation event. $\delta^{18}O$ fluctuations in stream input from lower storages and groundwater storages can be explained in a similar way.

6.8 DS 07_03

6.8.1 Characterization of DS 07_03

This event took place in the extremely hot and dry summer of 2003. According to *DWD* (*2003*), the mean daily temperature was 3.4°C above the mean reference temperature from the period 1961 to 1990. The area average of temperature during the months of June and August was the warmest since the start of measurements in 1901. The month of July was also warmer than the average of the reference period. Thus, 2003 was the hottest summer in the most parts of Germany since begin of measurements. In addition, the area average of sunshine duration was the greatest since 1951. The persistent high-pressure situations resulted also in a considerable deficit of precipitation, making the summer of 2003 the fifth driest since 1901. As a result of this exceptional climatic situation, the Dreisam discharges for the months of July, August and September were the lowest since 1941 (*IHF 2004*). At the beginning of July, the Dreisam discharge was subject to measurement problems caused by low water stages (measurement of negative runoff).

Due to this extreme drought, no comparable runoff situation could be found in the initialization timeserie from 1994 to 1999 for insertion of the data window (see chapter 6.4.2). Therefore, a low water situation had to be created artificially by deleting the precipitation from the initialization timeserie and waiting until storages ran low enough to produce the desired discharge.

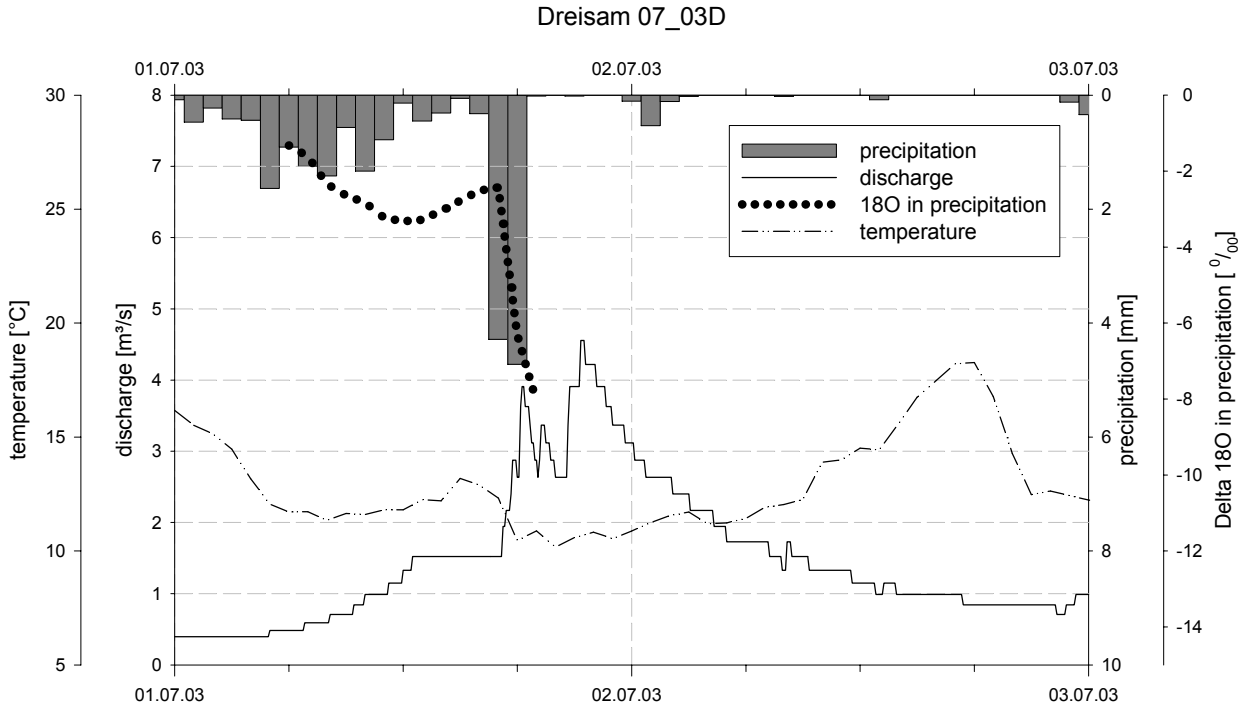

Figure 6.13: Event characteristics DS 07_03

Figure 6.13 shows the main characteristics of the event in July 2003. After a smooth first precipitation peak with intensity maxima of below 2 mm/h follow two hours of more intense rainfall with 4.3 and 4.7 mm/h. This erratic precipitation causes a multiple runoff peak in the range of 4 to 4.5 m^3/s starting from low-water discharges near zero (0.26 m^3/s). The $\delta^{18}O$-values show a dramatic decline from -2.5 to –8 during the two hours of intense precipitation. A very hot period with average catchment temperatures of 25°C and more was preceding the event.

PRECIPITATION was regionalized from the stations Ebnet, Buchenbach, Zasler, St.Wilhelm, Hinterzarten, St.Märgen and Rotbach (Falkensteig). **TEMPERATURE** gradients were calculated from the stations Zastler, St.Wilhelm and Schauinsland. **WIND** was measured at the two stations Schauinsland and St.Wilhelm. For the artificial creation of **SUNSHINE DURATION** data, the same procedure was applied as for DS 05_02. **ATMOSPHERIC HUMIDITY** was available from Zastler, St.Wilhelm and Schauinsland. Again, the average of those three stations was transferred to all other stations before regionalization. $\delta^{18}O$ was measured at the two stations Rotbach (Falkensteig) and Katzensteig near St.Wilhelm and then regionalized (see chapter 6.2).

6.8.2 Results of DS 07_03

Figure 6.14 shows the simulation result of event DS 07_03 for the entire Dreisam catchment.

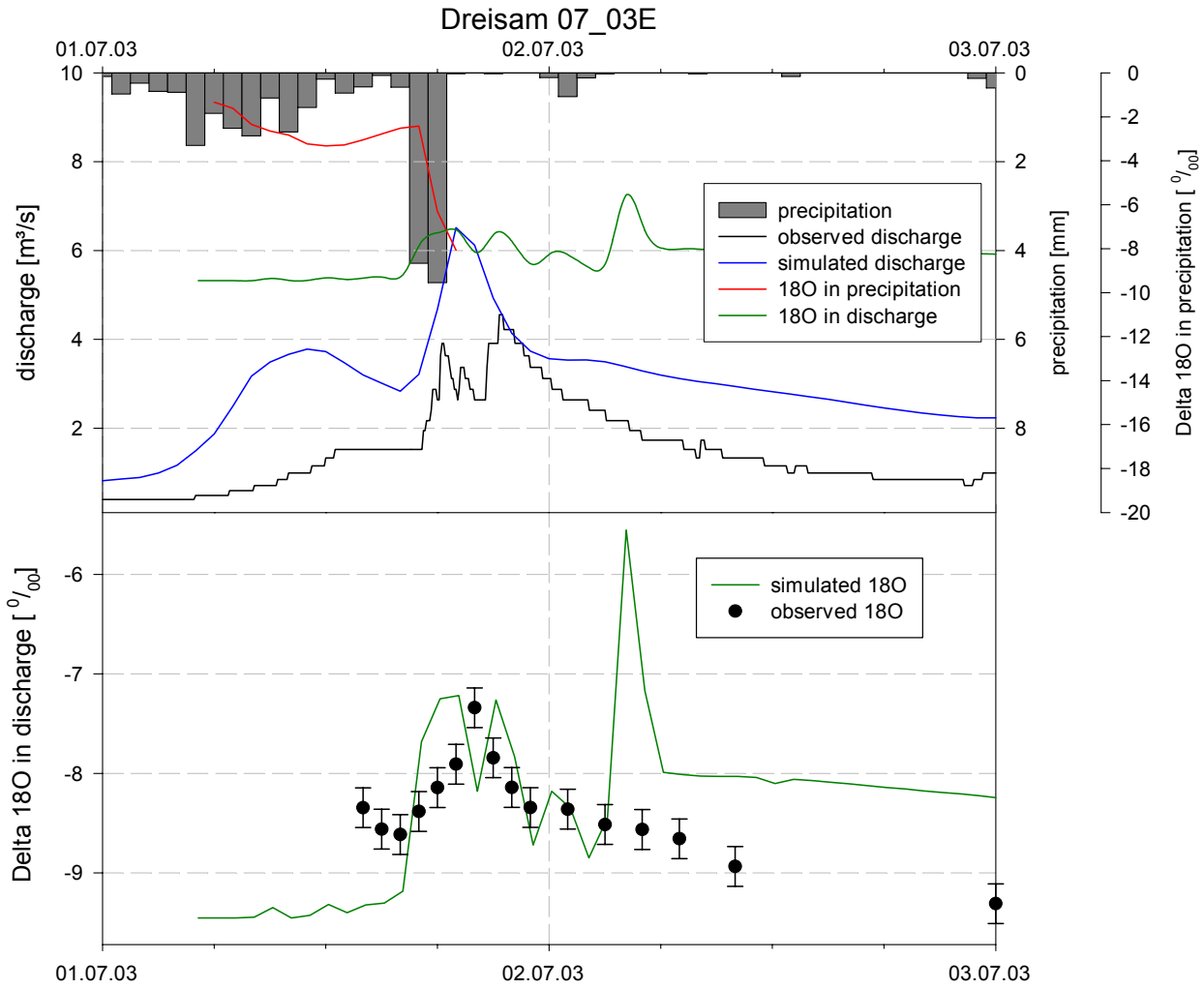

Figure 6.14: Results of DS 07_03 E; Dreisam

The upper part of Figure 6.14 displays the significant overestimation of runoff. The first simulated peak of event DS 07_03 is missing in the measurements. In return, the multiple peaks, which were observed during measurements is only represented by one simulated peak. $\delta^{18}O$-values in precipitation exceed those in the discharge during the whole event.

The output curve of $\delta^{18}O$ in discharge shows four distinct peaks. After a rise from values of -9.4‰ the first two peaks reach about -7.2‰ and -7.3‰. Before the curve rises towards the maximum peak near -5.5‰ at July 2, 4 a.m. values drop down to -8.8‰ with a small peak of -8.5‰ in between. After the maximum peak, $\delta^{18}O$-values drop down to -8.5‰ and remain at this plateau for the rest of the simulation. In contrary to this, measured values only form one single peak with -7.3‰ at the time of the first two simulated peaks and then decrease continuously down towards -9.3‰. Thus, the high and pointed peak in $\delta^{18}O$-values is not existent in measurements.

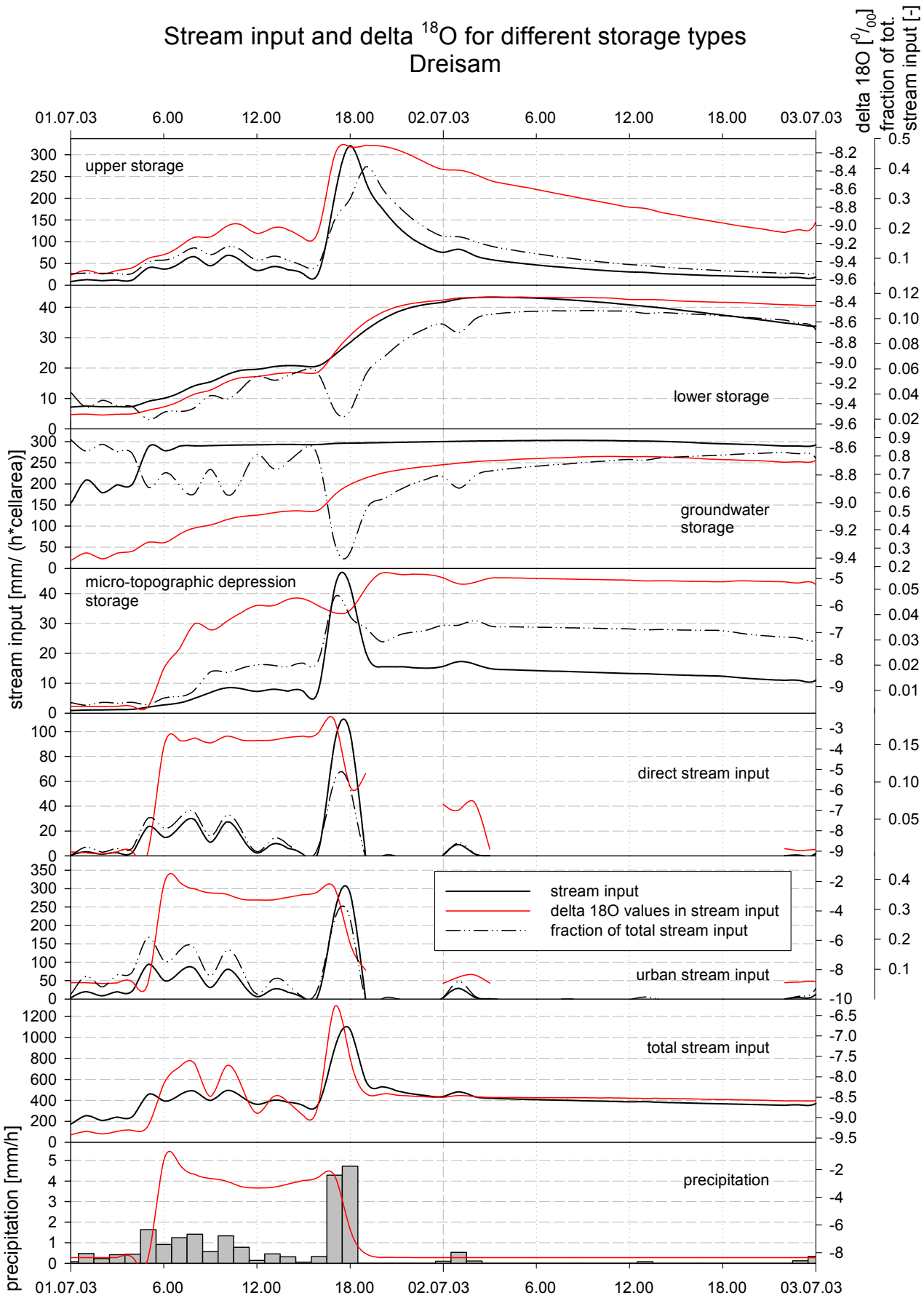

Figure 6.15: Stream input (black), fraction of total stream input (dash-dotted) and $\delta^{18}O$-values (red) from different storage types; DS 07_03 D; Dreisam catchment

Figure 6.15 identifies the dominant runoff components and their influence on simulated ^{18}O in total stream input. The largest amount of stream input is provided by the upper storages. Nevertheless, ^{18}O-values are mostly determined by direct runoff components from urban and open water areas, as those components carry nearly undiluted event water. Providing a maximum fraction of together 36% of total stream input, they are responsible for the maximum $\delta^{18}O$ peak of -6.5‰. In comparison to the other simulations, during the existing low water conditions direct runoff components provide an additional ratio of total stream input and therefore enhance their importance.

BRUGGA:

Figure 6.16 shows the results from the simulation 07_03 D for the Brugga subcatchment.

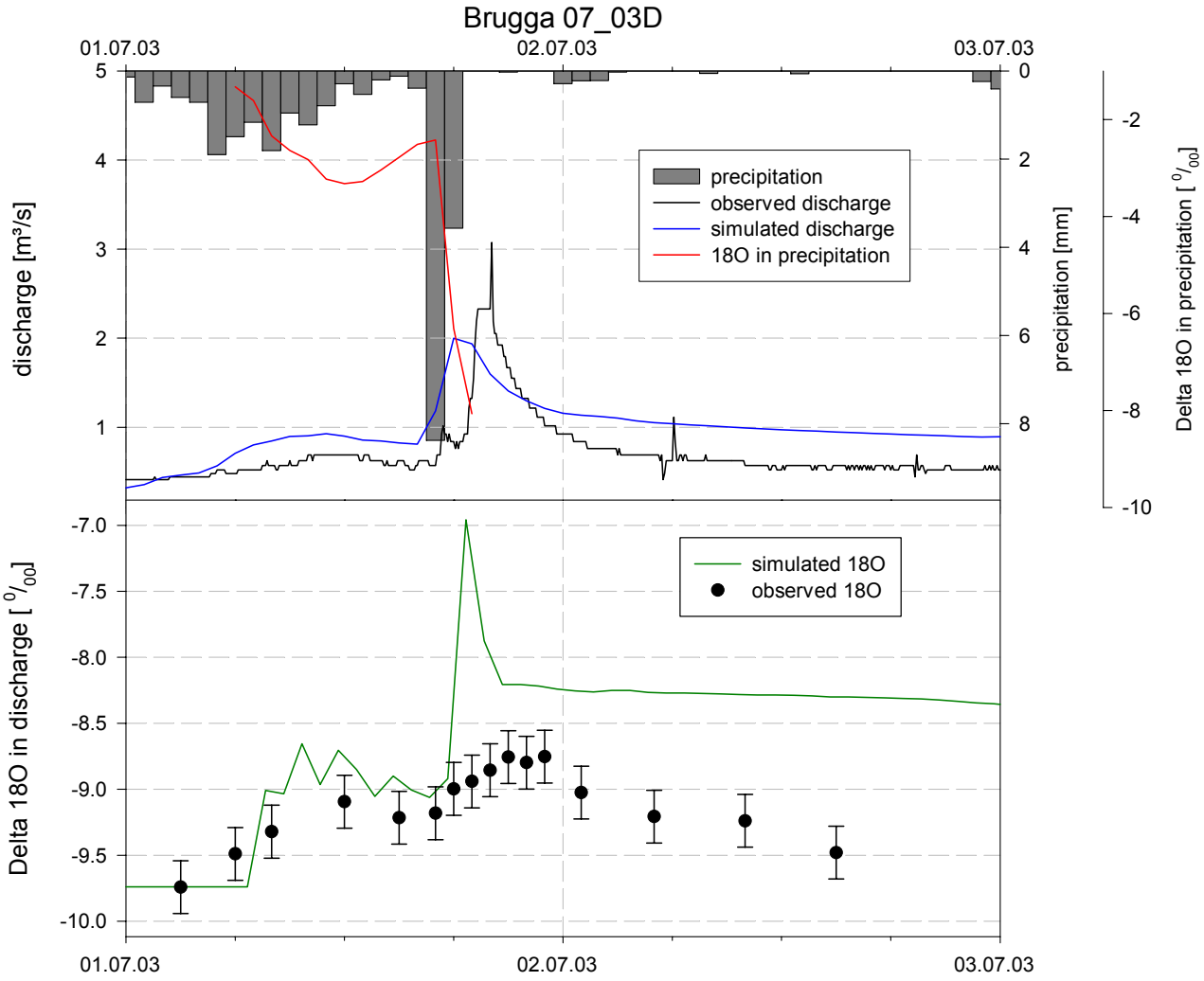

Figure 6.16: Results of DS 07_03 D; Brugga

The regionalization of precipitation shows a similar general pattern as for the Dreisam catchment besides one hour of elevated precipitation intensity with more than 8 mm/h. The runoff, which is resulting from the first precipitation peak is slightly overestimated whereas the second peak is underestimated and too early in its dynamics.

The curve of simulated $\delta^{18}O$ in discharge (lower part of Figure 6.16) shows a rise to about -8.7‰ and afterwards a decline to about -9‰. As in the Dreisam catchment, this minimum is followed by a pointed peak of -7.0‰ at July 1, 7 p.m. and a decline down to a plateau of -8.3‰. Measured values first rise similar to simulations but the maximum peak of -8.7‰ is by far lower than simulations. After this peak, measurements decline again towards starting values.

WAGENSTEIG:

Figure 6.17 shows the results from the simulation 07_03 E for the Wagensteig subcatchment. This graph shows as an example for very good simulation results.

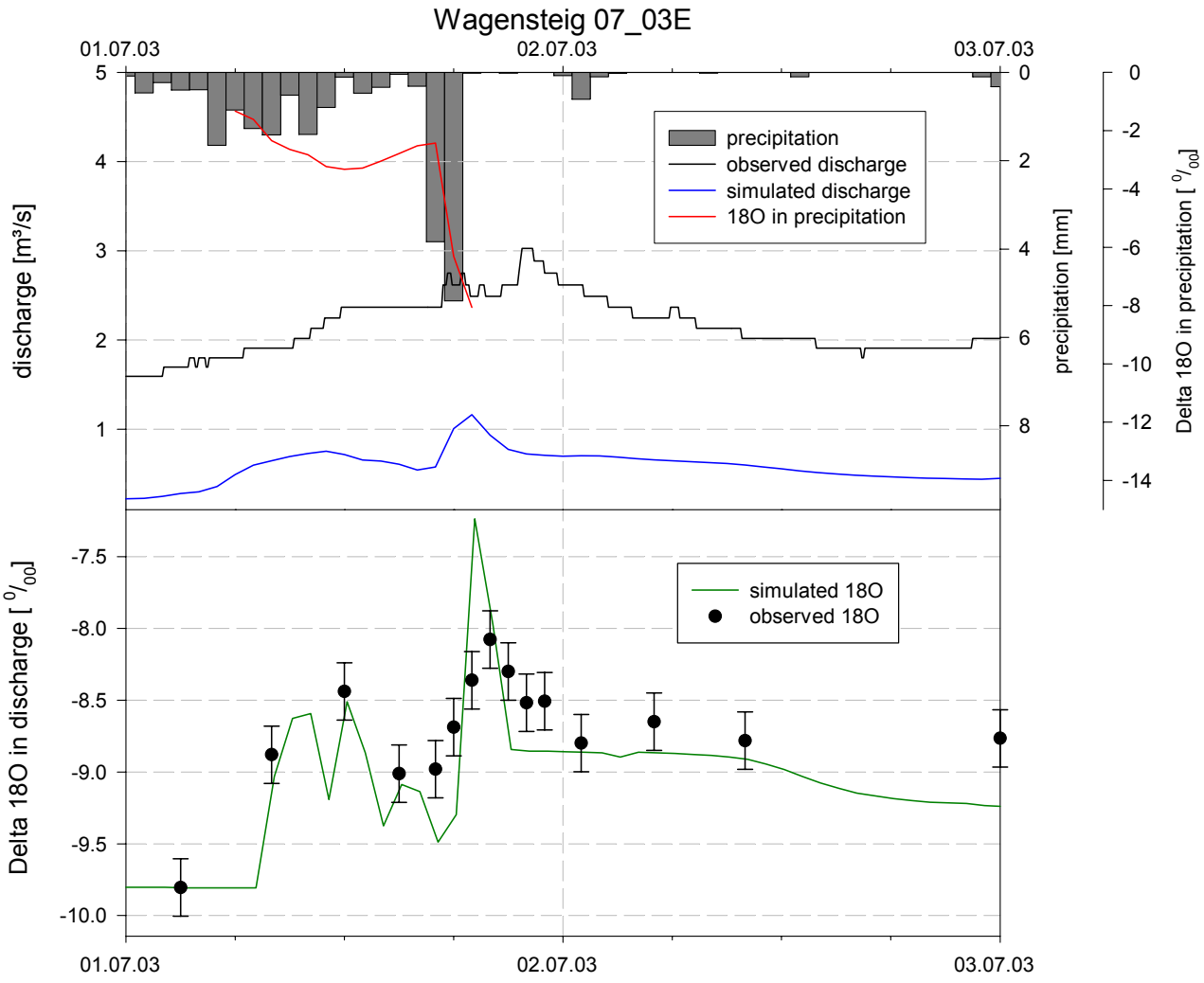

Figure 6.17: Results of DS 07_03 E; Wagensteig

The gauging station of water levels for this subcatchment is subject to significant sedimentation. Consequently, this station was officially retired by the water management authorities (GewässerdirektionsüdlicherOberrhein/Hochrhein) in 1998 (*DIDSZUN 2004*). Nevertheless, the general runoff dynamics can be recognized even though absolute measured values of discharge are displaced towards too high values. Simulated discharge shows the dynamics of regionalized precipitation with a first smooth peak and a second

more pointed maximum. In gauged discharge, this behavior is a lot more indistinct, although it shows multiple peaks. The pattern of regionalized precipitation in the Wagensteig subcatchment is similar to area precipitation in the entire Dreisam catchment.

Modeled $\delta^{18}O$-values in discharge follow the general picture in the other catchments. After a multiple first peak and a decline, a fourth, very distinct peak with values of up to -7.2‰ is observed. The plateau that follows this peak is not as pronounced as for the other catchments and $\delta^{18}O$ tends to lower values towards the end of the simulation. Nearly all measurements plot on the simulated curve within their analytic confidence interval.

6.8.3 Discussion of DS 07_03

DREISAM:

- Precipitation regionalization:

From the regionalized precipitation can be concluded that 07_03 is a convective event, with irregular spatial and temporal precipitation patterns (spottiness of rainfall). In addition, the general data situation is even worse than for 05_02. Thus, an adequate precipitation regionalization cannot be guarantied.

A significant overestimation of discharge can be observed in simulation results. Next to unrealistic moisture contents, this can be also well explained by the mentioned failure of precipitation regionalization. The multiple peaks in observations probably arise from irregular precipitation patterns, which are not captured by the regionalization routine. Also hourly resolution of rainfall data might be not high enough for an appropriate representation of intra storm variability. The absence of the first runoff peak in observations could be caused by a removal of river water for urban, agricultural and industrial use. It could also be explained with a failure of the soil routine under extremely dry conditions. Since the soil routine is based on an empirical relation between percolation and soil moisture, this relation might be unfounded under extremely dry soil moisture conditions

- δ18O regionalization:

Since also for this event δ18O-values have to be regionalized from only two stations, the same uncertainty in solute input is inherent as in DS 05_03.

Despite the unsatisfactory runoff simulation, the results for ^{18}O simulations show an acceptable agreement of modeled and measured values apart from the extremely high peak of -6.5‰ (see Figure 6.14). This peak can be clearly assigned to the convective two-hour storm with high intensities, as results from solute transport calculations within the river network show. In the case of extreme low-water situations, a mean residences time of 8h 12min was computed for solutes in the Dreisam catchments (see Table 6.3). The failure of ^{18}O simulations for this feature can be explained as follows:

- Sampling methods:

$\delta^{18}O$-values show a dramatic decline towards initial values in runoff during the second hour of the intense shower (Figure 6.13). However, the first hour with high $\delta^{18}O$-values is probably an artifact of sampling and regionalization methods. According to chapter 0, ^{18}O data samples reflect bulk mean values of the preceding sampling intervals. Samples are not bottled until a certain amount of precipitation is collected. If the bottle was nearly filled by the preceding period of low precipitation intensities, it contains only little water from the intense rainfall, to which the probe is assigned. The character of the short but intense event indicates that it originates from another convective cell than the preceding rainfall. Consequently, it is more obvious to assume a consistent isotope signature witin the 2 hour storm than to accept the extreme drop in $\delta^{18}O$-values. If a similar ^{18}O-value would be assigned to the first hour as was obtained for the second hour of the intense rainfall, the pronounced ^{18}O peak in runoff would disappear.

- Model uncertainties (direct runoff components, exfiltration from groundwater)

The enhanced dominance of direct runoff components, which carry undiluted event water, can be explained by the increase in their contribution to total stream input under low water conditions. The subsurface storage components are retarded because of low storage levels and consequently their importance is reduced. On the other hand, their fluctuations of ^{18}O are less damped because of a higher ratio of event water. Yet, the overall influence of direct stream input is still dominating. The elevated plateau of $\delta^{18}O$ after the event, where a decline of ^{18}O is measured, could result from neglecting exfiltration of pre-event water from groundwater storages (see chapter 5.7). Since exfiltration is especially important in low water conditions, it would lead to further dilution of event water and a decline of ^{18}O-values. The missing conceptualization of an immobile water volume enhances this effect (see results of Brugga).

BRUGGA:

Sampling methods:

The same exaggerated peak of $\delta^{18}O$ can be observed for the Brugga subcatchment at about 7 p.m. Because precipitation regionalization for the smaller Brugga catchment is more accurate, it is even more likely that this peak is an artefact sampling methods.

- Model uncertainty (immobile phase):

In the end of the simulation, modeled values of ^{18}O remain on an elevated level, whereas measurements recover from the influence of the precipitation input to some degree. This fact can be caused by an inadequate model conceptualization. In order to produce the required low water conditions the volume of water within the storage system has to be very low. As the model only accounts for mobile water, the total volume of stored water within the catchment is underestimated. Therefore, the fraction of event water in the catchment is comparatively large. Even if event and pre-event waters completely mix in the model, initial values of $\delta^{18}O$ will not be regained. However, in natural systems a large volume of water is fixed in an immobile phase. Although it does not take part in the water circle under dry conditions, it reacts with event water during a wetting phase. Equalization

of solute concentrations due to concentration gradients between an immobile and mobile phase (diffusion) takes place. Therefore, diffusion into and out of an immobile phase (retardation) results in a moderation of $\delta^{18}O$ reactions. In addition, part of the immobile water is displaced by mobile water without mixing and diffusion resulting in a further decline of $\delta^{18}O$-values. In the present solute model, both effects are disregarded.

WAGENSTEIG:
The absence of the first runoff peak and the following multiple peaks can be again explained by an incorrect precipitation regionalization and a failure of the soil routine.

The results of $\delta^{18}O$ simulations for the Wagensteig subcatchment show a very good agreement of measured and observed values. As the maximum peak of -7.2‰ is located in between two measurements its existence in runoff can be doubted. Therefore, the result of the simulation is not in stringent contradiction to the stated sampling inaccuracy for the ^{18}O. A uniform isotope signature with low $\delta^{18}O$-values for the two-hour storm event would result in a lower peak without affecting the agreement of modeled and observed values.

6.9 BRU 06_01

6.9.1 Characterization of BRU 06_01

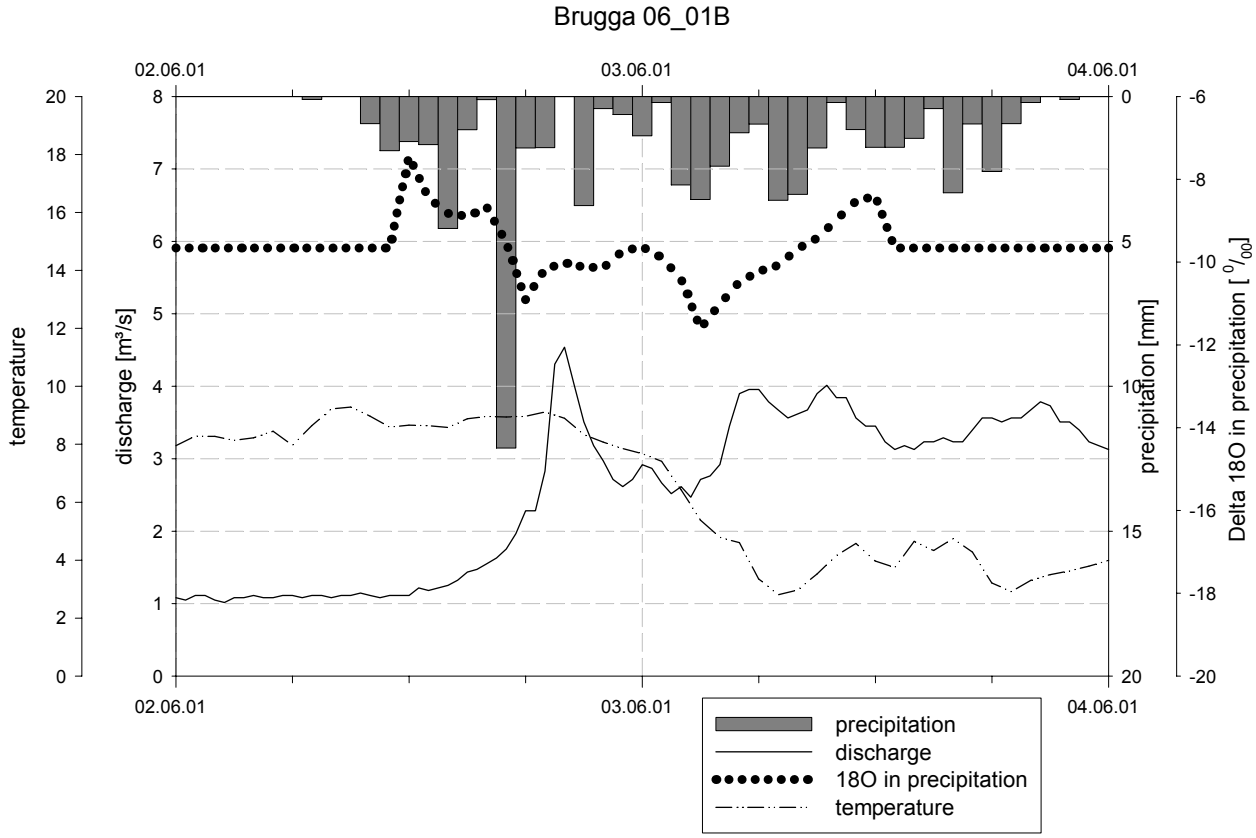

Figure 6.18: Event characteristics BRU 06_01

As mentioned before this event in June 2001 was only simulated for the Brugga catchment. Thus, discharge, regionalized precipitation and temperature only refer to this subcatchment. Figure 6.18 illustrates the main event characteristics. Precipitation with a maximum intensity of 12 mm/h and an average intensity of 2 mm/h lasts for more than 35 hours and produces a total input of 68.7 mm. Discharge at the gauging station in Oberried rises from 1 m³/s to a peak of 4.5 m³/s. After a short decrease, it stays within a range of 3 to 4 m³/s for the rest of the precipitation event. The ^{18}O signal varies between -7.5‰ and -11.5‰ with the higher values at the beginning and end of the event. For the beginning and the end of the event, no ^{18}O data of precipitation was available. Thus, the initial value in runoff was assigned to precipitation of those periods. Therefore, simulations are only valid for the shaded area of Figure 6.18.

For **PRECIPITATION** regionalization, the stations at St.Wilhelm, Zastler, Schauinsland and Hofsgrund were used. **TEMPERATURE** gradients were calculated in the same way as in 6.7.1. For **WIND**, again the average values from Schauinsland and St.Wilhelm were transferred to all other stations. The same was done for **ATMOSPHERIC HUMIDITY**

measurements at the three stations Zastler, St.Wilhelm and Schauinsland. **SUNSHINE DURATION** data was created synthetically according to chapter 6.7.1. $\delta^{18}O$ was regionalized from the stations Hofsgrund and Katzensteig, near St.Wilhelm. For the periods in the beginning and in the end of the event, initialization values had to be assigned to ^{18}O in precipitation because no measurements were available. Thus, the first measurements of ^{18}O in runoff had to be disregarded and the final part of the simulation is not meaningful.

6.9.2 Results of BRU 06_01

Figure 6.19 shows the simulation results of event BRU 06_02 for the Brugga catchment. The actual simulation window is again shaded.

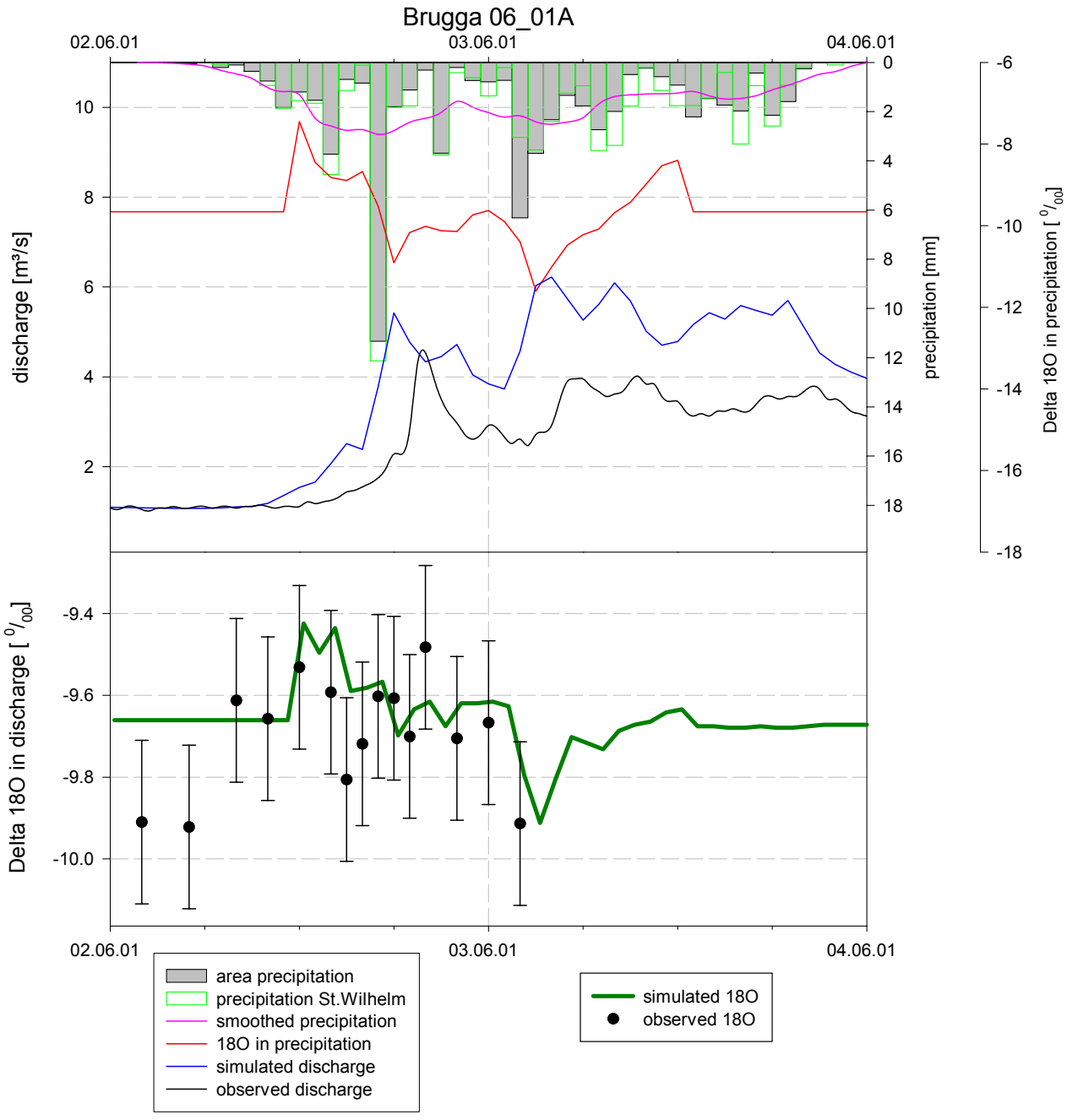

Figure 6.19: Results of BRU 06_01 A; Brugga

The 18 hours lasting event supplied the Brugga catchment with approximately 66.3 mm of precipitation (calculated from regionalized precipitation, grey in Figure 6.19). A maximum intensity of 12.1 mm/h was observed in St.Wilhelm. The measurements of this station are plotted in light green. In order to reveal a general pattern in precipitation, it was smoothed with an exponential filter (pink in Figure 6.19). According to this, precipitation appears in three waves. Those waves produce three major discharge peaks in the range of 4 m^3. Although the simulated discharge is overestimated by more than 2 m^3/s, its general dynamics are well reproduced. The first precipitation wave is signified by $\delta^{18}O$-values of mostly around –8‰ to -9‰ which is mostly higher than values in initial runoff (-9.66‰). Only in the end of this wave, $\delta^{18}O$ drops below values in runoff. The second precipitation wave is marked by $\delta^{18}O$-values of about -9.5‰ at the beginning decreasing towards -11.6‰.

Besides the disregarded first measurements, simulation results plot within the analytical measurement error. Fluctuations of ^{18}O in runoff closely reflect the $\delta^{18}O$ dynamics in precipitation input. Nevertheless, the absolute variation is strongly damped.

6.9.3 Discussion of BRU 06_01

Due to the precipitation characteristics (long duration with high intensities) the event can be called an advective storm. Further simulations have shown that when only the station in St. Wilhelm (light green in Figure 6.19) is used for area precipitation, the general runoff dynamics are not as well represented as for regionalized rainfall from the stations St.Wilhelm, Zastler, Schauinsland and Hofsgrund.

As mentioned, modeled $\delta^{18}O$ signatures lie well within the analytical error range of regarded measurements. Since measured $\delta^{18}O$ variations in runoff are small compared to analytical uncertainty, this result could be also achieved when the simulation would simply display the constant initial ^{18}O signature. Due to this fact, the simulation's significance is limited, although the general dynamics in ^{18}O fluctuations are well displayed.

6.10 Summarizing discussion of model applications

Table 6.4: Comparison of simulated events

EVENT	DS 05_02	DS 07_03	BRU 06_01
Catchment	Dreisam + subcatchments	Dreisam + subcatchments	Brugga
Max. discharge [m³/s]	8.3	4.6	4.5
Discharge prior to the event [m³/s]	2.6	~0.3	1.0
Max. precipitation intensity [mm/h]	4.6	4.7	12.1
Total precipitation [mm]	16.1	30.8	68.7
Duration of storm [h]	~15	~11	~42
Shape of runoff peak	Single peak	Multi-peaks	Multi-peaks
Category of storm	convective	convective	advective
$\delta^{18}O$ in precipitation crossing signature of runoff?	yes	no	yes
Comment on ^{18}O simulation	Time shift and overestimated fluctuations for Dreisam; good results for Brugga	Overestimated peak values for Dreisam and Bugga; good results for Wagensteig	Good results for Brugga; little relevance, because auf insignificant fluctuations

Table 6.4 gives a brief overview of the hydrological situation during the simulated events. None of the simulations was influenced by snowfall.

One of the main results of model applications is the identification of the great influence of direct runoff components, such as urban runoff and stream input from open water areas on ^{18}O concentrations in simulated runoff. Within a sealed area, the calibration parameter *cUrbanSplit* determines the runoff coefficient of urban stream input. For the present simulations, *cUrbanSplit* was set to 0.4, according to *PESCHKE ET AL.* (*1999*). Thus, 40% of precipitation input enters the stream nearly without any subsurface contact and dilution. The remaining 60% of precipitation input percolate to the runoff generation routine. *GUNKEL* (*1996*) mentions, that more than 30% of annual rainfall in urban areas is transferred to the streams via urban sewage. An investigation on the internet confirmed the range from 0.3 to 0.4 for runoff coefficients in low-density residential areas (*GSDA 2004, IGS 2004*). Nevertheless, the high fraction of direct runoff components to total stream input during peak discharges leads to an overestimation of ^{18}O fluctuations in catchments with a high fraction of urban area. This can be observed by comparing the results from DS 05_02 for the Dreisam catchment and the Brugga subcatchment. In the Brugga catchment, with a maximum stream input from sealed areas of ca. 8%, fluctuations are within the range of measurement errors. However, for the denser populated Dreisam catchment (max. urban stream input 25%) ^{18}O fluctuations were overestimated. In

general, the contribution of direct runoff components with more than 30% to total stream input during peak discharges is in strong contradiction to early studies (*UHLENBROOK ET AL. 2001, OTT 2002*). Since the urban routine of prior model versions inherited a multitude of defects and mistakes, this result has to be confirmed in further investigations. As the runoff coefficient for low-density residential areas of 0.4 seems to be realistic, the overestimated contribution of direct runoff components the most obvious explanation is the missing routing routine for these components. If urban runoff enters the stream within the time step of precipitation input, no other component has yet reached the stream (see chapter 5.8.4). Thus, its contribution to total stream input is overrated. Even a time lag of one hour would already lead to significant dilution with other runoff components.

In natural systems, direct runoff does not only consist of stream input from urban and open water areas. Here, also fast interflow and Piston Flow processes are relevant for runoff dynamics. As could be shown by *UHLENBROOK & LEIBUNDGUT* (*1997*), these components carry large fractions of pre-event water during floods. In the dynamic orientated conceptualization of $TAC^{d,}$ where those effects are represented by large storage coefficients, fast runoff components carry mostly event water. The effect of pre-event water supplying Piston Flow storages is not yet implemented (see chapter 7.4).

As shown by *UHLENBROOK ET AL.* (*2002*) also springs with no urban areas in their catchment show different reactions in runoff dynamics and sensitivity towards ^{18}O input. This was mainly explained by the strong influence of very heterogeneous drift and debris covers on the hillslopes of the Dreisam catchment. Sensitive springs were observed on the foot of forested hillslopes with blocky surface covers and underlying layers of high hydraulic conductivity due to macro pores. Springs, which show nearly no reaction on ^{18}O in precipitation were found on the foot of hillslopes with pasture land and underlying layers of lower hydraulic conductivities. These different runoff characteristics are already implemented in the model structure by the parameterization of runoff generation types with lower or higher storage coefficients. Nevertheless, the declaration of predominant runoff generation processes in cells is subject to large uncertainties because of strong heterogeneities throughout the catchment. On this note, ^{18}O simulation depends on parameterization of the water model as well as the accurate declaration of runoff generation types in the catchment.

It is very important to note that the graphs of stream input from different storage types only reflect the contribution of those cells with a direct connection to the stream channel. Therefore, the runoff generation type of the stream channel determines the origin of stream input components. The influence and contribution of different runoff generation types and their implemented storages on the overall catchment reaction is very difficult to assess.

A short summary of simulation uncertainties is given in the following:

Large **ANALYTICAL ERRORS** impede a detailed interpretation of events with small fluctuations of $\delta^{18}O$ in discharge (see chapter 6.9).
The uncertainty in $\delta^{18}O$ input via precipitation, which is caused by **SAMPLING METHODS**, is significant (see chapter 6.8). With an advanced assignment of sampling times, this could be improved. Sampling time should be assigned to the preceding period either centered or weighted by precipitation amounts.
Both **REGIONALIZATION OF PRECIPITATION AND ^{18}O SIGNATURE** leads to large uncertainties in water and ^{18}O input. Inaccuracy or even total failure of runoff simulations and ^{18}O dynamics are the result (see chapter 6.7). The influence of these uncertainties is hard to evaluate, as they are always immanent. Their importance can only be reduced by a close meshed network of precipitation and ^{18}O stations with a sufficiently high resolution in rainfall and ^{18}O dynamics.
As simulation results are predetermined by the applied **INITIALIZATION** procedures to a large degree, an initialization with natural input data from a period prior to the simulated event would be highly desirable. For a correct initialization of antecedent moisture conditions timeseries for climatic input are necessary. For initialization of ^{18}O, bulk mean δ-values of preceding precipitation events would be sufficient. The detailed influence of antecedent moisture conditions could be shown in chapter 6.7.
A multitude of effects, such as overestimated $\delta^{18}O$ fluctuations in discharge concentrations can be assigned to **MODEL UNCERTAINTIES**, even though their responsibility for inaccurate simulation results is not yet proven.

- As discussed, the influence of urban runoff is overestimated.
- Solute translation in river networks has to be revised, as the delayed reaction of $\delta^{18}O$ compared to measurements shows in chapter 6.7. In addition, dispersion and diffusions within the stream channels is not yet included in the solute model.
- Diffusion (adsorbtion/desorption) into and out of an immobile phase (retardation) is disregarded.
- Piston Flow effects, which deliver mostly pre-event water due to displacement of older water components cannot be modeled adequatly.
- Exfiltration from the groundwater and consequently, further dilution with pre-event water had to be neglected. This effect gains special importance under low water conditions.

For a more realistic treatment of direct runoff components, a routing routine should be implemented in module of urban runoff. An application of the kinematic wave approach (*kinematic*-function) with low Manning numbers would be appropriate. For improvement of process orientation of the model, the parameter *cUrbanSplit* and consequently the influence of urban runoff should be reduced to 0.3. Unfortunately, the sensitivity of *cUrbanSplit* has not been investigated by *SIEBER* (*2003*). For a representation of peak discharges during floods, other fast runoff generation processes have to be enhanced by the declaration of cells with fast interflow and therefore low storage coefficients. Storage coefficients of upper storages should be calibrated towards higher values. Piston Flow

processes with displacement of pre-event water should to be included in the solute model. Dispersion and diffusion of solute should be included in a new routing scheme for solute transport within the river network (e.g. by numerical dispersion in a kinematic wave routing scheme).

Overall, the greatest relevance for simulation uncertainties is seen in the limited availability of input data, especially station density for $\delta^{18}O$ regionalization. In order to assess uncertainties of model conceptualization, the model should be tested with better data situation. Especially sampling methods for $\delta^{18}O$ in precipitation should be adapted to model requirements (hourly bottling of bulk samples).

6.11 Conclusion of model applications

From the model applications of ^{18}O simulations the following conclusions can be drawn:

- If data requirements for the solute model are fulfilled, simulation accuracy is within the analytical error of laboratory measurements of ^{18}O. This claim has already been achieved by the presented applications within the Brugga subcatchment.
- The water model seems to overestimate the contribution of urban runoff to total stream input in catchments with a relatively high degree of urbanization.
- Other fast runoff components such as shallow translatory flow and saturated overland flow are only important when the cells under consideration are directly connected to the river network. Otherwise, their influence is swept off by dilution with pre-event water. (See Figure 6.10, Figure 6.12 and Figure 6.15)
- The incorporation of Piston Flow, an immobile subsurface phase and dispersion/ diffusion within the river network would lead to better results in ^{18}O simulations, because of their damping effect on $\delta^{18}O$ concentrations at the catchment outlet.
- In order to capture the time lag between stream input and discharge at the catchment outlet, the module for solute translation within the river network has to be revised.

The presented model applications have shown that the model for solute transport can be used as a diagnostic tool for the adequate conceptualization of water fluxes. The contribution of stream input from urban and open water areas within TAC^d is mainly responsible for the overestimated fluctuations of δ18O-values in simulations (see 05_02). The fact that urban runoff is contributing with nearly 30% to total stream input during peak discharges is in strong contradiction to early studies (*UHLENBROOK ET AL. 2001*). However, the program code of the urban runoff routine in earlier model versions inherited considerable mistakes leading to not negligible errors in the internal water balance. The overestimated stream input from urban areas is accredited to the missing routing routine. By simulating a conservative tracer under well known input and initial conditions the model of solute input can be used in terms of 'multi response calibration/validation' (*UHLENBROOK & LEIBUNDGUT 2002*).

For the solute model, data for the spatial distribution of input concentrations is as essential as is precipitation for the water model. It is shown by model applications that a sufficient density of measurement stations and their representative location within the catchment is crucial in order to decrease simulation uncertainties.

Similar to this, also sampling methods for $\delta^{18}O$ measurements in precipitation have to be adapted to the hourly input of precipitation into the model. Bulk mean samples should be bottles at equidistant time steps rather than at certain amounts of cumulated precipitation.

By simulating conservative transport of oxygen-18, only the first steps towards a general description of solute transport on the catchment scale have been made. Numerous runoff generation processes and effects of solute transport have to be incorporated to develop the presented model towards a physical description of flow and transport processes.

7 Proposal for further model developments

7.1 Kinematic solute transport within the river network

The implementation of mechanical and kinematic dispersion is mostly relevant for channel transport and in homogeneous aquifers. A kind of channel dispersion can be introduced by application of the kinematic function also for solute transport. Due to its numerical solving scheme, peaks of a propagating wave are smoothed (numerical dispersion). Hereby, also translation times and the effects of spatially distributed lateral inflow of solute can be captured. In this thesis, no satisfactory implementation of kinematic solute routing could be achieved although much time and effort was invested. However, the acquired knowledge would be of great use for solving this task in future model versions.

7.2 Retardation

Retardation due to adsorption/ desorption in an immobile phase can be introduced by the incorporation of a not runoff relevant passive water volume and a transition parameter, which determines the speed of diffusion.

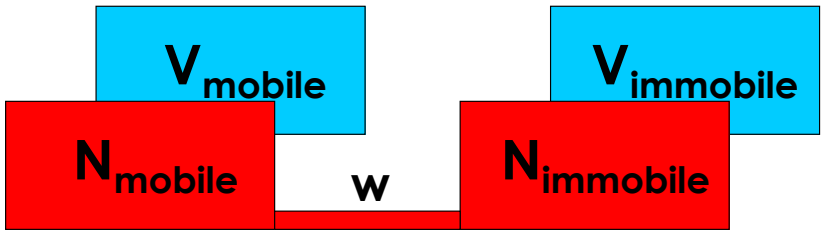

Figure 7.1: Conceptualization of retardation

The proposed conceptualization of retardation is illustrated in Figure 7.1.

$$\frac{dN_{mobile}}{dt} = \left(\frac{N_{mobile} - N_{immobile}}{V_{mobile} - V_{immobile}} \right) \cdot w$$

w: diffusion coefficient [1/time step]
N_{mobile}: mobile solute [quantitiy]
$N_{immobile}$: immobile solute [quantity]
V_{mobile}: mobile water volume [mm]
$V_{immobile}$: immobile water volume [mm]

7.3 Solute reactions

Due to the 2.5 dimensional structure of *TAC*^{d}, solute reactions like decomposition or decay can be implemented depending on the storage type. Moreover, they can be distributed

horizontally depending on the general runoff generation type, landuse or type of vegetation. Moreover, solute reactions can be controlled by time and space depending factors such as temperature, water content, atmospheric humidity or season. As a result, the model can be modified for solute transport simulations of reactive substances, with only little effort.

7.4 Piston flow

The conceptualization of Piston Flow via a storage system with large storage coefficients only reflects the dynamics of water fluxes. The fact that runoff out of those areas mainly consists of pre-event water cannot be accounted for in the present concept. In contrary to simulations of runoff dynamics, in solute transport simulations the water is identified by its solute concentration.

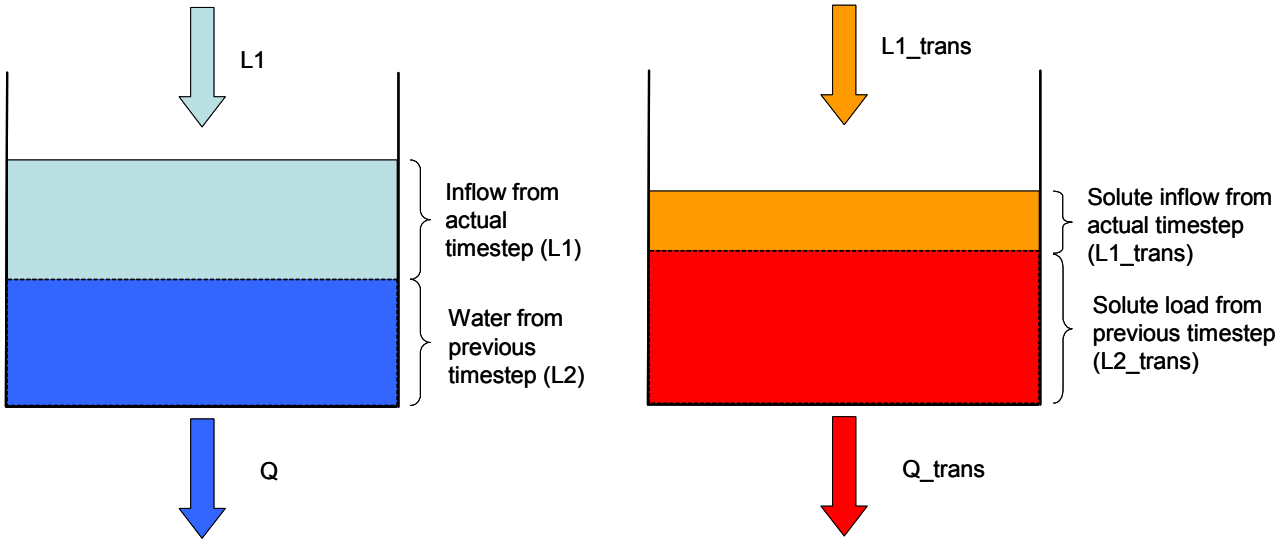

Figure 7.2: Conceptualization of Piston Flow

The suggested scheme of Piston Flow is illustrated in Figure 7.2. Due to this conceptualization, incoming water and solute fluxes do not mix with stored water from the prior time step until output fluxes were subtracted. Nevertheless, their volume and their pressure are still regarded when calculating output fluxes. Therefore, a displacement of pre-event water can be simulated with this simple conceptionalization.

The appropriate *PCRaster* model script for water fluxes could be formulated in the following way:

```
Q = (L1 + L2) * k;      k: Storage coefficient [-]
L2 = (L1 + L2) - Q;
```

The corresponding solute fluxes could be expressed like this:

```
# TRANSPORT TRANSPORT TRANSPORT TRANSPORT TRANSPORT
Q_trans = if (Q > L2, L2_trans + (Q - L2) * L1_trans/ L1, Q * L2_trans/ L2);
L2_trans = (L1_trans + L2_trans) - Q_trans;
# TRANSPORT TRANSPORT TRANSPORT TRANSPORT TRANSPORT
```

7.5 Test of model uncertainties

As mentioned before, it is only possible to evaluate the model uncertainties with continuous timeseries of input data, for climatic input as for solute input. In addition, a better spatial resolution of ^{18}O input measurements would be necessary. A high temporal resolution during the simulation event and bulk mean values of ^{18}O for the preceding events have to be provided. The declaration of runoff generation types has to be reconsidered in respect to their influence on solute transport.

7.6 Urban runoff routine

As for all fluxes, the drainage direction of urban flows is defined by a *PCRaster* map (*LDD*). The LDD used for urban runoff does not have to be concordant with the commonly used drainage direction map, which defines flow-directions according to the steepest elevation gradient. Thus, the fact that most urban runoffs follow artificial sewage networks can be accounted for in a quite simple way. It is also possible to direct urban runoffs into the stream only at the end of settlements. Those cells would be defined as urban cells and stream cells at the same time, which are located upstream of a non-urban cell. A simple *if*-query would have to be added to the model script. In addition, a kinematic wave routing scheme for urban runoff can be added by applying the predefined *PCRaster* function *kinematic* with low Manning parameters.

7.7 Darcy flow in porous groundwater aquifers

The conceptualization of the Zarten basin (*nRGType 6*) has considerable deficits in the treatment of lateral flows. A manually defined local drainage direction (*LDD*) is used to route lateral fluxes through this unit. This results in extremely high water levels at the border to the surrounding fractured Gneiss aquifer, where the contributing inflow enters the porous groundwater aquifer. When lateral subsurface water fluxes enter this unit, they are not transferred towards the middle of the aquifer with low water levels, because their flow is restricted to the *LDD*. This misconception could be significantly improved by breaking up the strict drainage direction via the *LDD* for this runoff generation type. For example, the direction of flow could be determined by the lowest water level in the neighbouring cells. Alternatively and more advanced, the water could be distributed in more than one surrounding cell according to the gradients of water levels. If in addition, the storage coefficients are multiplied by these gradients, they can be interpreted as k_f – values. A simple but by far more sophisticated and realistic groundwater model based on Darcian flow would be the result. In addition, the vertical aquifer geometry in the Zarten basin as well as its division in two groundwater stories with different k_f-values could be implemented.

8 Final remarks

Within the scope of this thesis, a distributed solute transport model was developed based on the catchment model *TAC*^{d}. With the present version, a multitude of input scenarios can be simulated for conservative, non-reactive solutes. The time-dependent effects of point source contaminations as well as area-wide diffuse input of liquid or solid solute with instantaneous or continuous input functions is computed for each cell of the catchment as well as river discharges. The model can be advanced with little effort by integrating any kind of solute reaction. Thus, it provides a framework for future simulation of reactive solutes like nitrate, sulfate or phosphorus.

Despite the mentioned multitude of simulation uncertainties, the successful application of the solute transport model for diffuse ^{18}O simulations has to be emphasized. Even with insufficient supply of input data, it was possible to simulate ^{18}O fluctuations in the Brugga catchment within the accuracy of laboratory measurements. Failing simulations can be mostly accredited to inaccuracy of input data. Input regionalization of precipitation for the simulated events is based on a very low station density. $\delta^{18}O$ was yet only measured in two locations which then had to be regionalized for the entire Dreisam catchment. Against this background, an application of a distributed solute transport model without any data for initialization appears to be bold. However, as the intended result was a general examination of model abilities this procedure is justified.

The stated model uncertainties are meant as propositions for further investigation. Their actual influence cannot be identified because of large data uncertainties. However, the two most prominent deficits are the module of solute routing in the river network and the generally overestimated influence of urban runoff. Other weaknesses of the model structure might explain unsatisfactory simulation results in case they are not caused by input data. However, before further enhancements are initiated, their contribution towards a more realistic description of catchment processes has to be evaluated. Here it is again referred to the quote of PILKEY: *"The state of the art is not necessarily close to the state of nature"* (PILKEY *1997, p. 265*). In further model developments, the gain in process-orientated description of nature should be carefully balanced against an increase of the unmanageable model complexity. A sound catchment model can only be established, if all its components are adjusted to the same degree of abstraction.

On this note, the limitations of the *TAC*^{d} model have to be respected. Since distributed solute transport can only be coupled to a physically correct description of water flow processes, the use of a conceptual water model is *a priory* subject to many unknowns. *TAC*^{d}'s distributed storage analogy is close enough to physical flow processes in mountainous meso-scale catchments to allow the implementation of solute transport. Therefore, *TAC*^{d} can be called a conceptual model with a high degree of physical agreement. The fundamental prerequisite for a coupling of the solute and water model

however, is the correct description of water fluxes and volumes within the storages. The solute model implements the complete mixture of water volumes in storages with different solute concentrations before output fluxes of these storages are calculated. This procedure is justified in aquifers with large macro-pores or in the fractured gneiss-aquifer. In an extended porous groundwater aquifer, however it would lead to unrealistic high dispersion coefficients.

Numerous practical tasks exist to which a distributed transport model for reactive solutes can be applied. One of them is the assessment of effects of area-wide human solutes input on concentrations in stream discharges. Thereby agricultural and industrial sources of nitrates, sulfates and many other contaminants are of special interest for water suppliers. Simulations of actual or potential stream contaminants are also essential for an estimation of effects on the biological river habitats. To advance the capabilities of *TACd* to a degree, where it can be distributed to water recourse management facilities much work still has to be invested (e.g. implementation of reactive solute transport, graphical user interface).

As the model of solute transport can also account for mineralization (e.g. of silicate) if mineralization rates are provided, simulations of silicate could be used to further evaluate the process-orientation of water fluxes within the model (multi response calibration/validation). Interesting results from a comparison to earlier studies, where fixed concentrations were assigned to storage types (*UHLENBROOK 1999*), and more insight into the complexity of interacting model processes can be expected.

By implementing solute transport, TAC^d was brought to a level where it competes with the most advanced river basin modeling systems like *WaSiM ETH, HBV-96, SHETRAN* or *MIKE SHE*. The door to a comprehensive treatment of water and solute transport in mountainous meso-scale catchments is pushed open.

References

Abbott, M.B., Bathurst, J.C., Cunge, J.A., O'Connell, P.E., & Rasmussen, J. (1986a): An introduction to the European Hydrologic System Systeme Hydrologique Europeen, SHE, 1: History and philosophy of a physically based, distributed modeling system. Journal of Hydrololgy, 87, pp. 45–59.

Abbott, M.B., Bathurst, J.C., Cunge, J.A., O'Connell, P.E., & Rasmussen, J. (1986b): An introduction to the European Hydrologic System Systeme Hydrologique Europeen, SHE, 2: Structure of a physically based, distributed modeling system. Journal of Hydrology, 87, pp. 61–77.

AIMWATER (1999): Survey of modelling approaches. European research project "AIMWATER", http://dataserv.cetp.ipsl.fr/AIMWATER/reports/modelsurvey_report.pdf, [Access date: 02.01.2005].

Arheimer, B. (2004): The HBV-N model. Swedish Meteorological and Hydrological Institute, SE-601 76 Norrköping, Sweden, http://www.smhi.se/sgn0106/if/hydrologi/documents/HBV-N_input.doc [Access date: 02.01.2005].

Arheimer, B.& Brandt, M. (1998): Modeling nitrogen transport and retention in the catchments of southern Sweden. AMBIO 27(6), pp. 471-480.

Becker, A. (1992): Methodische Aspekte der Regionalisierung. Mitteilung Nr. XI der Senatskommision für Wasserforschung, Regionalisierung in der Hydrologie, Deutsche Forschungsgemeinschaft.

Beckie, R. (2001): Advanced groundwater hydrology. Lecture notes, Department of Earth and Ocean Sciences, University of British Columbia, Canada.

Beek, T. aus der (2004): The further development of the process-based catchment model TAC^{d} and its application to the H.J. Andrews Experimental Forest, Oregon, USA. Diploma thesis at the Albert-Ludwigs-University Freiburg, Department of Hydrology, (unpublished).

Bergström, S. (1976): Development and application of a conceptual runoff model for Scandinavian catchments. Ph.D. thesis SMHI Reports RH, No. 7, Norrköping.

Bergström, S. (1992): The HBV model – its structure and applications. SMHI Reports RH, No. 4, Norrköping.

Beven, K.J. (1996): A discussion of distributed hydrological modeling. chapter 13A 255-279 in: Abbott, M. B.& Refsgaard, J. C. (1996): Distributed Hydrological Modelling. Kluwer Academic Publishers, Dortrecht, Netherlands.

Beven, K.J. (1997): Distributed Modelling in Hydrology: Application of the TOPMODEL concept, Wiley, Chichester.

Bold, S. (2000): Instationäre Grundwassermodellierung des Zartner Beckens. Diploma thesis at the Albert-Ludwigs-University Freiburg, Department of Hydrology, (unpublished).

Braden, H. (1985): Ein Energiehaushalts- und Verdunstungsmodell für Wasser- und Stoffhaushaltsuntersuchungen landwirtschaftlich genutzer Einzugsgebiete. Mitteilungen Deutsche Bodenkundliche Geselschaft No. 42, pp.294-299.

Chow, V.T., Maidment, D.R. & Mays, L.W. (1988): Applied Hydrology. McGraw Hill, New York.

DeVries, J.J., & Hromadka, T.V. (1993): Computer models for surface water. in: Maidment D.R. (1993): Handbook of hydrology. McGraw-Hill, New York.

Dingman, S.L. (1984): Fluvial Hydrology. W.H. Freeman and Company, New York.

DVWK (1996): Deutscher Verband für Wasserwirtschaft und Kulturbau e.V., Ermittlung der Verdunstung von Land- und Wasserflächen. Merkblätter zur Wasserwirtschaft, 238, Bonn.

DWD (2003): Deutsche Wetter Dienst, Der Rekordsommer 2003. http://www.dwd.de/de/FundE/Klima/KLIS/prod/spezial/temp/Rekordsommer_2003.pdf, [Access date: 02.01.2005].

Eisele, M. (2003): Stoffhaushalt und Stoffdynamik in Flusseinzugsgebieten: Ein Beitrag zum Bewertungsverfahren "Hydrologische Güte". Freiburger Hydrologische Schriften, volume 10, Department of Hydrology, Universität of Freiburg.

ESRI (2004): Environmental Systems Research Institute, http://www.esri.com/ [Access date: 02.01.2005].

Ewen, J., Parkin, G. & O'Connell, P.E. (2000): SHETRAN: distributed river basin flow and transport modeling system. ASCE J. Hydrologic Engineering, 5, pp. 250-258.

FEFLOW (2004): Finite Element Subsurface FLOW System, http://www.wasy.de/deutsch/produkte/feflow/; http://www.waterloohydrogeologic.com/software/feflow/feflow_prof_app.htm [Access date: 02.01.2005].

Fritz, A. (2001): Experimentelle Untersuchung der Abflusskonzentration in Bächen des Bruggaeinzugsgebiets. Diploma thesis at the Albert-Ludwigs-University Freiburg, Department of Hydrology, (unpublished).

Fuchs, P., Müller Westermeier, G. & Schmidt, A. (2001): Mittlere jährliche Niederschlagshöhe (ohne Korrektur). Hydrologischer Atlas von Deutschland, page 2.2, Publisher: Bundesministerium für Umwelt, Naturschutz und Reaktorsicherheit, Bonn/Berlin.

Glover, B.J. & Johnson, P. (1974): Variations in the natural chemical concentration of river water during flood flows, and the lag effect. Journal of Hydrology, 22, pp. 303 - 316.

GOOGLE (2004): internet search engine. http://www.google.de

GRASS (2004): Geographic Resources Analysis Support System, http://grass.itc.it/index.php [Access date: 02.01.2005].

GSDA (2004): GeoSpatial Data Aquisition, http://emrl.byu.edu/gsda/data_tips/tip_soiltype_table.html [Access date: 02.01.2005].

Gunkel, G. (1996): Renaturierung kleiner FLiessgewässer. Umwelt Forschung, Gustav Fischer Verlag Jena, Stuttrart.

HBV-96 (2004): http://dude.uibk.ac.at/Projects/HydAlp/demonstrator/hydalp/models/hbv.html [Access date: 02.01.2005].

HBV-NP (2004): The HBV-N model. Swedish Meteorological and Hydrological Institute, SE-601 76 Norrköping, Sweden, http://www.smhi.se/sgn0106/if/hydrologi/hbv_np.htm [Access date: 02.01.2005].

Hoyningen-Huene, J. von (1983): Die Interzeption des Niederschlags in landwirtschaftlichen Pflanzenbeständen. Schriftenreihe DVWK 57, pp. 1-53.

Hädrich, F. & Stahr, K. (1997): Die Böden in der Umgebung von Freiburg im Breisgau. in: Schwarzwald und Oberrheintiefland - Eine Einführung in das Exkursionsgebiet um Freiburg im Breisgau, Freiburger Geographische Hefte, Heft 36, Albert-Ludwigs-University Freiburg.

IHF (2004): Dürreperiode 2003. Department of Hydrology, Albert-Ludwigs-University Freiburg, http://www.hydrology.uni-freiburg.de/aktuell/dreisam/duerre_03.html [Access date: 02.01.2005].

IGS (2004): Indiana Geological Survey, Indiana University, http://igs.indiana.edu/survey/projects/hydrotools/html_files/element2.cfm [Access date: 02.01.2005].

Johst, M. (2003): Die Weiterentwicklung und Anwendung des prozessorientierten Einzugsgebietsmodells TACD im Löhnersbach-Einzugsgebiet, Kitzbüheler Alpen, Österreich. Diploma thesis at the Albert-Ludwigs-University Freiburg, Department of Hydrology, (unpublished).

Karssenberg, D. (2002): The value of environmental modelling languages for building distributed hydrological models. Hydrological Processes, 16, pp. 2751–2766.

Kendall, C. & McDonnell, J.J. (1998): Isotopes in Catchment Hydrology. Elsevier/North Holland Publ. Comp. Amsterdam.

LfU (2000): Landesanstalt für Umweltschutz, Pegelstatistik und hydrologische Hauptzahlen der Pegel Brugga, Dreisam, Rotbach, St. Wilhelmer Talbach, Zastlerbach und Wagensteigbach (unpublished).

Liehl, E. (1988): Oberflächenformen und Landschaftsgeschichte. in: Breisgau-Hochschwarzwald - Land vom Rhein über den Schwarzwald zur Baar, Landkreis Breisgau-Hochschwarzwald (Publisher), Schillinger Verlag GmbH, Freiburg i.Br.

LIFELONG LEARNERS (2004): Royal Institute of Technology, Stockholm, http://www.lifelong-learners.com/pde/ [Access date: 02.01.2005].

Lindström, G., Johansson, B., Persson, M.,Gardelin, M. & Bergström, S. (1997): Development and test of the distributed HBV-96 model. Journal of Hydrology 201, pp. 272-88.

LISEM (2004): Limburg Soil Erosion Model, => Basic => Basic theory, Faculty of Geographic Science, Utrecht University, http://www.geog.uu.nl/lisem/ [Access date: 02.01.2005].

Maloszewski, P. & Zuber, A. (1992): On the calibration and validation of mathematical models for the interpretation of tracer experiments in groundwater. Advances in Water Resources, 15: pp. 47-62.

Maloszewski, P. & Zuber, A. (1993): Principles and practice of calibration and validation of mathematical models for the interpretation of environmental tracer data. Advances in Water Resources, 16: pp. 173-190.

MATLAB (2004): http://www.mathworks.com/ [Access date: 02.01.2005].

Melching, C.S. (1995): Reliability Estimation. in: V.P. Singh (1995): Computer Models of Watershed Hydrology. Water Resources Publications, Colorado, USA, pp. 69-118.

Metz, B. (1997): Glaziale Formen und Formungsprozesse im Schwarzwald, in: Schwarzwald und Oberrheintiefland - Eine Einführung in das Exkursionsgebiet um Freiburg im Breisgau. Freiburger Geographische Hefte, Heft 36, Albert-Ludwigs-University Freiburg.

MIKE SHE (2004): http://www.dhisoftware.com/mikeshe/ [Access date: 02.01.2005].

MODFLOW (2004): MODular three-dimensional finite-difference ground-water FLOW model, http://water.usgs.gov/nrp/gwsoftware/modflow2000/modflow2000.html [Access date: 02.01.2005].

Monteith, J.L. (1975): Vegetation and the atmosphere. volume 1, Principles, Academic Press, London.

Moser, H. & Rauert, W. (1980): Lehrbuch der Hydrogeologie - Isotopenmethoden in der Hydrologie. Gebr. Bornträger, Berlin, Stuttgart.

Nash, J.E. & Sutcliffe, J.V. (1970): River flow forecasting through conceptual models. Part I - A discussion of principles. Journal of Hydrology, 10, pp. 282-290.

Nasr, A., Taskinen, A. & Bruen, M. (2003): Developing an independent, generic, phosphorus modelling component for use with grid-oriented, physically-based distributed catchment models. Diffuse Pollution Conference, Dublin.

Nolan, K.M. & Hill, B.R. (1990): Storm-Runoff generation in the Permanente Creek drainage basin, West Central California - An example of flood-wave effects on runoff composition. Journal of Hydrology, 113, pp. 343-367.

Ott, B. (2002): Weiterentwicklung des Einzugsgebietsmodells TACD und Anwendung im Dreisameinzugsgebiet. Diploma thesis at the Albert-Ludwigs-University Freiburg, Department of Hydrology, (unpublished).

Parlow, E. & Rosner H.J. (1997): Das Klima des Oberrheingrabens. in: Schwarzwald und Oberrheintiefland - Eine Einführung in das Exkursionsgebiet um Freiburg im Breisgau, Freiburger Geographische Hefte, Heft 36, Albert-Ludwigs-University Freiburg.

PCRaster (2004a): Homepage,
http://pcraster.geog.uu.nl/index.html [Access date: 02.01.2005].

PCRaster (2004b): Programm Documentation,
http://pcraster.geog.uu.nl/documentation/pcrman/book1.htm [Access date: 02.01.2005].

Peschke, G., Etzenberg,C., Müller, G., Töpfer J. & Zimmermann S. (1999): Das wissensbasierte System FLAB - ein Instrument zur rechnergestützten Bestimmung von Landschaftseinheiten mit gleicher Abflussbildung. IHI-Schriften, volume 10, Zittau.

Pilkey, O.H. (1997): The fox guarding the hen house. Reply to Hillary, T.M. and Stakhiv, E.Z., (1997): Discussion Pilkey, O.H. (1996). Journal of Costal Research, 13, pp. 265-267.

Refsgard J.C. (1996): Terminology, Modelling Protocol and Clssification of Hydological Model Codes. in: Abbott, M. B.& Refsgaard, J. C. (1996): Distributed Hydrological Modelling. Kluwer Academic Publishers, Dortrecht, Netherlands.

Rehfuess, K.E. (1990): Waldböden - Entwicklung, Eigenschaften und Nutzung. Pareys Studientexte, 29, Verlag Paul Parey, Hamburg und Berlin.

Ries, J. (1992): Exkursion zu den skitouristisch bedingten Landschaftsschäden am Schauinsland. in: Mäckel, R. & B. Metz (1992): Schwarzwald und Oberrheintiefland. Freib. Geogr. Hefte, Band 36.Inst. f. Phys. Geographie, Freiburg i.Br.

Roser, S. (2001): Flächendetaillierte Weiterentwicklung des prozessorientierten Einzugsgebietsmodells TAC und Visualisierung der Modellergebnisse in einem dynamischen GIS. Diploma thesis at the Albert-Ludwigs-University Freiburg, Department of Hydrology, (unpublished).

Sauer, K. (1988): Erd- und Landschaftsgeschichte. in: Landkreis Breisgau-Hochschwarzwald (1988): Breisgau-Hochschwarzwald - Land vom Rhein über den Schwarzwald zur Baar, Schillinger Verlag GmbH, Freiburg i.Br.

Schrempp, S. (2004): personal note.

Schulla J.& Jasper K. (2000): WaSiM ETH, Model discription, http://www.iac.ethz.ch/staff/verbunt/WaSiM/wasim00english.pdf [Access date: 02.01.2005].

Schulla, J. (1997): Hydrologische Modellierung von Flussgebieten zur Abschätzung der Folge von Klimaänderungen. Dissertation ETH 12ß18, Verlag Geographisches Institut ETH Zürich.

SHETRAN (2004): Water Recource Systems Research Laboratory, http://www.ncl.ac.uk/wrgi/wrsrl/rbms/rbms.html [Access date: 02.01.2005].

Sieber, A. (2003): Parameterstudien und Unsicherheitsanalysen mit dem Einzugsgebietsmodell TACD. Diploma thesis at the Albert-Ludwigs-University Freiburg, Department of Hydrology, (unpublished).

Simile (2004): Simulistics Ltd., Edinburgh Technology Transfer Centre,Edinburgh, Scotland, http://www.ierm.ed.ac.uk/simile/index.html [Access date: 02.01.2005].

Singh, V.P. (1995): Computer Models of Watershed Hydrology. Water Resources Publications, Colorado, USA.

Stober, I. (1995): Die Wasserführung des kristallinen Grundgebirges. Ferdinand Enke Verlag, Stuttgart.

Thompson, N., Barrie, I.A. & Ayles, M. (1981): The meteorological office rainfall and evaporation calculation system: MORECS. Hydrological Memorandum No. 45, The Met Office, Bracknell, UK.

Tilch, N., Uhlenbrook, S., Leibundgut, Ch., Zillgens, B, Kirnbauer, R. & Merz, B. (2003): Entschlüsselung von Abflussbildungsprozessen mit Hilfe tracerhydrologischer Ansätze in einem alpinen Einzugsgebiet, Österreichische Wasser- und Abfallwirtschaft, volume 1/2, pp. 9-17.

Trenkle, H. & Rudloff, H. von (1989): Das Klima im Schwarzwald, in: Sick E. & Sick W.D. (1989): Der Schwarzwald - Beiträge zur Landeskunde. Liehl, Konkordia Verlag GmbH, Bühl/Baden.

Uhlenbrook, S. & Leibundgut, Ch. (1997): Abflussbildung bei Hochwasser. Wasser und Boden, 9, pp. 13-22.

Uhlenbrook, S. (1999): Untersuchung und Modellierung der Abflussbildung in einem mesoskaligen Einzugsgebiet. Freiburger Hydrologische Schriften, Band 10, Institut für Hydrologie der Universität Freiburg.

Uhlenbrook, S., Holocher,J., Leibundgut, Ch. & Seibert J.(1998): Using a conceptual rainfall-runoff model on different scales by comparing a headwater with larger basins. Hydrology, Water Resources and Ecology in Headwaters, IAHS Publ. No. 248.

Uhlenbrook, S., Steinbrich, A., Tetzlaff, D. & Leibundgut, Ch. (2001): Zusammenhang zwischen extremen Hochwassern und ihren Einflussgrößen (Connection between extreme floods and their driving variables; in German), Arbeitskreis KLIWA (Klimaveränderung und Konsequenzen für die Wasserwirtschaft), KLIWA-Symposium, 29.-30.11.2000, Karlsruhe, KLIWA-Berichte, volume 1, pp. 187-204.

Uhlenbrook, S. & Leibundgut, Ch. (2002): Process-oriented catchment modelling and multiple-response validation. Hydrol. Processes 16, pp. 423-440.

Uhlenbrook, S., Didszun, J., Leibundgut, Ch. (2002): Runoff Generation Processes in Mountainous Basins and Their Susceptibility to Global Change. Mountain Research Initiative - Global Change and Mountain Regions (Publisher Huber U.), 12 pages, submitted and in state of review.

van Dam, J.C. (2000): Field-scale water flow and solute transport: SWAP model concepts, parameter estimation and case studies. Wageningen University Ph.D. Thesis, Wageningen, The Netherlands.

van Dam, O. (2000): Modelling solar radiation, evapotranspiration and soil water dynamics in tropical rainforest logging gaps in Guyana. in: Ibarra-Berastegi, G., Brebbia, C.A. & Zannetti, P. (2000). Development and Application of Computer Techniques to environmental Studies VIII, ENVIROFT2000 proc., 28-30 June 2000, Bilbao, Spain. WIT press, Southampton, pp. 289-298.

van Dam, O. (2004): Modelling incoming potential radiation on a land surface with PCRaster. from retired Internet-Site (01.2005), http://www.geog.uu.nl/fg/ovandam/potrad.htm.

van der Perk, M. & Slávik, O. (2003): Simulation of event-based and long-term spatial redistribution of Chernobyl-derived radiocaesium within catchments using GIS-embedded models. Hydrological Processes 17 Issue 5, pp. 943-957.

van der Perk, M. (2004): personal note.

van Deursen, W.P.A. (1995): Geographical Information Systems and Dynamic Models Development and application of a prototype spatial modelling language. Ph.D. thesis, Faculty of Spatial Sciences, University of Utrecht The Netherlands.

Wesseling, C.G. (2004): personal note.

Wesseling, C.G., Karssenberg, D., van Deursen, W.P.A. & Burrough, P.A. (1996b): Integrating dynamic environmental models in GIS: the development of a Dynamic Modelling language. Transactions in GIS 1, pp. 40-48.

Wesseling, C.G., van Deursen, W.P.A., Karssenberg, D. & Burrough, P.A. (1996a): Experience and applications of a GIS based dynamic modelling language. Proceedings Second Joint European Conference & Exhibition on Geographical Information, Barcelona, Spain, 1996.

Wicks, J. M. & Bathurst, J. C. (1996): SHESED: A physically based, distributed erosion and sediment yield component of the SHE hydrological modelling system. Journal of hydrology, volume 175, pp. 213-238.

Appendix

A. Parameter table

Table 8.1: Parameter table

PARAMETER	DESCRIPTION	ASSESSMENT	VALUE	UNITS
PRECIPITATION CORRECTION				
cWindA	wind correction factors	calibration	1.01	[-]
cWindB	for precipitation	"	0.01	[-]
PRECIPITATION REGIONALIZATON				
cPrecRadius	max. distance at IDW-method	dependent on station density	15000	[m]
cPrecIDWPArt	weighting of regionalization methods	estimation via coefficient of determination of elevation regression	0.8	[-]
SNOW ROUTINE				
TEMPERATURE THRESHOLDS				
cTT	snow fall	calibration (reference value from literature)	0.1	[°C]
cTT_urban	snow fall in urban areas	"	-0.1	[°C]
cTT_melt	snow melt	"	0.0	[°C]
cTT_urban	snow melt in urban areas	"	-1.0	[°C]
cTT_forest	snow melt in forested areas	"	1.5	[°C]
cSFCF	snow fall correction factor	calibration (reference value from literature)	1.08	[-]
cCFMAX	hour-degree-factor	calibration (reference value from literature)	0.15	[mm °C^{-1}h^{-1}]
cCFMAX_urban	hour-degree-factor in urban areas	"	0.2	[mm °C^{-1}h^{-1}]
cCWH	water holding capacity	literature (Bergström 1992)	0.1	[-]
cCFR	refreezing coefficient	literature (Bergström 1992)	0.05	[-]
DIRECT RUNOFF FROM URBAN AREAS				
cUrbanSplit	fraction of sealed areas	literature (Peschke et al. 1999)	0.4	[-]
SOIL ROUTINE				
cLP	reduction of potential evapotranspiration	literature (Menzel 1997)	0.6	[-]

	max. storage capacity of soil storage			
cFC_DH	percolation at plateaus	calibration	250	[mm]
cFC_DI	deleaye Interflow	"	130	[mm]
cFC_FI	fasr Interflow	"	90	[mm]
cFC_FLI	fast, lateral Interflow, Piston Flow	"	200	[mm]
cFC_EDI	strongly delayed Interflow	"	200	[mm]
cFC_DV	percolation at valley bottoms	"	220	[mm]
SOIL PARAMETERS				
cBETA_DH	percolation at plateaus	calibration	1.8	[-]
cBETA_DI	delayed Interflow	"	1.5	[-]
cBETA_FI	fast Interflow	"	1.25	[-]
cBETA_FLI	fast, lateral Interflow, Piston Flow	"	1.5	[-]
cBETA_EDI	strongly deleyed Interflow	"	1.5	[-]
cBETA_DV	percolation at valley bottoms	"	1.75	[-]
RUNOFF GENERATION				
ZONES WITH PERCOLATION AT PLATEAUS				
cDH_K	storage coefficient	calibration	0.001	[h^{-1}]
ZONES WITH DELEAYED INTERFLOW				
cDI_K_u	storage coefficient of upper storage	calibration	0.017	[h^{-1}]
cDI_K_l	storage coefficient of lower storage	"	0.0035	[h^{-1}]
cDI_T	percolation between upper and lower storage	"	0.2	[mm/h]
cDI_H	max. storage capacity of lower storage	"	400	[mm]
ZONES WITH FAST INTERFLOW				
cFI_K_u	storage coefficient of upper storage	calibration	0.1	[h^{-1}]
cFI_K_l	storage coefficient of lower storage	"	0.012	[h^{-1}]
cFI_T	percolation between upper and lower storage	"	0.6	[mm/h]
cFI_H	max. storage capacity of lower storage	"	80	[mm]
ZONES WITH FAST, LATERALEN INTERFLOW, PISTON FLOW				
cFLI_K_u	storage coefficient of upper storage	calibration	0.2	[h^{-1}]
cFI_K_l	storage coefficient of lower storage	"	0.007	[h^{-1}]
cFLI_T	percolation between upper and lower storage	"	0.6	[mm/h]
cFLI_H	max. storage capacity of lower storage	"	150	[mm]
ZONES WITH STRONGLY DELAYED INTERFLOW				

cEDI_K	storage coefficient	calibration	0.0035	[h^{-1}]
ZONES WITH PERCOLATION AT VALLEY BOTTOMS				
cDV_K_u	storage coefficient of upper storage	calibration	0.05	[h^{-1}]
cDV_K_l	storage coefficient of lower storage	"	0.005	[h^{-1}]
cDV_T	percolation between upper and lower storage	"	0.2	[mm/h]
cDV_H	max. storage capacity of lower storage	"	800	[mm]
cThres	threshold value for surface water<=> groundwater interaction	"	500	[mm]
c_Exf	exfiltration rate	from groundwater modeling (Bold 2000)	0.025	[mm/h]
c_Inf	infiltration rate	"	0.1	[mm/h]
cPump_1	pump rate of water suppliers	average 1996/97	0	[m^3/h]
cPump_2	"	"	3.4	[m^3/h]
cPump_3	"	"	322.4	[m^3/h]
cPump_4	"	"	403.8	[m^3/h]
cPump_5	"	"	32.7	[m^3/h]
cPump_6	"	"	16.7	[m^3/h]
cPump_7	"	"	8.4	[m^3/h]
cPump_8	"	"	20.8	[m^3/h]
cPump_9	"	"	51.5	[m^3/h]
cPump_10	"	"	110	[m^3/h]
cPump_11	"	"	118.5	[m^3/h]
cPump_12	"	"	135	[m^3/h]
cPump_13	"	"	58.6	[m^3/h]
cPump_14	"	"	31.3	[m^3/h]
cPump_15	"	"	0.8	[m^3/h]
cPump_16	"	"	8.1	[m^3/h]
ZONES WITH STAURATED OVERLAND FLOW				
cMTD_K	storage coefficient	calibration	0.01	[h^{-1}]
cMTD	max. storage capacity	"	30	[mm]
FRACTURED AQUIFER				
cGW_K	storage coefficient	calibration	0.005	[h^{-1}]
cGW_H	max. storage capacity	"	1000	[mm]
cAll_P	percolation over overlaying storages into fractured aquifer (apart from saturated overland flow and percolation in valley bottoms)	"	0.075	[mm/h]
GENERAL FOR ALL UPPER STORAGE TYPES				
cUS_H	max. storage capacity	calibration	800	[mm]
KINEMATIC WAVE ROUTING				
sStreamWidth	stream width	measured	0.3-14.8 [m]	

sStreamLength	average stream length per cell	topographic map analysis	208.5	[m]
cN	roughness parameter after Manning	estimation from stream characteristics	0.04-0.08 [$m^{1/3}s^{-1}$]	
cBeta	parameter of kinematic wave approach	literature (Chow et al. 1998)	0.6	[-]
cTimeStep	time step duration in loops of the kinematic wave method	dependent on space and time discretization	360	[s]
cNrSteps	number of internal loops for the kinematic wave routing			

B. Additional graphs of simulation results

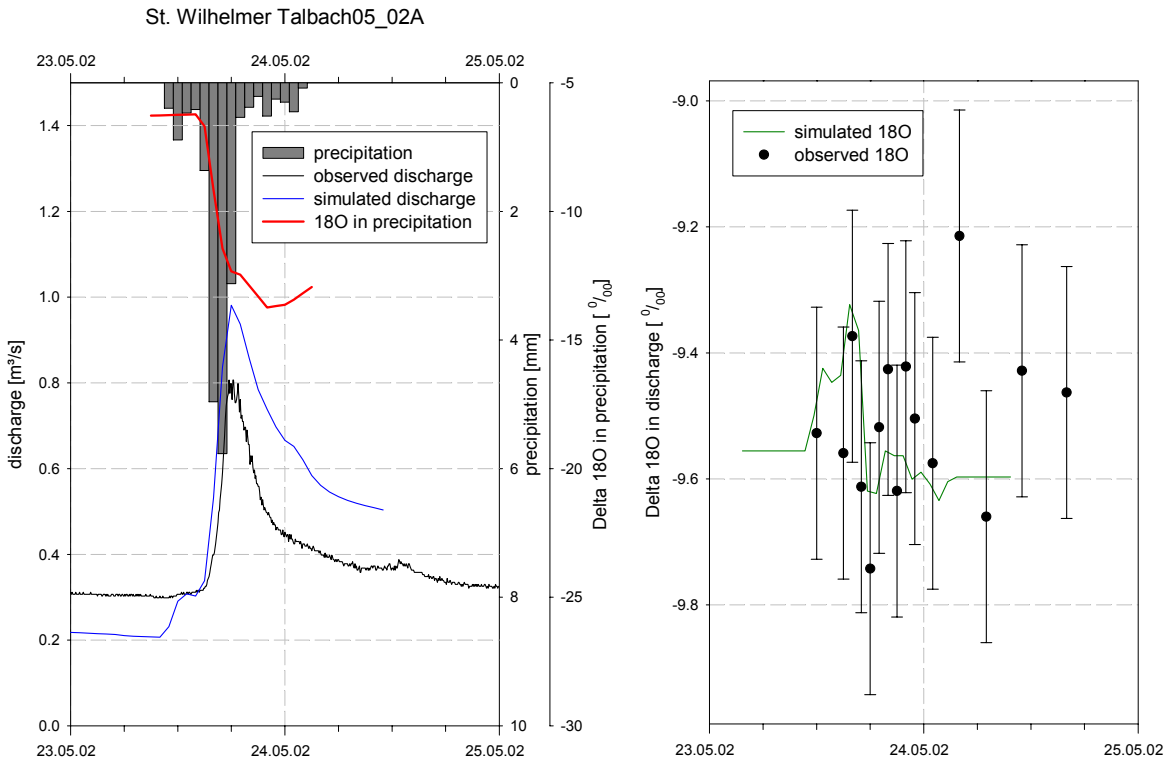

Figure 8.1: Results of DS 05_02A; St.Wilhelmer Talbach

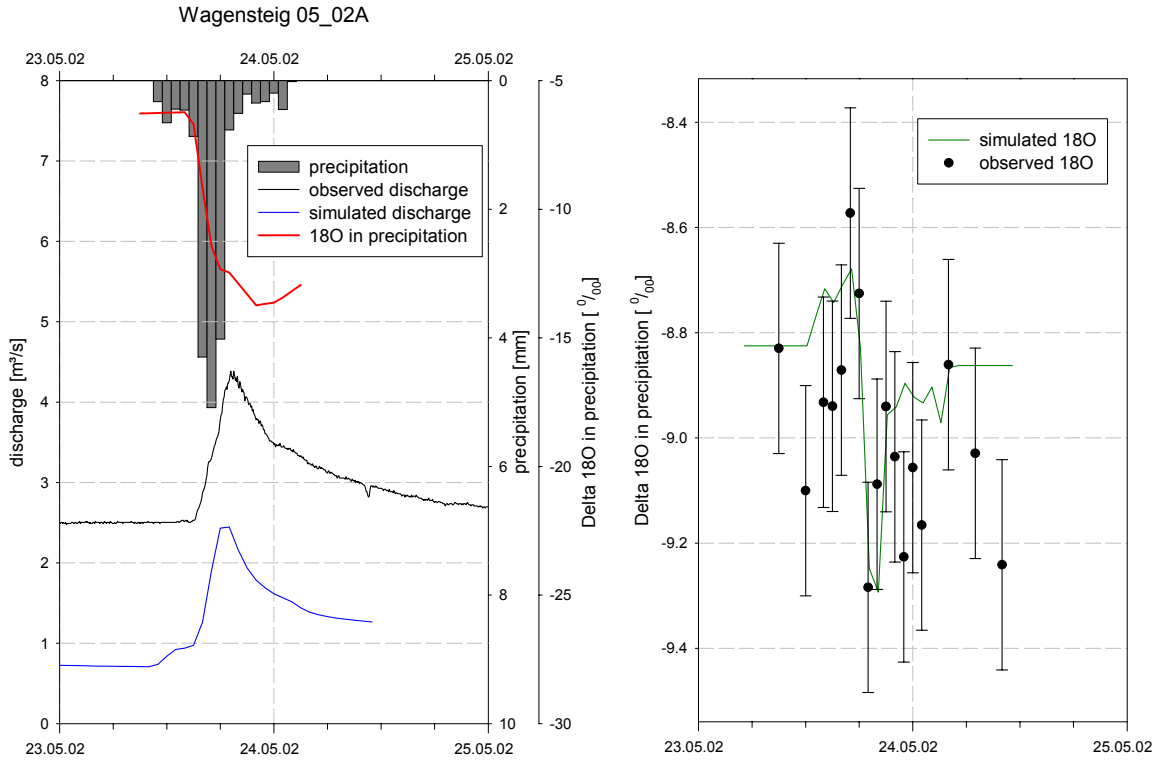

Figure 8.2: Results of DS 05_02A; Wagensteig Bach

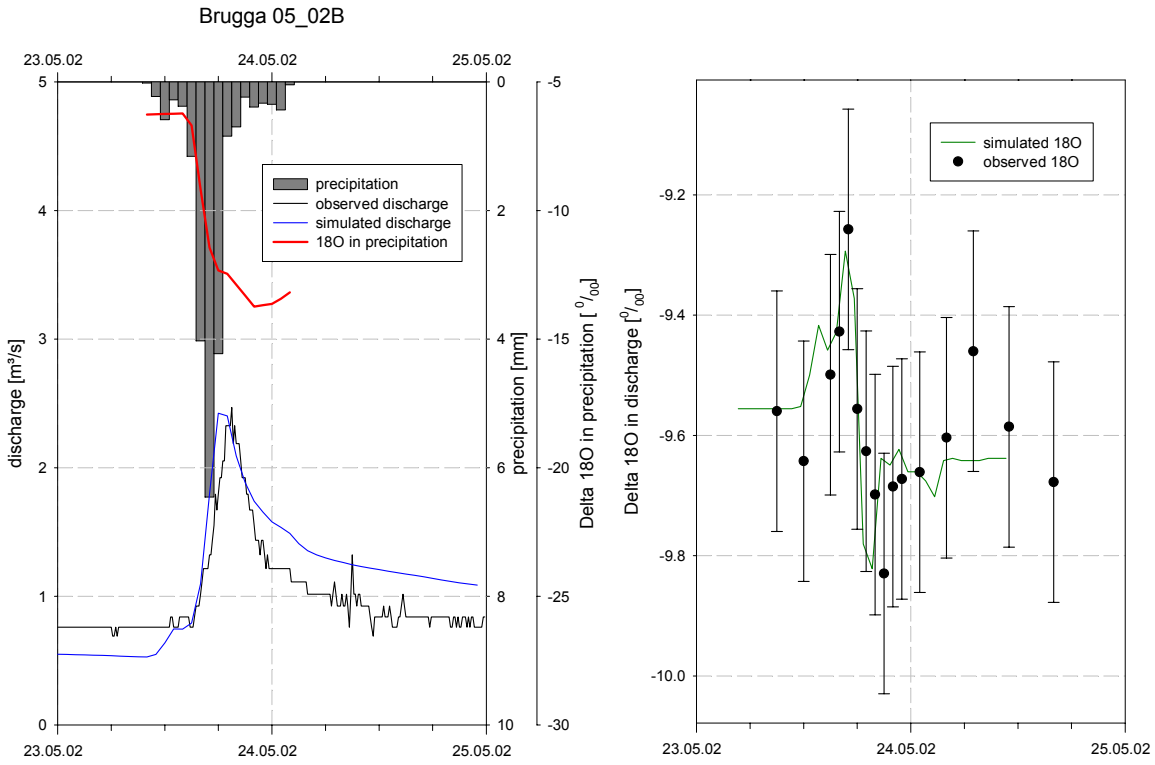

Figure 8.3: Results of DS 05_02B; Brugga

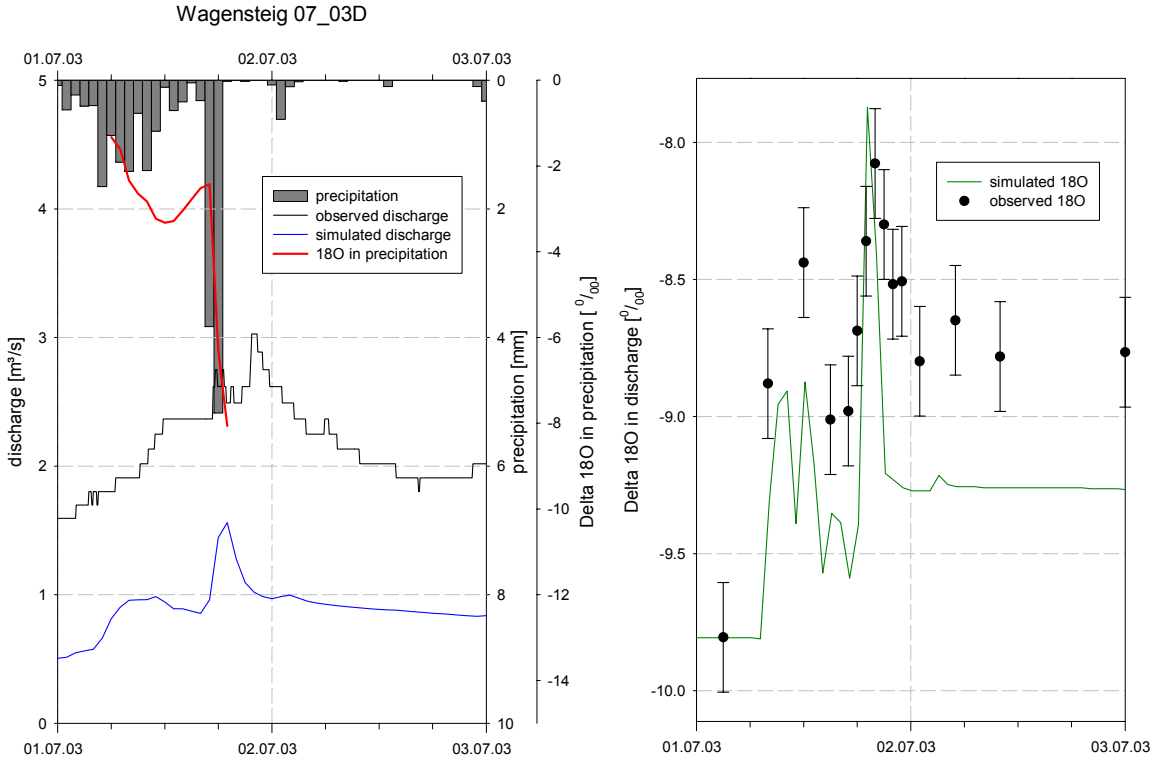

Figure 8.4: Results of DS 07_03D; Wagensteig Bach

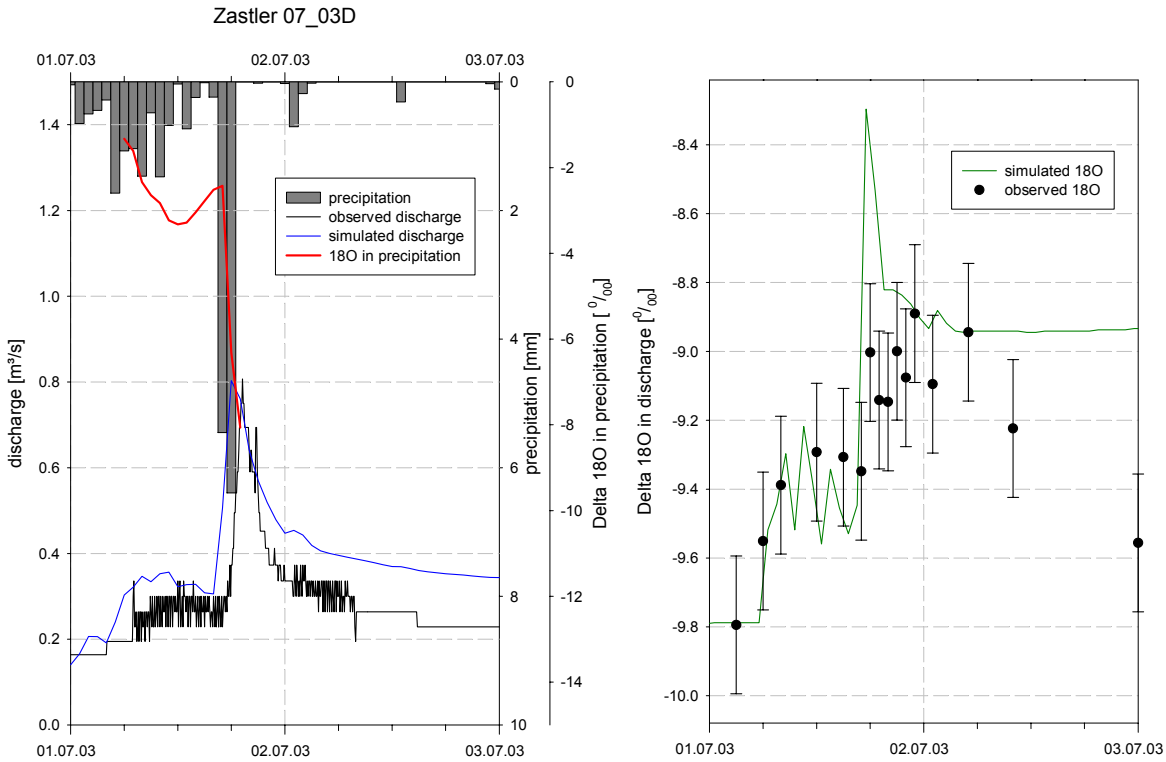

Figure 8.5: Results of DS 07_03D; Zastler Talbach

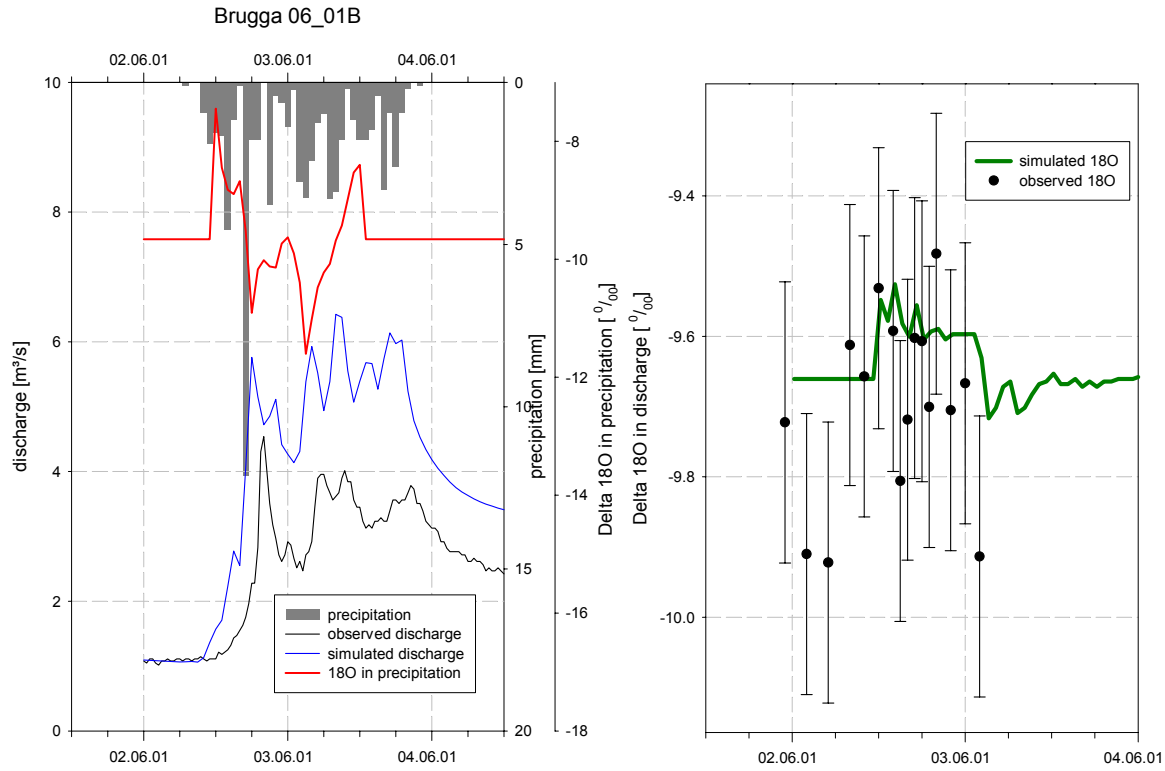

Figure 8.6: BRU 06_01B; Brugga

Dedicated to all the modelers on the globe (*SINGH 1995*)

EHRENWÖRTLICHE ERKLÄRUNG

Hiermit erkläre ich, dass diese Arbeit selbständig und nur unter Verwendung der angegebenen Hilfsmittel angefertigt wurde.

Freiburg i. Br., Januar 2005